Volume 73A
Number 4
July–August 1969
J. Res. Nat. Bur. Stand. (U.S.), A
CODEN: JNBAA 73A (4) 389–450 (1969)

Physics and Chemistry

U.S. DEPARTMENT OF COMMERCE

SECTION A

JOURNAL OF RESEARCH

NATIONAL BUREAU OF STANDARDS

Journal of Research

of the

National Bureau of Standards

A. Physics and Chemistry

July–August • 1969

VOLUME • 73A

NUMBER • 4

Editor: C. W. Beckett

Associate Editor: D. D. Wagman

Publication dates:
Feb. 1, Apr. 1, June 1, Aug. 1, Oct. 1, Dec. 1, 1969

JOURNAL OF RESEARCH

The National Bureau of Standards Journal of Research reports research and development in the fields of activity shown at right. Also included from time to time are survey articles on topics closely related to the Bureau's scientific and technical program.

The Journal is published in three separate sections as follows:

A. Physics and Chemistry

Contains papers of interest primarily to scientists working in these fields. Issued six times a year. Annual subscription: domestic, $9.50; foreign, $11.75. Single copy, varies.

B. Mathematical Sciences

Presents studies and compilations designed mainly for the mathematician and the theoretical physicist. Issued quarterly. Annual subscription: domestic, $5.00; foreign, $6.25. Single copy, $1.25.

C. Engineering and Instrumentation

Reports research and development results of interest chiefly to the engineer and the applied scientist. Issued quarterly. Annual subscription: domestic, $5.00 foreign, $6.25. Single copy, $1.25.

NATIONAL BUREAU OF STANDARDS

The National Bureau of Standards[1] was established by an act of Congress March 3, 1901. Today, in addition to serving as the Nation's central measurement laboratory, the Bureau is a principal focal point in the Federal Government for assuring maximum application of the physical and engineering sciences to the advancement of technology in industry and commerce. To this end the Bureau conducts research and provides central national services in four broad program areas. These are: (1) basic measurements and standards, (2) materials measurements and standards, (3) technological measurements and standards, and (4) transfer of technology.

The Bureau comprises the Institute for Basic Standards, the Institute for Materials Research, the Institute for Applied Technology, the Center for Radiation Research, the Center for Computer Sciences and Technology, and the Office for Information Programs.

THE INSTITUTE FOR BASIC STANDARDS provides the central basis within the United States of a complete and consistent system of physical measurement; coordinates that system with measurement systems of other nations; and furnishes essential services leading to accurate and uniform physical measurements throughout the Nation's scientific community, industry, and commerce. The Institute consists of an Office of Measurement Services and the following technical divisions:

Applied Mathematics — Electricity — Metrology — Mechanics — Heat — Atomic and Molecular Physics — Radio Physics[2] — Radio Engineering[2] — Time and Frequency[2] — Astrophysics[3] — Cryogenics.[3]

THE INSTITUTE FOR MATERIALS RESEARCH conducts materials research leading to improved methods of measurement standards, and data on the properties of well-characterized materials needed by industry, commerce, educational institutions, and Government; develops, produces, and distributes standard reference materials; relates the physical and chemical properties of materials to their behavior and their interaction with their environments; and provides advisory and research services to other Government agencies. The Institute consists of an Office of Standard Reference Materials and the following divisions:

Analytical Chemistry—Polymers—Metallurgy—Inorganic Materials—Physical Chemistry.

THE INSTITUTE FOR APPLIED TECHNOLOGY provides technical services to promote the use of available technology and to facilitate technological innovation in industry and Government; cooperates with public and private organizations in the development of technological standards, and test methodologies; and provides advisory and research services for Federal, state, and local government agencies. The Institute consists of the following technical divisions and offices:

Engineering Standards—Weights and Measures—Invention and Innovation—Vehicle Systems Research—Product Evaluation—Building Research—Instrument Shops—Measurement Engineering—Electronic Technology—Technical Analysis.

THE CENTER FOR RADIATION RESEARCH engages in research, measurement, and application of radiation to the solution of Bureau mission problems and the problems of other agencies and institutions. The Center consists of the following divisions:

Reactor Radiation—Linac Radiation—Nuclear Radiation—Applied Radiation.

THE CENTER FOR COMPUTER SCIENCES AND TECHNOLOGY conducts research and provides technical services designed to aid Government agencies in the selection, acquisition, and effective use of automatic data processing equipment; and serves as the principal focus for the development of Federal standards for automatic data processing equipment, techniques, and computer languages. The Center consists of the following offices and divisions:

Information Processing Standards—Computer Information—Computer Services—Systems Development—Information Processing Technology.

THE OFFICE INFORMATION PROGRAMS promotes optimum dissemination and accessibility of scientific information generated within NBS and other agencies of the Federal government; promotes the development of the National Standard Reference Data System and a system of information analysis centers dealing with the broader aspects of the National Measurement System, and provides appropriate services to ensure that the NBS staff has optimum accessibility to the scientific information of the world. The Office consists of the following organizational units:

Office of Standard Reference Data—Clearinghouse for Federal Scientific and Technical Information[3]—Office of Technical Information and Publications—Library—Office of Public Information—Office of International Relations.

[1] Headquarters and Laboratories at Gaithersburg, Maryland, unless otherwise noted; mailing address Washington, D.C. 20234.
[2] Located at Boulder, Colorado 80302.
[3] Located at 5285 Port Royal Road, Springfield, Virginia 22151.

U.S. DEPARTMENT OF COMMERCE
Maurice H. Stans, Secretary
NATIONAL BUREAU OF STANDARDS
A. V. Astin, Director

Order all publications from the Superintendent of Documents
U.S. Government Printing Office, Washington, D.C. 20402

Use of funds for printing this publication approved by the Director of the Bureau of the Budget (June 22, 1966).

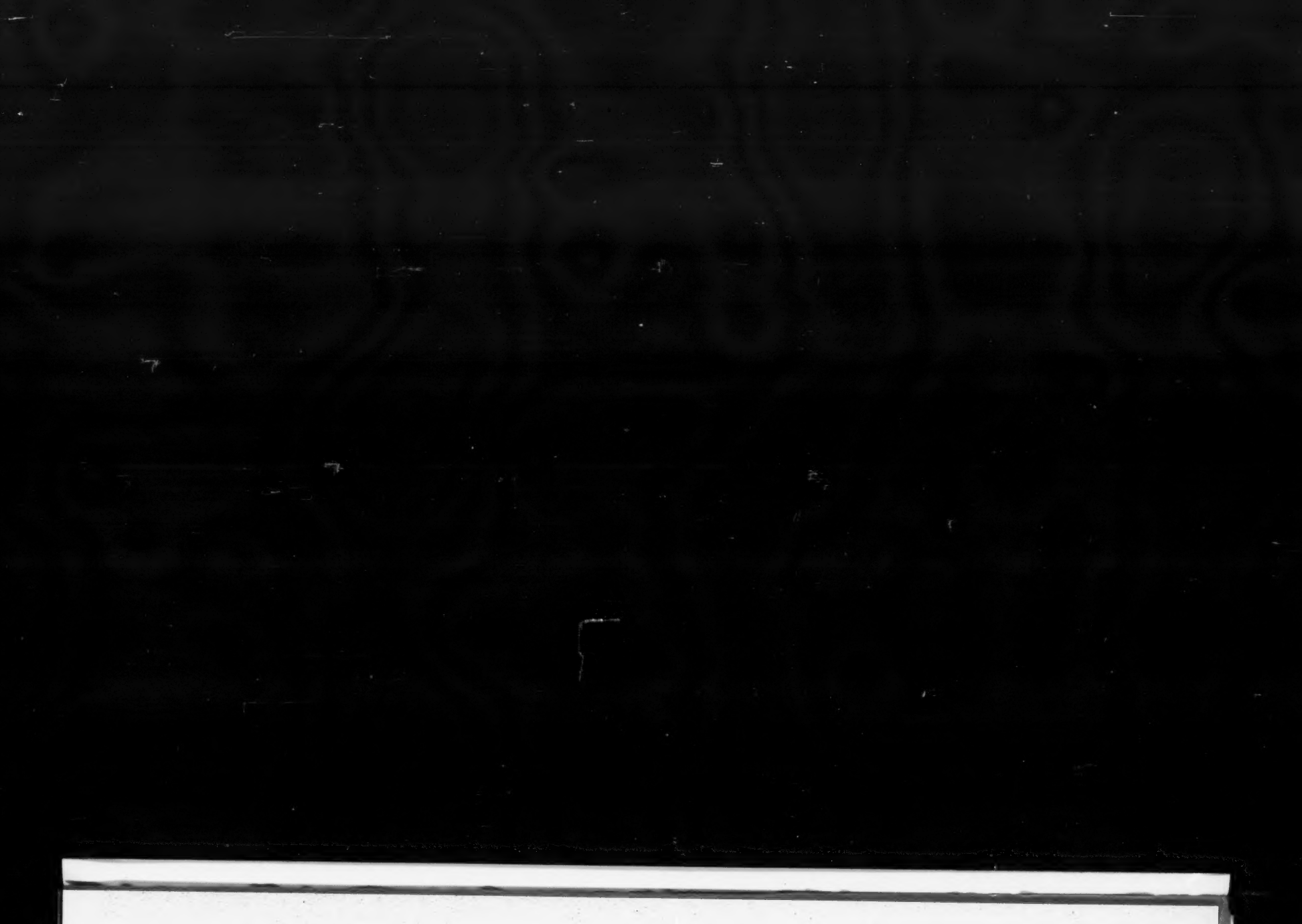

JOURNAL OF RESEARCH of the National Bureau of Standards—A. Physics and Chemistry
Vol. 73A, No. 4, July–August 1969

Classical Path Methods in Line Broadening. I. The Classical Path Approximation

Earl W. Smith,* C. R. Vidal,* and J. Cooper**

**Institute for Basic Standards, National Bureau of Standards
Boulder, Colorado 80302**

(February 24, 1969)

The classical path approximation is reviewed in a manner which permits definitive statements concerning its region of validity.

Key words: Classical path methods; line broadening theory.

1. Introduction

The classical path approximation which is used in most line broadening theories, as well as many other atomic and molecular problems, is not always clearly understood because it is based on rather heuristic arguments. Previous derivations have relied more on physical insight than mathematical analysis hence such features as the neglect of "back reaction" and the assumption that the density matrix is "diagonal in wave packet states" are not given to concise mathematical statements.

In this paper, statistical methods are used in deriving a precise mathematical expression for the "thermal average." The approximations used will be given as mathematical statements which are easily understood both physically and mathematically. It is hoped that this approach will be of some pedagogical value in understanding the foundations of the usual classical path methods.

In the following paper [1][1], henceforth referred to as II, this approach will be extended to show how the usual binary collision theories are obtained, and a systematic method for improving these theories is outlined.

2 Construction of a Mathematical Model

The line broadening problem for gases (or plasmas) is basically a study of the distribution of spectral radiation emitted or absorbed by the gas. The emission (or absorption) is usually produced by a small number of particles, and the spectral lines are shifted and broadened by the interaction between these radiators and the remainder of the particles in the gas. Since the number of radiators is usually a very small fraction of the total number of particles in the gas, the average distance between radiators will be large enough that any direct interactions between them are negligible. We will therefore regard the gas as being divided into a large number of cells in such a way that each cell contains one radiator and a large number of perturbing particles. We will assume that the particles at the border between adjacent cells are effectively at infinity with respect to the radiators; that is, the interaction between a radiator and a perturber at the edge of a cell is negligibly small. The distribution of particles at the border between cells will then be uniform (i.e., not altered by the presence of the radiators) and we may neglect all interactions between cells provided that we maintain this uniform distribution near the edges of the cells.

We have now represented the gas by a collection of noninteracting cells. Each cell may be described by a Hamiltonian of the form

$$H = H_a + H_p + V, \tag{1}$$

where H_a is an unperturbed Hamiltonian for the radiator, H_p is an unperturbed Hamiltonian for the remaining particles in the cell (henceforth called the perturbers), and V represents the interaction between the radiator and these perturbers.

The probability per unit time that a cell, initially in the state $|m>$, will make a spontaneous dipole transition to another state, $|n>$, is [2]

$$P_{mn} = (4\omega_{mn}^3/3\hbar c^3)\,|<m|\mathbf{d}|n>|^2 \tag{2}$$

*Radio Standards Physics Division, Plasma Physics, National Bureau of Standards Laboratories, Boulder, Colo. 80302.
**Joint Institute for Laboratory Astrophysics and Department of Physics and Astrophysics, University of Colorado, Boulder, Colo. 80302.

1 Figures in brackets indicate the literature references at the end of this paper.

where $|m>$ and $|n>$ are H eigenstates belonging to the eigenvalues E_m and E_n, ω_{mn} is the frequency difference $(E_m-E_n)/\hbar$, and $\mathbf{d}$ is the dipole moment of the cell. Since we are interested only in line spectra, we may exclude the continuum radiation produced by the perturbers (bremsstrahlung, etc.) by excluding the dipole moment of the perturbers. That is, $\mathbf{d}$ will be the dipole moment operator for the radiator, thus ignoring all transitions which do not involve a change in the dipole moment of the radiator. The power radiated when a cell makes a dipole transition from $|m>$ to $|n>$ is just $\hbar\omega_{mn}P_{mn}$, and the contribution this makes to the total power spectrum emitted by the gas is $\hbar\omega_{mn}P_{mn}\delta(\omega-\omega_{mn})$ or

$$P(\omega)=(4\omega^4/3c^3)\delta(\omega-\omega_{mn})|<m|\mathbf{d}|n>|^2 \qquad (3)$$

if we use delta functions as natural lines. If one wishes to use very narrow Lorentzian natural lines [3], it is necessary only to use a complex frequency variable in place of ω; this is of little practical importance although it is a mathematical convenience for some problems. In $P(\omega)$, negative values of ω (or ω_{mn}) represent absorptive transitions.

The total power spectrum emitted by the gas is obtained by adding the contributions, $P(\omega)$, from each of the cells. Since all cells have the same spectrum of accessible states (H eigenstates), this will turn out to be a weighted sum of eq (3) over all possible initial and final states. If the total number of cells (total number of radiators in the gas) is N_R and if the probability of finding a cell (one radiator plus its perturbers) in the initial state $|m>$ is ρ_m, then the number of cells initially in the state $|m>$ is $N_R\rho_m$. Since P_{mn}, given by eq (2), is the probability that a cell initially in the state $|m>$ will make a dipole transition to the state $|n>$, any given transition $|m>\rightarrow|n>$ will occur in $N_R\rho_mP_{mn}$ of the cells in the gas. The power radiated by this group of cells is $\hbar\omega_{mn}N_R\rho_mP_{mn}$ and their contribution to the total power spectrum is $\hbar\omega_{mn}N_R\rho_mP_{mn}\delta(\omega-\omega_{mn})$. We obtain the total power spectrum for the gas by summing this expression over all possible $|m>\rightarrow|n>$ transitions. The total power radiated per unit frequency interval is thus given by

$$P_T(\omega)=(4N_R\omega^4/3c^3)\Sigma_{mn}\delta(\omega-\omega_{mn})|<m|\mathbf{d}|n>|^2\rho_m. \qquad (4)$$

This expression is equivalent to summing eq (3) over all $|m>\rightarrow|n>$ transitions, weighting each term by $N_R\rho_m$, the number of cells initially in the state $|m>$.

In most line broadening problems one is interested only in a small range of frequencies which pertains to a single broadened line. In such a case the factor ω^4 in eq (4) does not change appreciably, and most of the frequency dependence of $P(\omega)$ is contained in the sum over $\delta(\omega-\omega_{mn})$. We thus define a line shape function, $I(\omega)$, by

$$P(\omega)=(4N_R\omega^4/3c^3)I(\omega) \qquad (5)$$

$$I(\omega)=\Sigma_{mn}\delta(\omega-\omega_{mn})|<m|\mathbf{d}|n>|^2\rho_m. \qquad (6)$$

The evaluation of $I(\omega)$ is the central problem of line broadening theories. Since eq (6) is not multiplied by N_R, we see that it is necessary to consider only a single cell (with appropriate weighting of the initial states) when evaluating $I(\omega)$. For this reason, most line broadening theories start out with a mathematical model which contains a single radiator immersed in a gas of perturbing particles. We have included this section merely to justify the use of such a model, and in all following sections we will refer to this model rather than the gas as a whole.

3. The Weak Coupling Approximation

Using the results of the previous section, it can easily be shown [4, 5, 6] that the line shape for spectral radiation is given by

$$I(\omega)=(2\pi)^{-1}\int_{-\infty}^{\infty}e^{i\omega t}C(t)dt$$

$$=\pi^{-1}\mathrm{Re}\int_0^{\infty}e^{i\omega t}C(t)dt \qquad (7)$$

where $C(t)$ is a correlation function which has the property $C^*(t)=C(-t)$. For dipole radiation, $C(t)$ is an autocorrelation function of the dipole operator $\mathbf{d}$ for the radiator. This function may be given by

$$C(t)=Tr\{\mathbf{d}\cdot T^{\dagger}(t)\mathbf{d}T(t)\rho\} \qquad (8)$$

where $T(t)$ and ρ are the time development operator [7] and density matrix for the system (a radiator and its perturbers) and the trace is over all states of the system.

The autocorrelation function $C(t)$ may be given various physical interpretations. Some of these interpretations are discussed in detail in section 7.

Following Fano [8, 9], we regard the system as being composed of two weakly coupling subsystems; subsystem "a" is the radiator (e.g., an atom, molecule, etc.) while subsystem "p" is the gas of perturbers. The Hamiltonian, H, for the system has been given in eq (1) by (H_a+H_p+V) where H_a and H_p are Hamiltonians describing the radiator and perturber subsystems and V represents a coupling interaction between these subsystems [10].

We assume that the radiator and the gas of perturbers are statistically independent; that is, the state of the perturbers does not depend explicitly on the state of the radiator, and vice versa. This is the neglect of "back reaction" in the density matrix. A mathematical statement of this approximation has been given by Fano [9] in terms of the density matrix:

$$\rho=\rho^{(a)}\rho^{(p)}, \qquad (9)$$

where $\rho^{(a)}$ and $\rho^{(p)}$ depend only on radiator and perturber variables respectively. As a first approximation we assume that each subsystem is in equilibrium:

$$\rho^{(a)} = \rho^{(a)}(H_a)$$
$$\rho^{(p)} = \rho^{(p)}(H_p). \tag{10}$$

For a canonical ensemble, $\rho \propto \exp\{-H/kT\}$; this requires that $\exp\{-V/kT\}$ be replaced by unity leaving $\rho \propto \exp\{-(H_a+H_p)/kT\}$ which has the form required by eqs (9) and (10). The interpretation of this approximation is a matter of some importance and it will be discussed in detail in section 8.

The assumption of statistical independence, eq (9), permits one to write the correlation function, eq (8), in the form

$$C(t) = Tr_a\{\mathbf{d}\cdot Tr_p\{T^\dagger(t)\mathbf{d}T(t)\rho^{(p)}\}\rho^{(a)}\}$$
$$= Tr_a\{\mathbf{d}\cdot < T^\dagger(t)\mathbf{d}T(t) > \rho^{(a)}\} \tag{11}$$

where the subscripts on the trace operations denote a trace over states of the indicated subsystem [9]. The bracket $\langle \ldots \rangle$ represents an ensemble average over the perturber subsystem. This average takes the place of the usual "thermal average."

4. The Perturber Ensemble

We have assumed that the radiator and the perturber subsystems are statistically independent. The density operator, $\rho^{(p)}$, for the perturber subsystem will therefore be the same as the density operator for an isolated gas of N particles in a volume $\mathscr{V}$ (the volume of a cell) maintained at a constant temperature T. Given the restrictions $(N, \mathscr{V}, T)$, there are many possible configurations of positions, $\mathbf{x} = (\mathbf{x}_1, \mathbf{x}_2 \ldots, \mathbf{x}_N)$, and velocities, $\mathbf{v} = (\mathbf{v}_1, \mathbf{v}_2, \ldots, \mathbf{v}_N)$, for the particles which are consistent with these macroscopic constraints. Speaking quantum mechanically, we say that there are many different state functions, $\varphi(\mathbf{x}, t)$, which could describe such an isolated gas. We may index each of these possibilities with a superscript (i), and we imagine a collection of perturber gases, called an ensemble [11]. Each $\varphi^{(i)}(\mathbf{x}, t)$ must be a solution of the Schrödinger equation,

$$i\hbar \frac{\partial}{\partial t}\varphi^{(i)}(\mathbf{x}, t) = H_p\varphi^{(i)}(\mathbf{x}, t), \tag{12}$$

which is normalized to unity:

$$\int |\varphi^{(i)}(\mathbf{x}, t)|^2 d\mathbf{x} = 1. \tag{13}$$

Due to its mathematical nature, the concept of an ensemble is not readily given to simple physical interpretations. However, in the following section it will be shown that, by neglecting the influence of the radiator on the state of the perturbers which surround it (i.e., "back reaction" effects in the wave functions), a physical interpretation of the ensemble is possible. In that case we may regard each of the cells discussed in section 2 as being a member of the ensemble (provided that there are enough cells); that is, each $\varphi^{(i)}$ will then represent one of the possible states for the perturbers in a cell and, for a given state of the radiator, the superscript i may then be used to index the cells. It must be emphasized that *in this section* we are not representing the wave function for the perturbers in the cells by $\varphi^{(i)}$. At this point we are simply constructing an approximate density operator for these perturbers which is based on an isolated gas. In the following section we will use the $\varphi^{(i)}$ as *basis functions* in constructing wave functions for the perturbers in the cells, however, the treatment of the *wave functions* in the following section is distinct from the discussion of the *statistics* in this section.

For an isolated gas, energy would be a constant of the motion hence each $\varphi^{(i)}$ will be an eigenfunction of H_p [13]. If we define a complete orthonormal set of H_p eigenfunctions $\{f_k(\mathbf{x})\}$ by

$$H_p f_k(\mathbf{x}) = E_p^{(k)} f_k(\mathbf{x}) \tag{14}$$

$$\int f_k^*(\mathbf{x}) f_j(\mathbf{x}) d\mathbf{x} = \delta_{k,j}, \tag{15}$$

then, from eqs (12) and (13), it is obvious that

$$\varphi^{(i)}(\mathbf{x}, t) = f_i(\mathbf{x}) \exp(-itE_p^{(i)}/\hbar). \tag{16}$$

Using the notation

$$f_k(\mathbf{x}) = \langle \mathbf{x}|k\rangle$$
$$\varphi^{(i)}(\mathbf{x}, t) = \langle \mathbf{x}|\varphi^{(i)}; t\rangle \tag{17}$$

Equation (16) may also be written in the form

$$|\varphi^{(i)}; t> = |i> \exp(-itE_p^{(i)}/\hbar). \tag{18}$$

The probability of finding the gas of perturbers in a particular state $\varphi^{(i)}$ will be denoted by $q^{(i)}$, and the $q^{(i)}$ will be normalized so that

$$\Sigma_i q^{(i)} = 1. \tag{19}$$

The density operator, $\rho^{(p)}$ is then defined [9] by a sum over all possible states $\varphi^{(i)}$, weighting each by its probability of occurrence $q^{(i)}$:

$$\rho^{(p)} = \sum_i |\varphi^{(i)}; t > q^{(i)} < \varphi^{(i)}; t|$$
$$= \sum_i |i > q^{(i)} < i|. \tag{20}$$

For the macroscopic constraints N, $\mathscr{V}$, and T, the statistical weights are given by

$$q^{(i)} = \exp\{-E_p^{(i)}/kT\}/\sum_i \exp\{-E_p^{(i)}/kT\} \tag{21}$$

where $E_p^{(i)}$ are the H_p eigenvalues. Since the states $\varphi^{(i)}$ are H_p eigenfunctions, they are also eigenfunctions of the operator $\exp(-H_p/kT)/Tr_p\{\exp(-H_p/kT)\}$

having the eigenvalues $q^{(i)}$ as given by eq (21). Using this property and a closure relation for the $\varphi^{(i)}$ we may combine eqs (20) and (21) to obtain a more familiar form for $\rho^{(p)}$.

$$\rho^{(p)} = \exp(-H_p/kT)/Tr_p\{\exp(-H_p/kT)\}. \quad (22)$$

It is obvious, from this equation, that the perturber density matrix is diagonal between eigenstates of H_p. Since the states $\varphi^{(i)}(\mathbf{x}, t)$ *are eigenfunctions of* H_p, the density matrix will be diagonal between these states. In the following section it will be assumed that $\varphi^{(i)}(\mathbf{x}, t)$ may, under certain conditions, be viewed as a product of wave packets for each of the perturbers. We will then be able to state that the density matrix is "diagonal in wave packet states."

5. Approximate Wave Functions

In this section, approximations will be made concerning the form of the wave functions for the system (radiator and perturbers). We will derive the wave functions used by Baranger [4], retaining the superscript (i) notation of the previous section in order to clarify the influence of the perturbers in these wave functions.

The wave functions for the system must be solutions of the Schrödinger equation

$$i\hbar \frac{\partial}{\partial t} \Psi(\mathbf{R}, \mathbf{x}, t) = (H_a + H_p + V)\Psi(\mathbf{R}, \mathbf{x}, t), \quad (23)$$

where $\mathbf{x}$ is a $3N$-vector $(\mathbf{x}_1, \mathbf{x}_2, \ldots, \mathbf{x}_N)$, which denotes the positions of the N perturbers, and $\mathbf{R}$ denotes the internal coordinates of the radiator (e.g., for an atom, $\mathbf{R}$ denotes the positions of the orbital electrons).

We wish to expand the wave functions $\Psi(\mathbf{R}, \mathbf{x}, t)$ in terms of some complete set of basis functions for the system. Since the functions $f_k(\mathbf{x})$, introduced in the previous section, form a complete set for the perturber subsystem and the H_a eigenfunctions, which we shall call $g_j(\mathbf{R})$, form a complete set for the radiator subsystem, we may expand $\Psi(\mathbf{R}, \mathbf{x}, t)$ in the following manner:

$$\Psi(\mathbf{R}, \mathbf{x}, t) = \sum_{jk} a_{jk}(t) g_j(\mathbf{R}) f_k(\mathbf{x}), \quad (24)$$

where the $a_{jk}(t)$ are to be determined by using eq (23) and some boundary condition on Ψ.

Using eq (16) we may rewrite eq (24) in the form

$$\Psi(\mathbf{R}, \mathbf{x}, t) = \sum_k \chi^{(k)}(\mathbf{R}, t)\varphi^{(k)}(\mathbf{x}, t) \quad (25)$$

where the coefficients

$$\chi^{(k)}(\mathbf{R}, t) = \sum_j a_{jk}(t) g_j(\mathbf{R}) \exp(iE_p^{(k)}t/\hbar) \quad (26)$$

must be determined by requiring that Ψ satisfy the Schrödinger equation, eq (23), as well as some boundary condition.

At some initial time, $t = 0$, we may require that the perturber gas be represented by one of the wave functions $\varphi^{(i)}$:

$$\Psi(\mathbf{R}, \mathbf{x}, 0) = \chi^{(i)}(\mathbf{R}, 0)\varphi^{(i)}(\mathbf{x}, 0). \quad (27)$$

That is, at some instant in time, the coupling interaction V will be small and the perturbers will behave like an isolated gas at that instant. Equation (27) constitutes the boundary condition for Ψ. Substituting eq (25) into the Schrödinger equation, eq (23), and using the orthogonality of the $\varphi^{(k)}$, we obtain a set of *coupled* equations for the coefficients $\chi^{(k)}$:

$$i\hbar \frac{\partial \chi^{(k)}}{\partial t} = [H_a + V^{(k)}(t)]\chi^{(k)} + \sum_{j \neq k} V^{(k,j)}(t)\chi^{(j)} \quad (28)$$

where

$$V^{(k)}(t) = \langle \varphi^{(k)}; t | V | \varphi^{(k)}; t \rangle \quad (29)$$

$$V^{(j,k)}(t) = \langle \varphi^{(j)}; t | V | \varphi^{(k)}; t \rangle. \quad (30)$$

We will now assume that the state of the perturbers is not affected by the interaction V; that is,

$$\langle \varphi^{(i)}; t | V | \varphi^{(j)}; t \rangle \ll \langle \varphi^{(j)}; t | V | \varphi^{(i)}; t \rangle. \quad (31)$$

With this approximation the states $\varphi^{(i)}$ may be regarded as approximate V eigenfunctions,

$$V|\varphi^{(i)}; t> = V^{(i)}|\varphi^{(i)}; t>, \quad (32)$$

as well as H_p eigenfunctions. This relation provides a mathematical statement of the neglect of "back reaction" in the wave functions. Since the state of the perturbers is now unaffected by the presence of the atom, the coupling term in eq (28) vanishes and, using the boundary condition given in eq (27), we readily obtain the approximate wave function

$$\Psi^{(i)}(\mathbf{R}, \mathbf{x}, t) = \chi^{(i)}(\mathbf{R}, t)\varphi^{(i)}(\mathbf{x}, t), \quad (33)$$

where $\chi^{(i)}$ satisfies the equation

$$i\hbar \frac{\partial}{\partial t} \chi^{(i)} = [H_a + V^{(i)}(t)]\chi^{(i)}. \quad (34)$$

Comparing eqs (12), (29), (33), and (34) with eqs (16), (17), (21), and (22) of reference [4], we see that the approximate wave function $\Psi^{(i)}$ is identical with the approximate wave function introduced by Baranger. The superscript (i) now indicates the dependence of the total wave function, $\Psi^{(i)}$, on the various possible perturber configurations in a cell (as mentioned in the previous section). Although this dependence is implied by Baranger, it is not illustrated by such a parameter.

It is obvious that a function $\Psi^{(i)}(\mathbf{R}, \mathbf{x}, t)$ having the form given in eq (33) cannot rigorously satisfy the Schrödinger, equation, eq (23), because the latter

is, in general, not separable equation. It would be possible to find solutions of the form $\chi^{(i)}(\mathbf{R}, \mathbf{x}, t)\varphi^{(i)}(\mathbf{x}, \mathbf{t})$, but the "radiator wave function," $\chi^{(i)}$, would then depend explicitly on the perturber coordinates, $\mathbf{x}$, as well as $\mathbf{R}$ and t. By neglecting "back reaction," according to eq (32), we have obtained an approximate wave function of the form $\chi^{(i)}\varphi^{(i)}$ where $\chi^{(i)}$ does not depend *explicitly* on perturber coordinates. The superscript (i) which appears on this "radiator wave function" indicates that $\chi^{(i)}$ does depend *implicitly* on the state of the perturbers through the effective potential $V^{(i)}(t)$; that is, we get different functions $V^{(i)}$ for each of the possible states $\varphi^{(i)}$.

A general procedure for approximating the solution of the Schrödinger equation (23) by a function $\Psi^{(i)}$ having the form stated in eq (33) would be an iterative one. The first approximation uses $\varphi^{(i)}$ and $\chi^{(i)}$ as given by eqs (12) and (34). If we chose to, we could obtain the next approximation to $\varphi^{(i)}$ by substituting $\Psi^{(i)} = \varphi^{(i)}\chi^{(i)}$ into the Schrödinger equation (23), using eq (34) to remove some of the $\chi^{(i)}$ terms. Multiplying by $\chi^{(i)*}$ and integrating over dR then gives a differential equation for $\varphi^{(i)}$ which is similar in form to eq (34). That is, in addition to the H_p which appears in eq (12) we would have a potential energy function which is averaged over R. The $\varphi^{(i)}$ solution of this new equation is presumably an improvement over the solution of eq (12) since the former contains some back reaction effects; however, the improved $\varphi^{(i)}$ would no longer be an H_p eigenfunction. Since it is desirable that $\varphi^{(i)}$ be an H_p eigenfunction and thus diagonalize $\rho^{(p)}$, we will use the first approximation to $\varphi^{(i)}$ (i.e., the solution of eq (12)). If back reaction effects are important, it is not sufficient to use this first approximation. If a higher order approximation is used, the density matrix, $\rho^{(p)}$, will not be diagonal, as noted by Griem [14]. [In sec. 8 it will be shown that when these back reaction effects become important, the classical path approximation is breaking down anyway.] In this case, it would be more convenient to use the H_p eigenfunctions as a *basis set* in evaluating the trace over perturber coordinates (i.e., the thermal average as defined by eq (11)). The perturber density matrix would then be diagonal, but it would be necessary to make a fully quantum mechanical calculation of the time development operator (similar to that discussed by Baranger [4, 5]). Such a procedure would not be a classical path calculation and we will not consider this case any further.

In keeping with the usual classical path treatment, we next assume that each wave function $\varphi^{(i)}(\mathbf{x}, t)$ may be expressed as a product of wave packet states $\varphi_j^{(i)}(\mathbf{x}_j, t)$ for each of the perturbers:

$$\varphi^{(i)}(\mathbf{x}, t) = \prod_j \varphi_j^{(i)}(\mathbf{x}_j, t). \tag{35}$$

The wave packets, $\varphi_j^{(i)}$, are assumed to be sharply localized during the times of interest in line broadening. Although one does not usually think of energy eigenstates as being wave packets, it is nonetheless possible for a wave packet state to be an *approximate* eigenfunction of both H_p and V (as required by eq (32)) having eigenvalues $E_p^{(i)}$ and $V^{(i)}(t)$ which are classical functions of perturber coordinates. The validity of this approximation is discussed in section (8).

We now note that the influence of the perturbers which is implicit in $V^{(i)}(t)$ may be specified by giving the locations, $\mathbf{x}_j^{(i)}$, of the peaks of the packets $\varphi_j^{(i)}$, as well as their group velocities, $\mathbf{v}_j^{(i)}$. We thus complete the classical path picture by regarding the wave packets $\varphi_j^{(i)}$ as classical particles described by their positions

$\mathbf{x}^{(i)} = (\mathbf{x}_1^{(i)}, \mathbf{x}_2^{(i)}, \ldots, \mathbf{x}_N^{(i)})$ and velocities

$$\mathbf{v}^{(i)} = (\mathbf{v}_1^{(i)}, \mathbf{v}_2^{(i)}, \ldots, \mathbf{v}_N^{(i)}).$$

Since the wave packets $\varphi_j^{(i)}$ are assumed to be sharply localized, we may replace $V^{(i)}(t)$ by a classical potential function. That is,

$$\int \varphi^{(i)*}(\mathbf{x}, t) V \varphi^{(i)}(\mathbf{x}, t)\, \mathbf{dx} = V^{(i)}(\mathbf{R}, \mathbf{x}^{(i)}, \mathbf{v}^{(i)}, t) \tag{36}$$

where $V^{(i)}(\mathbf{R}, \mathbf{x}^{(i)}, \mathbf{v}^{(i)}, t)$ is a classical potential function of the $3N$-vectors $\mathbf{x}^{(i)}$ and $\mathbf{v}^{(i)}$, the operator $\mathbf{R}$, and the time t.

6. The Thermal Average

To obtain an expression for the "thermal average" in eq (11), we must first obtain an expression for the time development operator, $T(t)$, for the total system. Since we are approximating the wave function $\Psi(\mathbf{R}, \mathbf{x}, t)$ by $\Psi^{(i)}(\mathbf{R}, \mathbf{x}, t)$, we will need the corresponding time development operator $T^{(i)}(t)$ which is defined by

$$\Psi^{(i)}(\mathbf{R}, \mathbf{x}, t) = T^{(i)}(t)\Psi^{(i)}(\mathbf{R}, \mathbf{x}, 0). \tag{37}$$

From eqs (33) and (34), we see that this operator may be written in the form

$$T^{(i)}(t) = \exp\{-itH_p/\hbar\}\; T_a^{(i)}(t) \tag{38}$$

where $T_a^{(i)}(t)$ is the solution of

$$i\hbar \frac{\partial}{\partial t} T_a^{(i)}(t) = [H_a + V^{(i)}(\mathbf{R}, \mathbf{x}^{(i)}, \mathbf{v}^{(i)}, t)]\, T_a^{(i)}(t) \tag{39}$$

with the boundary conditions $T_a^{(i)}(0) = 1$.

Since $\mathbf{d}$ (see eq (11)) is the dipole operator for the radiator, it will commute with the perturber Hamiltonian H_p and we may write

$$T^{(i)\dagger}(t)\mathbf{d}T^{(i)}(t) = T_a^{(i)\dagger}(t)\,\mathbf{d}T_a^{(i)}(t). \tag{40}$$

Substituting this identity into the "thermal average" in eq (11), we obtain

$$\langle \ldots \rangle = Tr_p\{T_a^{(i)\dagger}(t)\mathbf{d}T_a^{(i)}(t)\rho^{(p)}\}$$
$$= \sum_{kk'} \langle k|T_a^{(i)\dagger}\mathbf{d}T_a^{(i)}(t)|k'\rangle\, \langle k'|\rho^{(p)}|k\rangle, \tag{41}$$

where $|k>$ denotes an arbitrary basis vector for the perturber subsystem. Since $T_a^{(i)}(t)$ has no *explicit* dependence on perturber coordinates (i.e., it depends on perturbers *implicitly* through the coordinates $\mathbf{x}^{(i)}$, $\mathbf{v}^{(i)}$ of the wave packets $\varphi^{(i)}$), we have

$$<k|T_a^{(i)\dagger}(t)\mathbf{d}T_a^{(i)}(t)|k'>=\delta_{k,k'}T_a^{(i)\dagger}(t)\mathbf{d}T_a^{(i)}(t)\cdot \qquad (42)$$

Substituting this identity into eq (41), we see that we need only the diagonal matrix elements of $\rho^{(p)}$ in the states $|k>$. Using the matrix elements of $\rho^{(p)}$ as given by eq (20) and noting the normalization condition of eq (16), we obtain

$$<\ldots>=\sum_i q^{(i)}T_a^{(i)\dagger}(t)\mathbf{d}T_a^{(i)}(t). \qquad (43)$$

To complete our evaluation of the "thermal average," we must express this weighted average in a form which is amenable to practical calculations.

Since $q^{(i)}$ is a function of $E_p^{(i)}$, defined by eq (21), we may express $q^{(i)}$ as a function of $\mathbf{x}^{(i)}$ and $\mathbf{v}^{(i)}$ by using

$$<\varphi^{(i)};\, t|H_p|\varphi^{(i)};\, t>=E_p^{(i)}(\mathbf{x}^{(i)}, \mathbf{v}^{(i)})$$
$$=\sum_j \tfrac{1}{2}m\mathbf{v}_j^{(i)2}+V_p(\mathbf{x}^{(i)}),$$

where V_p denotes the interaction between perturbers. If the radiator is an ion in a plasma, we may add a Coulomb interaction, $V_0(\mathbf{x}^{(i)})$, to H_p [10]. This expression is consistent with the wave packet interpretation of $\varphi^{(i)}(\mathbf{x}, t)$.

In the classical limit, the sum over (i) is replaced by an integral over $\mathbf{x}^{(i)}$ and $\mathbf{v}^{(i)}$. We may thus write $q^{(i)}$ in the form

$$q^{(i)}(\mathbf{x}^{(i)}, \mathbf{v}^{(i)})=\exp\{-E_p^{(i)}(\mathbf{x}^{(i)}, \mathbf{v}^{(i)})/kT\}/Q, \qquad (45)$$

where Q is the classical partition function

$$Q=\int\int \exp\{-E_p^{(i)}(\mathbf{x}^{(i)}, \mathbf{v}^{(i)})/kT\}d\mathbf{x}^{(i)}d\mathbf{v}^{(i)}. \qquad (46)$$

We may now write the "thermal average" in the form

$$<\ldots>=Q^{-1}\int\int d\mathbf{x}^{(i)}d\mathbf{v}^{(i)}\exp\{-E_p^{(i)}(\mathbf{x}^{(i)}, \mathbf{v}^{(i)})/kT\}$$
$$T_a^{(i)\dagger}(\mathbf{x}^{(i)}, \mathbf{v}^{(i)}, t)\mathbf{d}T_a^{(i)}(\mathbf{x}^{(i)}, \mathbf{v}^{(i)}, t) \qquad (47)$$

where the time development operator $T_a^{(i)}(\mathbf{x}^{(i)}, \mathbf{v}^{(i)}, t)$ is obtained by solving eq (39) with the classical potential $V^{(i)}(\mathbf{R}, \mathbf{x}^{(i)}, \mathbf{v}^{(i)}, t)$. This expression will be reduced to the more familiar averages over collision variables (velocity, impact parameter, etc.) in II.

7. The Autocorrelation Function

7.1. The Influence of the Density Matrix and the Wave Functions

Before discussing the validity of the approximations concerning the density matrix and the wave functions (sec. 8), it is useful to first consider the roles they play in determining the line shape. Since the line shape has been given as a Fourier transform of the autocorrelation function, eq (7), it is convenient to study this function as well.

The autocorrelation function was defined in eq (8) by $C(t)=Tr\{\mathbf{d}\cdot\mathbf{d}(t)\rho\}$ where $\mathbf{d}(t)=T^\dagger(t)\mathbf{d}T(t)$ and ρ is an equilibrium density matrix for a radiator and its perturbers. Since both ρ and $T(t)$ are functions of H (see eq (1)), they will commute at all times (i.e., ρ is stationary) and we may write

$$Tr\{\mathbf{d}\cdot\mathbf{d}(t)\rho\}=Tr\{\mathbf{d}(t_0)\cdot\mathbf{d}(t+t_0)\rho\} \qquad (48)$$

for *any* time t_0. This relation is characteristic of a stationary random process and it indicates that when we speak of an initial time, we are referring to any arbitrarily chosen instant, not some time infinitely far in the past. In writing $C(t)=Tr\{\mathbf{d}\cdot\mathbf{d}(t)\rho\}$ we have arbitrarily chosen $t=0$ as our initial time. Autocorrelation functions [15] such as $C(t)$ fall to zero as t increases; this represents the loss of correlation between the dipole moment at the time $t=0$ and its value at some later time.

We may regard the trace, in the defining relation for $C(t)$, as a sum over all possible initial configurations of perturbers and initial states of the radiator; each term in this sum is weighted by the matrix element of ρ which gives the probability of finding the corresponding initial state. We may also interpret this trace as a sum over cells, with each initial state corresponding to a given radiator-perturber configuration as discussed in section 2. For each initial state there will be a dipole moment, $\mathbf{d}$, and at some time t later this moment will have changed to $\mathbf{d}(t)$. Once the initial state has been specified, the temporal change in $\mathbf{d}$ is determined solely by the time development operator $T(t)$, and is not influenced by the statistics (density matrix) in any way.

We may now think of the line shape as being obtained by taking the Fourier transform of the $\mathbf{d}\cdot\mathbf{d}(t)$ contribution from each initial state, and then summing these Fourier transforms, weighting each term by the appropriate density matrix element (the probability of occurrence of a given configuration in a cell). It is thus apparent that the density matrix can influence the line shape only by its weighting of each $\mathbf{d}\cdot\mathbf{d}(t)$ contribution; the wave functions influence $I(\omega)$ only by their effect on the calculation of each $\mathbf{d}\cdot\mathbf{d}(t)$ term. The influence of the density matrix is quite distinct from the influence of the wave functions, and similarly, approximations relevant to the statistics (density matrix) are completely independent of the approximations relevant to the dynamics (time development operator or wave functions).

7.2. Classical Correspondence

a. Classical Theories

In discussing any quantum mechanical theory it is frequently beneficial to have a classical correspondence available as an aid to understanding the physical

properties underlying the mathematical description. In a classical path description of line broadening, the perturbers are regarded as classical particles, and there is little difficulty in understanding the physical properties of this subsystem. The radiator is treated quantum mechanically however, and it is useful to develop its classical analog to clarify the influence of collisions on the spectral radiation.

In classical line broadening theories one considers a classical oscillating dipole which emits a continuous wave train (referred to as the light train). The light train is described by the classical dipole moment $d(t)$, and the line shape is given by a Fourier transform of the dipole autocorrelation function $C(t) = < dd(t) >$ just as in eq (7); in this case $< \ldots >$ denotes a classical average over collisions. In the Lorentz interruption theory (see p. 571 of ref. [16]), it is assumed that a collision terminates the unperturbed light train $d(t) = d \exp(-i\omega_0 t)$ where ω_0 is the unperturbed frequency. The autocorrelation function is therefore given by, $C(t) = d^2 \int P(t_0) U(t < t_0) \exp(-i\omega_0 t) dt_0$, where $P(t_0)$ is the probability that a collision will occur after a time t_0, and $U(t < t_0)$ is a step function which equals 1 before the collision occurs (i.e., when $t < t_0$) and equals zero after the collision. Although the line shape is not always given in this form (cf. eq (1.2) of ref. [16] noting that $P(t_0) = \nu_c \exp(-\nu_c t_0)$), the results are the same. In another classical theory Weisskopf, and later Lindholm, assumed that collisions can change the phase of the light train [16, 17]. The line shape is again given by the Fourier transform of the light train autocorrelation function (see also eq (1.13a) of ref. [16] or eq (11.13) of ref. [17]) hence a phase shift decreases the phase correlation thereby broadening the Fourier spectrum (line shape). In these phase shift theories, $d(t)$ has the form $\exp[-i\omega_0 t - i\eta(t)]$ where $\eta(t)$ represents the phase shifts produced by collisions. The autocorrelation function is $C(t) = d^2 \exp(-i\omega_0 t) \langle \exp[-i\eta(t)] \rangle$ where $< \ldots >$ denotes an average over phase shifts (thermal average). The Weisskopf theory assumed that small phase shifts (less than unity) have no effect on $C(t)$, whereas large phase shifts (greater than unity) destroy the phase correlation of the light train and cause $C(t)$ to fall to zero. This effect is only apparent after one performs an average over a probability distribution of phase shifts. To show this, we consider a collision which occurs in the time interval $(t, t+\Delta t)$ and produces a phase shift η_0. If the duration of this collision τ is very short, $\tau < \Delta t$, then we have $C(t+\Delta t) = C(t) \langle \exp(-i\eta_0) \rangle$ (the two factors are independent and are averaged separately as in the impact approximation; see sec. (11.3.2) of ref. [17]), where $\langle \exp(-i\eta_0) \rangle = \int \exp(-i\eta_0) P(\eta_0) d\eta_0$ and $P(\eta_0)$ denotes the probability of finding a phase shift of magnitude η_0. If $P(\eta_0)$ does not vary rapidly, then the rapid oscillation of $\exp(-i\eta_0)$ for $\eta_0 > 1$ will produce

$$\int_1^\infty \exp(-i\eta_0) P(\eta_0) d\eta_0 \ll 1$$

(the integral from $-\infty$ to -1 is also much less than 1) whereas the integral from -1 to $+1$ is on the order of unity. Thus, for $\eta_0 > 1$, we have $C(t+\Delta t) \simeq 0$ and for $\eta_0 < 1$, $C(t+\Delta t) \simeq C(t)$. While the average over η_0 is given more accurately by later phase shift theories (e.g., Lindholm's theory), the qualitative results for the line shape stated by Weisskopf for $\eta_0 > 1$ are basically unchanged. It is in this sense that we will regard a large phase shift as an effective termination of the light train.

b. Quantum Mechanical Theory

In the quantum mechanical problem the radiators in a gas emit a series of spectral lines which are broadened due to the perturbation V. We are usually interested in just one of these broadened lines corresponding to some given unperturbed frequency ω_0. The photons which contribute to this particular line are emitted in radiative transitions between some particular initial and final energy levels of the radiator (which may be perturbed). In this case, the light train is the wave function for a photon emitted in such a transition; the amplitude of the light train gives the probability of finding a photon emitted after some time t. Baranger has shown that the function $C(t)$ defined in eq (8) may be interpreted as the autocorrelation function for the light train amplitude (see p. 498 of ref. [4]). Thus the line shape is obtained from the Fourier transform of the light train autocorrelation function just as in the classical theories.

The effects of a collision may be roughly divided into two categories: adiabatic and nonadiabatic. We will discuss these separately although a single collision may have both effects. An adiabatic collision will simply shift the energy levels thereby producing a phase shift (which may be time dependent) in the time development operator $T(t)$. Such collisions will reduce the phase correlation between $\mathbf{d}(0)$ and $\mathbf{d}(t) = T^\dagger(t)\mathbf{d}T(t)$ just as the collisions in the classical phase shift theories. A nonadiabatic collision will induce a radiationless transition out of the initial state. This type of transition usually "terminates" the probability that the radiator will emit a photon with a frequency near ω_0. However, if there is another state whose energy is very close to that of the initial state, nonadiabatic collisions may simply produce transitions back and forth between these two states without completely destroying the probability of emission near ω_0. The latter situation is usually referred to as the problem of overlapping lines (although it is sometimes called a "phase-memory" effect) [18]. In a classical oscillator having more than one mode of oscillation, a nonadiabatic collision simply changes the oscillation from one mode to another. The Lorentz interruption theory implicitly assumes that the mode whose frequency is ω_0 is the only mode of interest and a (nonadiabatic) collision terminates this mode. However, if there were another mode with a frequency very close to ω_0, nonadiabatic collisions could switch the oscillator back and forth between these two modes without destroying the phase coherence of the light train (overlapping line case). For example, an oscillator in the mode ω_0 will have a phase $\omega_0 t$ at some time t (apart from an

arbitrary initial phase). If this oscillator is switched to the mode ω_1 at some time t and, after a time t_0, is switched back to ω_0, the resulting phase shift in the natural oscillation is $\eta \simeq [\omega_0(t+t_0)-(\omega_0 t+\omega_1 t_0)]=(\omega_0-\omega_1)t_0$. Estimating t_0 by the mean free time $(1/\nu_c)$ and noting that the collision frequency ν_c may be identified with the halfwidth $\Delta\omega_{1/2}$, (in a Lorentz picture), we have $\eta \simeq (\omega_0-\omega_1)/\Delta\omega_{1/2}$. If $(\omega_0-\omega_1) > \Delta\omega_{1/2}$ (isolated lines), we have $\eta > 1$ and we may say that the light train is terminated by nonadiabatic collisions (as the Lorentz theory assumes). If $(\omega_0-\omega_1) < \Delta\omega_{1/2}$ (overlapping lines), we may say that the light train has retained a "memory of its initial phase." Thus we see that nonadiabatic collisions are analogous to those considered by the Lorentz interruption theory only in the case of isolated lines. In the case of overlapping lines, nonadiabatic collisions are not treated by any classical theories although the classical analog is obvious. We also note that a collision which produces both adiabatic and nonadiabatic effects cannot be conveniently treated by classical theories either.

To make our discussion of the quantum mechanical $C(t)$ more quantitative we will consider the case of a quantitative three-state radiator having a ground state with energy E_0 and two excited states with energies E_1 and E_2. We will also assume that the ground state is not perturbed by the interaction $V(t)$ and we use $V_{00}=V_{01}=V_{02}=0$ (as well as $V_{ij}=V_{ji}$). A generalization to more complicated cases may be achieved by means of an obvious extension of the following arguments. The time development operator for the radiator (see eq (39)) will be written in an interaction representation defined by

$$T_a(t) = \exp(-itH_a/\hbar)T'(t), \tag{49}$$

where

$$T'(t) = \mathcal{O}\exp\left[-(i/\hbar)\int_0^\tau V'(t')dt'\right],$$

$$V'(t) = \exp(itH_a/\hbar)V(t)\exp(-itH_a/\hbar), \tag{50}$$

and $\mathcal{O}$ is the time ordering operator [19]. Notice that $V_{0j}=V_{j0}=0$ implies that $T'_{00}=1$ and $T'_{0j}=T'_{j0}=0$ for $j\neq 0$; this simplification is the reason for neglecting ground state interactions.

If we are interested only in the line whose unperturbed frequency is $\omega_{10}=(E_1-E_0)/\hbar$, we do not need all of the terms in the trace over states of the radiator (see eq (11)). We need only consider the terms

$$C(t) = \sum_j d_{j0}d_{01}\langle T'_{1j}\rangle\rho_j^{(a)}\exp(-i\omega_{10}t) + \sum_j d_{j0}d_{02}\langle T'_{2j}\rangle\rho_j^{(a)}\exp(-i\omega_{20}t), \tag{51}$$

where $\rho_j^{(a)} \propto \exp(-E_j/kT)$. The natural oscillation $\exp(-i\omega_{10}t)$ in the first term may be regarded as an unperturbed light train which causes the Fourier transform of this term (eq (7)) to be large in the vicinity of ω_{10}. Thus, when calculating the line ω_{10} we need only consider those terms in eq (11) whose natural oscillation is close to ω_{10}. The second term in eq (51) describes radiation near ω_{20}; this term will be important (when calculating the ω_{10} line) only if the lines ω_{10} and ω_{20} overlap (i.e., if their halfwidths are on the order of $(\omega_{10}-\omega_{20})$). It will be shown later in this section that the phase of the off-diagonal terms such as T'_{12} varies according to the line spacing ω_{12}; thus when the average time between collisions (which is on the order of $1/\Delta\omega_{1/2}$) is small compared with $1/\omega_{12}$, these off-diagonal terms will become important and phase memory effects (overlapping lines) will have to be considered. If ω_{10} and ω_{20} are isolated lines (i.e., their halfwidths are much smaller than ω_{12}), the second term in eq (51) (as well as the off-diagonal T' matrix elements) may be neglected. For some lines in the microwave region it may happen that the halfwidth of ω_{10} is on the order of ω_{10}; in this case it would be necessary to add the "negative resonance" terms, $\exp(-i\omega_{01}t)$, to eq (51).

If we factor the natural oscillation out of $C(t)$, we may write $C(t)=\exp(-i\omega_{10}t)\tilde{C}(t)$ where $\tilde{C}(t)$ is a decreasing function of t [15]. The line shape (see eq (7)) is proportional to $\int \exp(it\Delta\omega)\tilde{C}(t)dt$ where $\Delta\omega=(\omega-\omega_{10})$. Since $\exp(it\Delta\omega)$ oscillates rapidly for $t > 1/\Delta\omega$, the intensity at the point $\Delta\omega$ is determined primarily by the part of $\tilde{C}(t)$ for which

$$0 \leq t \leq 1/\Delta\omega. \tag{52}$$

For this reason, $1/\Delta\omega$ is frequently referred to as the time of interest in evaluating the intensity at the point $\Delta\omega$.

If the duration of a collision is much longer than the time of interest, the perturber may be regarded as stationary during this time. This quasi-static approximation is frequently employed in the description of ions in a plasma [4, 6]. Such static perturbations simply add a constant to the oscillation frequencies ω_{10}, ω_{20}, etc. The influence of dynamic perturbations, for which the collision time is less than or the order of the time of interest, is obtained by calculating $\langle T'_{1j}\rangle$ and $\langle T'_{2j}\rangle$.

We are interested in the classical correspondence for the quantum mechanical $C(t)$ primarily as an aid in establishing a criterion for the so-called strong collisions (this will be done in sec. 7.3). When a single collision is capable of reducing $C(t)$ to zero, it is referred to as a strong collision. To study this effect we need only consider the influence of a single collision on $C(t)$. We will consider some particular type of collision (e.g., given values of impact parameter, velocity, etc.) which is described by the interaction potential $V(t)$. We will assume that this is the first collision to occur after some arbitrarily chosen starting time $t=0$ (if a collision does not reduce $C(t)$ to zero, it is "weak," and to find a strong collision criterion we may neglect the effects of all previous "weak" collisions). The collision will begin at some time $t_0 \geq 0$, and we define a collision time τ such that $V(t)=0$ unless $t_0 \leq t \leq t_0+\tau$. From eq (50) we see

that $T'(t)=1$ when $t<t_0$; when $t>(t_0+\tau)$, we change the variable of integration to $t''=(t'-t_0)$ and obtain

$$T'(t)=\exp(it_0H_a/\hbar)S\exp(-it_0H_a/\hbar), \quad (53)$$

where S is the S-matrix for the collision,

$$S=1-(i/\hbar)\int_0^t \tilde{V}(t)dt - (1/\hbar)^2\int_0^\tau\int_0^t \tilde{V}(t)\tilde{V}(t')dt'dt+\cdots, \quad (54)$$

and

$$\tilde{V}(t)=\exp(itH_a/\hbar)V(t+t_0)\exp(-itH_a/\hbar). \quad (55)$$

The contribution to $C(t)$ from this collision will be called $C(V(t),\ t)$; this function will have the same form as $C(t)$ in eq (51) except that there will be no average $<\ldots>$ over collisions. To obtain $C(t)$ we would simply average $C(V(t),\ t)$ over the collision parameters for the first collision (and all successive collisions if the first collision is not strong).

c. Isolated Lines

If the lines ω_{10} and ω_{20} are isolated, $C(V(t),\ t)$ is given by $\Sigma_j d_{j0}d_{01}T'_{1j}\rho_j^{(a)}\exp(-i\omega_{10}t)$. In this series $T'_{10}=0$ (no ground state interaction) and T'_{12} is unimportant (for isolated lines only). As mentioned earlier, to show that T'_{12} is unimportant it is necessary to average over t_0. This has been done for the line wings in eq (19) of ref. [20] and the second term in this equation, which contains the off-diagonal elements of the time development operator, is negligible in the case of isolated lines (see also the following section on overlapping lines). Using this fact we have

$$C(V(t),\ t)\propto d_{10}^2\rho_1T'_{11}(t)\exp(-i\omega_{10}t). \quad (56)$$

Since the complex function $T'_{11}(t)$ can always be written in the classical form $\exp[-i\eta(t)-\epsilon(t)]$, the classical correspondence for $C(V(t),\ t)$ becomes obvious. Collisions for which $\epsilon=0$ are equivalent to the collisions in the classical phase shift theories and those for which $\epsilon\gtrsim 1$ are equivalent to the nonadiabatic collisions in the Lorentz theory. To illustrate the functional form of η and ϵ, we will evaluate $T'_{11}(t)$, for $t>(t_0+\tau)$, to lowest order in $V(t)$. We will use $V_{11}=V_{22}=0$ since V has no diagonal matrix elements in most problems (i.e., V usually has nonvanishing matrix elements only between states with different angular momenta). Using eqs (53), (54), and (55) we obtain

$$T'_{11}(t)=1-\hbar^{-2}\int_0^\tau\int_0^t V_{12}(t+t_0)V_{21}(t'+t_0)\exp\{i\Delta E_{21}(t'-t)/\hbar\}dt'dt$$

$$\simeq 1-i(\bar{V}_{12}^2/\hbar\Delta E_{21})\int_0^\tau[\exp\{it\Delta E_{21}/\hbar\}-1]dt, \quad (57)$$

where $\Delta E_{21}=(E_2-E_1)$ and $\bar{V}_{21}$ denotes the average value of $V_{21}(t)$ during the collision. For fast collisions $(\Delta E_{21}\tau/\hbar)\ll 1$, we have

$$T'_{11}(t)\simeq 1-\tfrac{1}{2}(\bar{V}_{21}\tau/\hbar)^2. \quad (58)$$

For slower collisions $(\Delta E_{21}\tau/\hbar)\gg 1$, we replace τ by ∞ when integrating the exponential in eq (57). We then replace ΔE_{21} by $(\Delta E_{21}+i\delta)$, perform the integral, and then take the limit $\delta\to 0$. The justification for this procedure is the "radiation damping" which produces the natural line width (see sec. 13.A of ref. [3]). In this manner we obtain

$$T'_{11}(t)\simeq 1+i(\bar{V}_{21}^2\tau/\hbar\Delta E_{21}). \quad (59)$$

These results may be summarized by

$$C(V(t),\ t)\propto d_{10}^2\rho_1\exp(-i\omega_{10}t+i\eta-\epsilon), \quad (60)$$

where

$$\eta=\begin{cases}0 & (\Delta E_{21}\tau/\hbar)\ll 1\\ (\bar{V}_{21}^2\tau/\hbar\Delta E_{21}) & (\Delta E_{21}\tau/\hbar)\gg 1\end{cases} \quad (61)$$

and

$$\epsilon=\begin{cases}\tfrac{1}{2}(\bar{V}_{21}\tau/\hbar)^2 & (\Delta E_{21}\tau/\hbar)\ll 1\\ 0 & (\Delta E_{21}\tau/\hbar)\gg 1.\end{cases} \quad (62)$$

Notice that if the perturbation is not strong enough to mix adjacent levels, $\bar{V}_{21}\ll\Delta E_{21}$, then $\epsilon\ll 1$ and we have only a phase shift. That is, all collisions are adiabatic if $\bar{V}_{21}\ll\Delta E_{21}$. If adjacent levels are mixed, we will have phase shifts produced by slow (adiabatic) collisions and inelastic transitions produced by fast (nonadiabatic) collisions.

For a series of collisions which do not overlap in time (or for which this overlap is negligible) the classical form is preserved and the net result is a phase shift η and a damping ϵ which are obtained by adding up the phase shifts and damping constants from each of the collisions. When two collisions overlap, quantum mechanical mixing effects occur and the classical form is destroyed.

d. Overlapping Lines

If the lines ω_{10} and ω_{20} are not isolated we must consider all terms in eq (51):

$$C(V(t),\ t)\propto[\rho_1d_{10}^2T'_{11}+\rho_2d_{20}d_{01}T'_{12}]\exp(-i\omega_{10}t) + [\rho_2d_{20}^2T'_{22}+\rho_1d_{10}d_{02}T'_{21}]\exp(-i\omega_{20}t). \quad (63)$$

The $\rho_1T'_{11}$ term gives the probability that a radiator initially in the state E_1 will remain in that state after a time t; the $\rho_2T'_{12}$ term gives the probability that a radia-

tor initially in the state E_2 will make a radiationless transition to E_1 during the time t; together these two terms describe the probability, at the time t, that a radiator will emit a photon with a frequency near ω_{10}. The remaining terms in eq (63) describe the probability of emission near ω_{20} (we must consider these terms when the lines ω_{10} and ω_{20} overlap).

When $t < t_0$, the radiator is unperturbed hence $T'_{11} = T'_{22} = 1$ and $T'_{12} = T'_{21} = 0$; in this case, $C(V(t), t) \propto [\rho_1 d_{10}^2 \exp(-i\omega_{10}t) + \rho_2 d_{20}^2 \exp(-i\omega_{20}t)]$. When the collision occurs, we get a probability for switching between the modes ω_{10} and ω_{20} as discussed earlier; that is, T'_{12} and T'_{21} increase in amplitude while T'_{11} and T'_{22} decrease. To show this effect, we will calculate the T' matrix elements for $t > (t_0 + \tau)$.

The condition for overlapping lines is $(\Delta E_{21}/\hbar) \lesssim \Delta\omega_{1/2}$; since we may identify $\Delta\omega_{1/2}$ with ν_c where $(1/\nu_c)$ is the mean free time between collisions and since τ is usually much less than $1/\nu_c$ (at least for strong collisions), we must have $(\Delta E_{21}\tau/\hbar) \ll 1$. Noting the results of eqs (57) and (58), we see that when $(\Delta E_{21}\tau/\hbar) \ll 1$, the S matrix elements may easily be evaluated to all orders with the following results:

$$S_{11} = S_{22} = \cos(\bar{V}_{21}\tau/\hbar)$$

$$S_{12} = S_{21} = -i \sin(\bar{V}_{21}\tau/\hbar). \tag{64}$$

Using eqs (55), (63), and (64) we may give an explicit expression for $C(V(t), t)$ in terms of $(\bar{V}_{21}\tau/\hbar)$. To simplify the following discussion we will use $C(V(t), t) = C_1(V(t), t) + C_2(V(t), t)$, where

$$C_1(V(t), t) \propto \rho_1 [d_{10}^2 \exp(-i\omega_{10}t) \cos(\bar{V}_{12}\tau/\hbar) - id_{20}^2 (d_{10}/d_{20}) \exp(-i\omega_{20}t + i\omega_{21}t_0) \sin(\bar{V}_{21}\tau/\hbar)], \tag{65}$$

and $C_2(V(t), t)$ contains the two ρ_2 terms in eq (63). (C_2 may be obtained by interchanging the indices 2 and 1 in C_1.) We will discuss only C_1 since the interpretation of C_2 is obviously identical.

$C_1(V(t), t)$ describes the behavior of a radiator which was initially in the state E_1. Before the collision

$$C_1(V(t), t) \propto \rho_1 d_{10}^2 \exp(-i\omega_{10}t) \tag{66}$$

and after the collision, $t > t_0 + \tau$, C_1 is given by eq (65). $\cos^2(\bar{V}_{21}\tau/\hbar)$ gives the probability that the radiator will be in the state E_1 after the collision, and $\sin^2(\bar{V}_{21}\tau/\hbar)$ gives the probability that the collision will induce a radiationless transition to the state E_2. If $(\bar{V}_{12}\tau/\hbar) = (\pi/2)$, the collision will *definitely* cause a transition to E_2 and we would have

$$C_1(V(t), t) \propto \rho_1 d_{20}^2 (d_{10}/d_{20}) \exp(-i\omega_{20}t + i\omega_{21}t_0) \tag{67}$$

after the collision. Equation (67) describes a light train for the line ω_{20} with a phase shift $\omega_{21}\, t_0$ just as in the classical oscillator discussed earlier (the factor d_{10}/d_{20} represents the arbitrary initial phase difference between the two modes as well as an amplitude difference if one should exist). This result is identical with the result for a two mode classical oscillator because, when $(\bar{V}_{12}\tau/\hbar)$ equals some odd multiple of $(\pi/2)$, there is definitely a change of mode; for other values of $(\bar{V}_{12}\tau/\hbar)$, the quantum mechanical expression, eq (65), shows only a probability for this mode switching effect. Notice that the mode switching or phase-memory effects are described by the off-diagonal T' matrix elements. These off-diagonal elements were not needed in the description of isolated lines because the average phase shift $\omega_{21}t_0$ is greater than unity (recall that the average value of t_0 is the mean free time $(1/\nu_c)$ which is estimated by $1/\Delta\omega_{1/2}$) and these elements vanish after the t_0 average.

In the case of overlapping lines, $C(V(t), t)$ does not have the simple classical form which was obtained for isolated lines. In this case we would average $C(V(t), t)$ over collision parameters by defining a quantity $\epsilon = (\bar{V}_{12}\tau/\hbar)$ and a function $P(\epsilon)$ which gives the probability that the collision will produce a $(\bar{V}_{12}\tau/\hbar)$ whose magnitude is ϵ. The average over $C(V(t), t)$ contains terms like

$$\int P(\epsilon) \cos \epsilon d\epsilon \text{ and } \int P(\epsilon) \sin \epsilon d\epsilon.$$

If $P(\epsilon)$ does not vary rapidly then we may say that collisions for which $\epsilon > 1$ effectively terminate the wave train (this argument is analogous to the treatment of large phase shifts in the classical theories).

7.3. Strong Collisions

In discussing the approximations relevant to the density matrix and the wave functions, our general procedure will be to show that each approximation breaks down only during a "strong collision." It is thus convenient at this point to clarify our meaning of strong collisions and to discuss briefly the dynamics of certain types of collisions.

In the previous section it was shown that each collision produces a phase shift and changes the amplitude of the light train. In this manner, a series of collisions will eventually destroy the correlation between $d(t)$ and $d(0)$ and reduce $C(t)$ to zero. It may happen that a *single collision* is capable of reducing $C(t)$ to zero; such an event is defined to be a *strong collision*. From the results of the previous section we see that a strong collision is one which produces a large phase shift, $\eta > 1$, or a large decrease in amplitude, $\epsilon > 1$. Such collisions terminate the light train and therefore satisfy the hypotheses of the Lorentz interruption theory when $\epsilon > 1$, or Weisskopfs phase shift theory when $\eta > 1$. The general program of classical path theories is to describe all but the strong collisions assuming that these will be treated by some other method such as a Lorentz-Weisskopf approximation [21].

From the results of the previous section, we see that a strong collision will occur when

$$(V\tau/\hbar) \gtrsim 1 \tag{68}$$

unless the level spacing is greater than V (cf eq. (61) using $\Delta E_{21} > \bar{V}_{21}$). If $\Delta E_{21} > \bar{V}_{21}$ we must replace the V in eq (68) by $V_{\text{eff}} = \bar{V}_{21}^2/\Delta E_{21}$; in this case, V_{eff} is the actual perturbation of the radiator since we have used $V_{11} = 0$. It is in this sense that we use eq (68) as a working definition of strong collisions. It should be noted that our definition of a strong collision as one which terminates the light train is basically equivalent to the strong collisions in the impact theory [21] which are said to occur when the terms in the S-matrix expansion (see eq (54)) are on the order of unity or larger.

Most classical potential functions are inversely proportional to some power of the perturber position $\mathbf{r}(t) \simeq \boldsymbol{\rho}_0 + \int_0^t \mathbf{v}(t')\,dt'$, where $\boldsymbol{\rho}_0$ is the radiator-perturber separation at the time of closest approach and $\mathbf{v}(t)$ is the instantaneous perturber velocity. The maximum value of the potential where $|\mathbf{r}(t)|$ is smallest, namely when $\mathbf{r}(0) = \boldsymbol{\rho}_0$. The half maximum occurs when $|\mathbf{r}(\tau)| = |\boldsymbol{\rho}_0 + \int_o^\tau \mathbf{v}(t')\,dt'| \simeq 2\rho_0$ (which may be taken as a definition of the collision time τ). If $\mathbf{v}(t)$ changes very little during a collision we may use $\mathbf{v}(\tau) \simeq \mathbf{v}(0) = \mathbf{v}_0$ or $|r(\tau)| \simeq |\boldsymbol{\rho}_0 + \tau\mathbf{v}_0| \simeq 2\rho_0$. Since $\boldsymbol{\rho}_0 \cdot \mathbf{v}_0 = 0$, the collision time is on the order of

$$\tau = \rho_0/v_0 \tag{69}$$

where v_0 is the velocity at the time of closest approach. It can be shown by a rather lengthy analysis of hyperbolic trajectories, that this estimate is valid even when the radiator is an ion which accelerates a charged perturber.

If the radiator is electrically neutral, we may estimate v_0 by the thermal velocity $v_{\text{av}} = \sqrt{3kT/m}$. If both radiator and perturber are charged particles, we may estimate v_0 by

$$v_0^2 = v_{\text{av}}^2 - 2Z_r Z_p e^2/m\rho_0 \tag{70}$$

where Z_r and Z_p denote the charge of the radiator and perturber respectively.

8. Validity Criteria

8.1. General

An expression for the "thermal average" has been derived, eq (47), using a classical path treatment. This expression, or one like it, is the starting point for most of the modern semiclassical line broadening theories and it may be regarded as the end result of the classical path approximation. It is therefore worthwhile to examine the validity criteria for this expression.

It has been shown that the classical path approximation, as it is used in line broadening theories, actually embodies several types of approximations. As we have stated them, they may be roughly divided into three classes; (1) the representation of the gas by a collection of noninteracting cells, (2) simplifications of the density matrix, and (3) a classical treatment of the perturber wave functions.

In order to justify the mathematical model which is used by most line broadening theories, we have assumed that the average spacing between radiators is large enough that all direct and indirect interactions between radiators are negligible. (By indirect interactions we mean that one radiator may influence a perturber which is interacting with another radiator.) It is probably possible to justify the mathematical model with more relaxed assumptions, however, since our assumptions are satisfied for virtually all problems of interest, this may not be necessary. For resonance broadening in neutral gases, this approximation may have to be reconsidered.

It should be noted that the radiator Hamiltonian H_a should describe translational motion of the radiators as well as their internal structure (i.e., bound states). In practice, however, one usually neglects this translational motion and calculates only the discrete spectrum. This procedure neglects Doppler shifts which also broaden a given line. The Doppler broadening may be reinstated, in an approximate manner, by means of convolution integrals [6]. This folding procedure should be valid if the radiators trajectory, during the time of interest, is not appreciably altered by collisions with other particles. For most plasma line broadening problems this criterion is well satisfied however, for some foreign gas broadening problems one may have to treat Doppler effects more carefully.

8.2. Density Matrix

The approximations relevant to the density matrix are for the purpose of achieving a product form, eq (8), which permits us to factor the trace operations, as in eq (11), and thereby perform the average over perturber states without affecting the sum over states of the radiator. In this weak coupling approximation, the subsystems are statistically independent and this is what is meant by the neglect of back reaction as it applies to the statistics (density matrix). This approximation has been made by replacing the term exp $\{-V/kT\}$ in the Boltzmann factor by unity; that is, we have assumed that all V matrix elements (or at least those which pertain to the spectral line of interest) will satisfy $V \ll kT$. It should be noted that in obtaining this inequality we have tacitly assumed that the radiators and perturbers are in thermal equilibrium at a temperature T. For many line broadening experiments, however, the radiators and perturbers have different temperatures. Nonetheless, if the perturbers are in thermal equilibrium at a temperature T_p, the weak coupling approximation will still be valid for $V \ll kT_p$ and the perturber statistics will be described by a Boltzmann factor as in eq (47). In such a case, the statistical weights for the atomic states (matrix elements of $\rho^{(a)}$) would be determined from the rate equations which describe the population and depopulation of atomic levels. We will henceforth take

$V \ll kT$, where T is the perturber temperature, as the validity criterion for the weak coupling approximation. It is obvious that this inequality will be violated for some interactions, however, it will be shown that the errors made by this approximation are important only in the far wings of a line where $\hbar\Delta\omega \gtrsim kT$.

If the perturbation $V \gtrsim kT$ is produced by a static ion (one which does not move appreciably during the time of interest, see eq (52)) in a plasma, the Stark splitting is on the order of kT, and it is immediately obvious that this will influence only the far wings, $\Delta\omega > kT/\hbar$, of a line.

When the perturbation $V > kT$ is produced during a collision with a dynamic perturber (we will consider electrons as representatives of dynamic perturbers), the radiator-perturber separation must be on the order of $\lambda\!\!\!^{-}_{\rm av} = \hbar/\sqrt{3mkT}$ (the thermal wavelength, or average de Broglie wavelength, for the perturber) or smaller [22]. Using $V = kT$, $\rho_0 = \lambda\!\!\!^{-}_{\rm av}$ and $v_0 = v_{\rm av}$ in eq (68), we see that, for neutral radiators, $V \gtrsim kT$ can occur only during a strong collision (for most neutral radiators the energy spacing between adjacent states is less than kT and it is not necessary to consider $V_{\rm eff}$ as discussed in sec. 7.3). If a charged perturber collides with an oppositely charged radiating ion, it will be accelerated by the Coulomb attraction V_0, hence $v_0 > v_{\rm av}$. Using $V = kT$, $\rho_0 = \lambda\!\!\!^{-}_{\rm av}$, and $v_0 = v_{\rm av}(v_0/v_{\rm av})$ in eq (68), we find that $(V\tau/\hbar)$ is on the order of $(v_{\rm av}/v_0)$, which is less than 1. Thus, in this case, $V \gtrsim kT$ need not correspond to a strong collision. In a collision involving a radiating ion and a charged perturber of like sign, the perturber will be decelerated, and it is unlikely that it will come close enough to the radiator to produce $V \gtrsim kT$. To show this, we note that the smallest value of ρ_0 given by eq (70) is $(2e^2/m\rho_0) = v_{\rm av}^2$ or $\rho_0 = \lambda\!\!\!^{-}_{\rm av}(2e^2/\hbar)\sqrt{m/3kT}$; in order that ρ_0 be on the order of $\lambda\!\!\!^{-}_{\rm av}$, it is necessary that T be larger than 10^8 deg K.

Regarding $C(t)$ as a weighted sum of $\mathbf{d}\cdot\mathbf{d}(t)$ terms as discussed in section 7.1, it is clear that the approximate density matrix $\rho^{(a)}\rho^{(p)}$ will incorrectly weight only those $\mathbf{d}\cdot\mathbf{d}(t)$ terms which correspond to a radiator *initially* undergoing a $V \gtrsim kT$ collision (i.e., the density matrix weights each term according to the state at $t = 0$). This does not preclude the possibility that $V \gtrsim kT$ collisions may occur at later times, $t > 0$, in the remaining, correctly weighted, $\mathbf{d}\cdot\mathbf{d}(t)$ terms. Such events will indeed occur, however, they are determined by the dynamics of the system and this has no connection with the statistical weighting (density matrix) of the corresponding initial states. If we define a collision frequency ν_{kT} for the $V \gtrsim kT$ collisions then the probability that such a collision will occur within a time τ of $t = 0$ is $\nu_{kT}\tau$. The number of incorrectly weighted $\mathbf{d}\cdot\mathbf{d}(t)$ terms will therefore be $\nu_{kT}\tau N_T$, where N_T is the total number of terms. The number of correctly weighted terms will be $(1-\nu_{kT}\tau)N_T$, and the error resulting from the use of the weak coupling density matrix will be on the order of $\nu_{kT}\tau/(1-\nu_{kT}\tau)$. Since the duration, τ, of a $V \gtrsim kT$ collision will be much smaller than the time between such collisions, we may replace $(1-\nu_{kT}\tau)$ by 1 and the error estimate becomes $\nu_{kT}\tau$. The error will be largest when all collisions produce $V \gtrsim kT$; in this case we may *estimate* the collision frequency by $\Delta\omega_{1/2}$, the halfwidth of the observed line. The largest value of $\tau = \rho_0/v_0$ for a $V \gtrsim kT$ collision occurs for $\rho_0 = \lambda\!\!\!^{-}_{\rm av}$ and $v_0 = v_{\rm av}$ (decelerated perturbers, $v_0 < v_{\rm av}$, are not likely to produce $V \gtrsim kT$). The largest value of τ is $\hbar/kT$ hence the largest error is on the order of $\hbar\Delta\omega_{1/2}/kT$. Since $\hbar\Delta\omega_{1/2}$ is much less than kT for virtually all lines of interest, this error is negligible. A more detailed analysis of the incorrectly weighted terms shows that this error estimate breaks down when $\Delta\omega \gg \Delta\omega_{1/2}$. In this case the time of interest is less than the average time between collisions (recall that $\Delta\omega_{1/2} \cong \nu_{kT}$ for the worst case), and some of the correctly weighted $\mathbf{d}\cdot\mathbf{d}(t)$ terms will not suffer a collision during the time of interest. These "unperturbed" terms will have little influence on the line shape in the region $\Delta\omega > \Delta\omega_{1/2}$ (their dominant influence is in the line center when $\Delta\omega < \Delta\omega_{1/2}$). We must therefore compare the number of incorrectly weighted terms with $(\nu_{kT}/\Delta\omega)(1-\nu_{kT}\tau)N_T$ (the number of correctly weighted terms which have undergone a collision during the time of interest, $1/\Delta\omega$). In this case the error estimate becomes $\hbar\Delta\omega/kT$ which is small if $\Delta\omega \ll kT/\hbar$. It must be emphasized that these error estimates are only an upper bound for the true error which, in most cases, is much less than $(\hbar\Delta\omega_{1/2}/kT)$ or $(\hbar\Delta\omega/kT)$.

For *neutral* radiators $V \gtrsim kT$ occurs only during a strong collision. Since a strong collision completely disrupts the light train, the weighted sum of all $\mathbf{d}\cdot\mathbf{d}(t)$ terms which correspond to a strong collision at $t = 0$ will have fallen to zero by the time these collisions are completed. That is, the halfwidth for the sum of all incorrectly weighted $\mathbf{d}\cdot\mathbf{d}(t)$ terms will be on the order of $\tau = \hbar/kT$ or smaller. The corresponding Fourier transform will thus be a constant for $\hbar\Delta\omega < kT$. Since the incorrectly weighted terms add only a constant to $I(\omega)$ for $\hbar\Delta\omega < kT$, the approximate density matrix will not affect the shape of $I(\omega)$ for neutral radiators. Since most $V \gtrsim kT$ collisions are strong collisions even when the radiator is an ion, the above argument may be loosely applied to ion lines as well. We may therefore give the condition for validity of the weak coupling density matrix as

$$\hbar\Delta\omega \ll kT. \tag{71}$$

This condition was also obtained by Baranger [5, 23] within the framework of a quantum mechanical impact theory. We note, in passing, that the region of validity for the impact approximation is given $\tau_0\Delta\omega \ll 1$ where τ_0 is some representative collision time (see sec. 5.1 of ref. [4]). Since $\tau_0 \gtrsim \hbar/kT$, we may state that when the impact approximation is valid the weak coupling density matrix may be used; the converse of this statement is not necessarily true.

8.3. Wave Functions

The dynamics of the system are needed only to calculate $\mathbf{d}(t)$ from $\mathbf{d}(0)$ for each given initial state; this requires a knowledge of $T(t)$ but not $\Psi(\mathbf{R}, \mathbf{x}, t)$.

That is, since we are working with a trace, eq (8), it is not necessary to know the wave functions $\Psi(\mathbf{R}, \mathbf{x}, t)$ for the system (although it is necessary to define a set of basis functions). Semiclassical approximations have been made in the wave functions simply to permit the use of a classical potential function, $V^{(i)}(\mathbf{R}, \mathbf{x}^{(i)}, \mathbf{v}^{(i)}, t)$, in the time development operator. These semiclassical approximations, which are the hallmark of the classical path approximation, permit a simple physical interpretation of the dynamics of the system. More powerful quantum mechanical treatments are available [3,4]; however, in many cases, the results of these theories differ only slightly from the classical path treatment and the physical insight afforded by the latter is frequently advantageous.

The wave packet assumption was used to obtain the relation

$$V(\mathbf{R}, \mathbf{x})\varphi^{(i)}(\mathbf{x}, t) = V^{(i)}(\mathbf{R}, \mathbf{x}^{(i)}, \mathbf{v}^{(i)}, t)\varphi^{(i)}(\mathbf{x}, t), \quad (72)$$

where $V^{(i)}$ is a classical function of the classical position and velocity coordinates $\mathbf{x}^{(i)}$ and $\mathbf{v}^{(i)}$. $V(\mathbf{R}, \mathbf{x})$ can be expressed as a sum of interactions $V(\mathbf{R}, \mathbf{x}_j)$ between the radiator and each perturber (recall that $\mathbf{x} = (\mathbf{x}_1, \mathbf{x}_2, \ldots \mathbf{x}_N)$), thus we need only require that

$$V(\mathbf{R}, \mathbf{x}_j)\varphi^{(i)}(\mathbf{x}_j, t) = V^{(i)}(\mathbf{R}, \mathbf{x}_j^{(i)}, \mathbf{v}_j^{(i)}, t)\varphi^{(i)}(\mathbf{x}_j, t) \quad (73)$$

when $V(\mathbf{R}, \mathbf{x}_j) \neq 0$ in order to obtain eq (72). Messiah [24] has shown that eq (73) is obtained if the perturber is represented by a classical wave packet [25, 26] and if the potential field seen by the perturber does not vary appreciably (as compared with the perturbers kinetic energy) over the width of the wave packet.

The conditions for validity of eq (73) are discussed in detail by Messiah and we shall only outline this discussion as it applies to our problem. We must show; (1) that it is possible to construct a wave packet which does not overlap with the wave functions for the other particles, (2) that this wave packet does not spread appreciably during a collision (i.e., when $V(\mathbf{R}, \mathbf{x}_j)$ is nonzero), and (3) that the potential seen by the perturber does not vary appreciably over the width of a wave packet. The potential seen by the perturbers may be obtained by iterating the Schrödinger equations for $\chi^{(i)}$ and $\varphi^{(i)}$ to the next higher order as discussed in section 5. This potential will be the matrix elements of $V(\mathbf{R}, \mathbf{x})$ between atomic states or, in some cases, it will be V_{eff} as discussed in section 7.3, (or some other type of optical potential) [27]. The momentum of a perturber moving in the potential $V(\mathbf{R}, \mathbf{x})$ is given by $p = \sqrt{2m(E-V)}$, where E denotes the perturber energy. From this expression we see that $\Delta p = m\Delta V/p$, where Δp and ΔV denote the variation in p and V over the width of a wave packet. The condition that $\Delta V \ll p^2/2m$ is thus equivalent to

$$\Delta p \ll p \quad (74)$$

which is the usual condition for validity of WKB calculations (see eq (7.13) of ref. [28] noting that $\lambda(dp/dx)$ may be replaced by Δp). We will assume for the moment that this inequality can be satisfied, and it will be shown that the other validity conditions are easily met.

We wish to represent those perturbers which are not interacting with the radiator by Gaussian wavepackets of width Δx_g and momentum spread $\Delta p_g \ll p_{\text{av}}$ at some instant of time. For this wave packet construction we must require that Δx_g be much less than the average particle spacing $n^{-1/3}$ (n is the perturber density) so that the wave packets do not overlap. Using $\Delta x_g \Delta p_g \simeq \hbar$ (for a Gaussian wavepacket), we see that the condition $\Delta p_g \ll p_{\text{av}}$ also requires $\Delta x_g \gg \hbar/p_{\text{av}} = \lambda\!\!\!^{-}_{\text{av}}$. We must therefore be able to satisfy.

$$\lambda\!\!\!^{-}_{\text{av}} \ll \Delta x_g \ll n^{-1/3}. \quad (75)$$

For virtually all problems of interest we have $\lambda\!\!\!^{-}_{\text{av}} \ll n^{-1/3}$, hence it will be possible to construct Gaussian wave packets for the overwhelming majority of perturbers at some instant of time.

Since static perturbers (e.g., ions in a plasma) are regarded as stationary during the time of interest, it is only necessary that they be represented by wave packets at some instant of time. As discussed above, this will be possible for the overwhelming majority of perturbers if $\lambda\!\!\!^{-}_{av} \ll n^{-1/3}$. The treatment of static perturbers will be discussed further in II and for the remainder of this section we will consider only dynamic perturbers.

During a collision a wave packet will generally increase both its width, Δx, and its momentum spread, Δp. If $\Delta p \ll p$ (or $\Delta V < p^2/2m$, which will be verified shortly), the increase in momentum spread will be negligible, and for a collision of duration $\tau = \rho_0/v_0$, the wave packet will increase its width to a maximum of $\Delta x_\tau = (\Delta x + \tau\Delta p/m)$. To prevent overlap with the radiators wave function during the collision Δx_τ should satisfy $(\Delta x_\tau + R_0) < \rho_0$, where R_0 denotes the effective "extent" of the perturber wave function. Using $\tau = \rho_0/v_0$ and $\Delta p \ll p$, we see that $(\tau\Delta p/m) \ll \rho_0$ hence we need only require $(\Delta x + R_0) < \rho_0$.

For a collision involving a neutral radiator the perturber momentum may be taken to be p_{av}, hence we may use $\Delta x \simeq \Delta x_g$ and $\Delta p \simeq \Delta p_g$ (which will then satisfy $\Delta p \ll p$). Since Δx may be within an order of magnitude of $\lambda\!\!\!^{-}_{\text{av}}$ (and still satisfy $\Delta x \gg \lambda\!\!\!^{-}_{\text{av}}$), we may obtain an order of magnitude estimate of the overlap condition, $(\Delta x + R_0) < \rho_0$, by considering $(\lambda\!\!\!^{-}_{\text{av}} + R_0) < \rho_0$. If $R_0 \lesssim \lambda\!\!\!^{-}_{\text{av}}$, the wave functions will overlap only when $\rho_0 \lesssim \lambda\!\!\!^{-}_{\text{av}}$, and for neutral radiators, this produces a strong collision (see sec. 8.2). If $R_0 \gg \lambda\!\!\!^{-}_{\text{av}}$, a more detailed analysis of the perturbation potential is required; as an example we will consider the Stark broadening interaction, $V \simeq e^2R_0/\rho_0^2$, for which $(V\tau/\hbar) \simeq (R_0/\rho_0)(e^2/\hbar v_{\text{av}})$. Since $(e^2/\hbar v_{\text{av}}) \gtrsim 1$ for temperatures of 10^6 K or less (for electron perturbers), we see that the overlap condition, $R_0 > \rho_0$, is violated only during a strong collision. Thus, for neutral radia-

tors, the wave functions will overlap only during a strong collision. In the case where a radiating ion accelerates a charged perturber the deBroglie wavelength of the perturber is decreased, $\lambda\!\!\!^{-}_0 = \hbar/mv_0 \lesssim \lambda\!\!\!^{-}_{av}$. If v_0 is not much larger than v_{av}, there is essentially no difference between this case and the neutral radiator discussed above. If $v_0 \gg v_{av}$ the situation is somewhat different. In this case the perturber will come very close to the radiator and it is necessary to construct the initial wave packet with a width Δx much smaller than $\lambda\!\!\!^{-}_{av}$. Since $\lambda\!\!\!^{-}_0 \ll \lambda\!\!\!^{-}_{av}$, we construct the wave packet so that $\Delta x > \lambda\!\!\!^{-}_0$ which, using $\Delta x \Delta p \gtrsim \hbar$, implies that $\Delta p < p_0$. Such a wave packet will not hold together very long, however, it will hold together for a time on the order of $\tau = \rho_0/v_0$ which is all that is required by eq (73). In this case we will have $\lambda\!\!\!^{-}_0 \ll R_0$ and the wave functions will overlap when $\rho_0 \lesssim R_0$. The perturbation potential will be

$$V \simeq Ze^2R_0/\rho_0^2 \text{ and } (V\tau/\hbar) = (Ze^2R_0/\hbar\rho_0 v_0);$$

we do not need to consider a V_{eff} as discussed in section 7.3 because when $\rho_0 \lesssim R_0$, V is comparable to the ionization energy for ions [29]. If $v_0 \gg v_{av}$ then, from eq (70), we have $v_0 \simeq (2Ze^2/m\rho_0)^{1/2}$ and

$$(V\tau/\hbar) \simeq [(Z/2)(R_0^2/\rho_0 a_0)]^{1/2}$$

where $a_0 = \hbar^2/me^2$ is the Bohr radius (we have chosen m as the electron mass; for an ion perturber $(V\tau/\hbar)$ would be even larger). Since R_0 is larger than a_0, we see that the overlap of wave functions again produces a strong collision.

It is interesting to note that, for Stark broadening in plasmas we have $(V\tau/\hbar) \simeq (Ze^2R_0/\hbar\rho_0 v_0) \gtrsim (ZR_0/a_0 l)$, where $l = m\rho_0 v_0/\hbar$ is the angular momentum of the perturber. Since $R_0 > a_0$, we will have strong collisions when $l \lesssim 1$. Other interaction potentials may be treated in a similar manner with the same general results. In any case, the wave functions will not overlap if $\lambda\!\!\!^{-}_0 < \rho_0$; using $\lambda\!\!\!^{-}_0 = \hbar/mv_0$ and $l = m\rho_0 v_0/\hbar$, we find that the radiator and perturber will be distinct (i.e., their wave functions do not overlap) when

$$l > 1. \tag{76}$$

It is also interesting to note that the perturbers will look like classical particles as they pass the radiator only if $\Delta x \ll x$ and $\Delta p \ll p$; using $\Delta x \Delta p \simeq \hbar$, we again obtain the inequality $\hbar < m\rho_0 v_0$ or $l > 1$. We note further that $\Delta l = \pm 1$ in a dipole transition, thus $\Delta l < l$ and it is in this sense that the angular momentum of a perturber is conserved during a collision, as it must be if we are to use classical mechanics to describe the perturbers.

We have now shown that the validity criteria for the use of classical wavepackets are all easily satisfied if $\Delta p \ll p$, or equivalently, $\Delta V \ll p^2/2m$. That is, the essential validity criterion for the classical wavepackets is the same as the condition for validity of a WKB calculation. This was also noted by Baranger [4] who found that the results of a quantum mechanical impact theory reduce to the classical path results when a WKB treatment of the wave functions is employed.

To show that the condition $\Delta V < p^2/2m$ is satisfied we note that V increases monotonically as the radiator-perturber separation is decreased, thus $\Delta V \leqslant V$ and it is sufficient to show that $V < p^2/2m$. Again V may be replaced by V_{eff} if V is not strong enough to mix adjacent states. Using $p^2/2m = mv_0^2/2$, $\tau = \rho_0/v_0$, and $l = m\rho_0 v_0/\hbar$, we obtain

$$(V\tau/\hbar l) < 1. \tag{77}$$

Noting eqs (68) and (76), it is clear that this inequality can be violated only during a strong collision (recall that $l \lesssim 1$ produces a strong collision).

Equation (73) requires that a perturber be represented by a wave packet when it collides with the radiator. If we let $\varphi^{(j)}_{w.p.}(\mathbf{x}_j)$ denote a Gaussian wave packet for the jth particle then the wave function $\varphi^{(j)}(\mathbf{x}_j, t) = T_j(t)\varphi^{(j)}(\mathbf{x}_j, 0)$, where T_j is the time development operator for this particle, will be a Gaussian packet at some time t_j if we construct $\varphi^{(j)}(\mathbf{x}_j, 0)$ such that

$$\varphi^{(j)}(\mathbf{x}_j, 0) = T_j(-t_j)\varphi^{(j)}_{w.p.}(\mathbf{x}_j) \text{ (note that } T_j(t_j)T_j(-t_j) = 1).$$

In this manner we can arrange the wave function $\varphi^{(j)}(\mathbf{x}, t) = \prod_j \varphi^{(j)}(\mathbf{x}_j, t)$ in such a way that all particles which collide with the radiator during the time of interest are represented by Gaussian wavepackets at the time of their collision. In general these particles will not be represented by wavepackets before or after their collisions, but this does not matter as far as eq (73) is concerned.

We have now shown that it is possible to represent the perturbers by classical wavepackets as required by eq (73) unless a strong collision occurs (in which case we do not use wavepackets). It is interesting to note that it may be possible to treat some strong collisions by classical path methods. That is, eq (77) could be satisfied when $(V\tau/\hbar) \gtrsim 1$ if l is sufficiently large. If one wished to do this, it would be necessary to reexamine the validity criteria in more detail. For the purposes of this paper, however, it is sufficient to state that the use of classical wavepackets is justified for all collisions which are not strong collisions.

8.4. An Approximate Classical Potential

Although we have justified the use of a classical potential as given by eq (73), we have not yet specified its functional form. If back reaction effects in $\varphi^{(j)}$ are negligible, the potential $V^{(j)}$ will result from a perturber passing by the radiator on a straight line trajectory (or a hyperbola if both radiator and perturber are charged particles). If back reaction effects are important, the trajectory will be a rather complicated function of velocity, acceleration, etc. A wavepacket formed by WKB calculations (the iterative procedure discussed in sec. 5) may be

able to account for the true classical trajectory, however, the perturber wave function $\varphi^{(i)}$ would no longer be an H_p eigenfunction. While this may not matter for some scattering problems, it makes a great deal of difference in line broadening.

In section 6 we used the fact that $\varphi^{(i)}$ is an H_p eigenfunction to obtain the classical energy expression $E_p^{(i)}(\mathbf{x}^{(i)}, \mathbf{v}^{(i)})$ in eq (44). If the perturber wave function were not an energy eigenfunction, the perturber density matrix would not be "diagonal in wave packet states" and the average over perturber states, eq (41), would be intractable in a wave packet representation. We must therefore show: (1) that $\varphi^{(i)}$ may be an H_p eigenfunction (i.e., back reaction effects in $\varphi^{(i)}$ are negligible), and (2) that the energy eigenvalues may be represented by $E_p^{(i)}(\mathbf{x}^{(i)}, \mathbf{v}^{(i)})$ as stated in eq (44).

Since energy eigenvalues are not time dependent, we need only show that $E_p^{(i)}$ represents the H_p eigenvalue at some instant of time. This problem is essentially the same as eq (73) except that *all* perturbers must be represented by classical wave packets at some instant. Since we have a large number of perturbers in our system (a cell), there will always be some wave functions which overlap; however, for virtually all problems of interest we have $\varkappa_{\text{av}} \ll n^{-1/3}$ and it is possible to construct wave packets for the overwhelming majority of perturbers at some instant of time (cf. eq (75)). It is in this sense that eq (44) is satisfied.

To show that back reaction effects in $\varphi^{(i)}$ are negligible, we consider the perturbation $V^{(i)}(\mathbf{x}^{(i)}, \mathbf{v}^{(i)}, t)$ which results when a perturber moves past a neutral radiator on a straight line trajectory (the trajectory will be a hyperbola if both perturber and radiator are charged particles). The true perturber trajectory will deviate from a straight line (or hyperbola) because of accelerations (back reaction) resulting from the potential V seen by the perturbers (this potential may be V_{eff} as discussed in sec. 7.3). The approximate trajectory will be valid if this deviation does not appreciably alter the potential $V^{(i)}$ seen by the *radiator* during the collision (i.e., during the time $\tau \simeq \rho_0/v_0$, or the time of interest $1/\Delta\omega$, if this should be shorter). $V^{(i)}$ is influenced by the perturber trajectory through its dependence on $\mathbf{r}(t)$, the position of the perturber at the time t. If the deviation, $\Delta\mathbf{r}(t)$, produced by the perturbation is small enough that $\mathbf{r}(t) + \Delta\mathbf{r}(t) \simeq \mathbf{r}(t)$, the approximate trajectory will provide a good estimate of the true perturbation potential (whether the radiator is an ion or a neutral).

For a time on the order of τ, the magnitude of the deviation may be estimated by $\Delta r = |\mathbf{F}|\tau^2/2m = |\nabla V|\tau^2/m$ where $\mathbf{F} = -\nabla V$ is the back reaction force which causes the perturber to deviate from the approximate trajectory. Since V is inversely proportional to some power of $r(t)$ we have $|\nabla V| \simeq V/r(t)$. Using $r(t) \geqslant \rho_0$ we have

$$\frac{\Delta r}{r} \leqslant \frac{V\tau^2}{2m\rho_0^2} < \frac{V\tau}{\hbar l} \ll \frac{V\tau}{\hbar} \tag{78}$$

where $\tau = \rho_0/V_0$, $l = m\rho_0 v_0/\hbar$, and $l > 1$. This result shows that $(\Delta r/r) \ll 1$ unless a strong collision occurs.

The above argument shows that the approximate trajectory is valid (unless a strong collision occurs) for *elastic* collisions. If an *inelastic* collision should occur, the radiator and perturber will exchange an amount of energy ΔE. This will produce a sudden change in the perturber velocity, $\Delta E = mv\Delta v$, which will give rise to a deviation $\Delta r \leqslant \tau\Delta v$ in the trajectory. Again using $\tau_0 = \rho_0/v_0$, $l = mv_0\rho_0/\hbar$, and $l > 1$, we obtain

$$\frac{\Delta r}{r} \leqslant \frac{\Delta v}{v_0} \simeq \frac{\Delta E}{\frac{1}{2}mv_0^2} \simeq \frac{\tau\Delta E}{\hbar l} < \frac{\tau\Delta E}{\hbar}. \tag{79}$$

In section 7.2 it was shown that the probability for inelastic transitions is essentially zero unless $(\tau\Delta E/\hbar) \lesssim 1$ (for a more detailed treatment see ref. [30]). Thus the approximate trajectory is valid for both elastic and inelastic collisions.

It is interesting to note, that the change in the perturbers kinetic energy during the collision is a small fraction of its total kinetic energy.

9. Summary and Comments

It has been found that if the approximations which are used in the classical path treatment of line broadening break down, then a strong collision, defined by eq (68), is occuring. It should be noted that the converse of this statement is not necessarily true; that is, it may be possible to extend the classical path treatment of some problems into the region where $(V\tau/\hbar) \simeq 1$. In this case the validity conditions must be considered in more detail.

In the application of classical path methods, strong collisions are usually treated by interruption approximations based on the Lorentz-Weisskopf theory; the influence of all other collisions is evaluated by means of the time development operator $T_a^{(i)}(t)$ as discussed in section 6.

In section 8.4 it was shown that back reaction effects on the perturber trajectory are negligible whenever a classical path calculation is justified. That is, the validity criteria for the use of classical wave packets break down at the same time as (or in some cases before) the validity conditions for the use of unperturbed trajectories.

It was noted that our definition of strong collisions, eq (68), is essentially the same as the result obtained by setting the lead terms in an S-matrix expansion to unity. However, using this S-matrix expansion until the lead terms are on the order of unity may be a very poor approximation of the S-matrix; indeed, most errors attributed to strong collisions stem from this series approximation. To avoid possible confusion, we wish to emphasize that this approximation concerning the S-matrix is not part of the classical path approximation and any errors resulting from it have no bearing on the validity of classical path methods. It is therefore quite possible to improve upon these so-called strong collision problems within the framework of the classical path approach. The series approximation has been

improved for Lyman alpha lines [31], by summing terms in the series and, for hydrogen lines in general [32], by an approximate treatment of the exponential definition of the S-matrix.

The region of validity for the weak coupling density matrix has been given as $\Delta\omega < kT/\hbar$. We wish to emphasize once again that the approximations relevant to this density matrix are not influenced by the semiclassical treatment of the wave functions which is a part of the classical path approximation. The weak coupling density matrix may be (and has been [3, 4]) used in more rigorous quantum mechanical theories.

10. References and Notes

[1] Smith, E. W., Vidal, C. R., and Cooper, J., J. Res. Nat. Bur. Stand. (U.S.), **73A** (4), 405–420 (1969).

[2] Schiff, L. I., Quantum Mechanics, p. 261. (McGraw-Hill Book Co., Inc., New York, 1955).

[3] Smith, E. W., and Hooper, C. F., Jr., Phys. Rev. **157,** 126 (1967).

[4] Baranger, M., Atomic and Molecular Processes, chap. 13, edited by D. Bates (Academic Press Inc., New York, 1962).

[5] Baranger, M., Rand Corporation Report No. (RM-2118-AEC) ASTIA Document No. (AD 150692), Feb. 1958.

[6] Griem, H. R., Plasma Spectroscopy, chap. 4. (McGraw-Hill Book Co., Inc., New York, 1964).

[7] $T(t)$ governs the time development of the system from any arbitrary time τ to the time $t+\tau$; this operator may also be written $T(t+\tau, \tau)$.

[8] Fano, U., Phys. Rev. **131,** 259 (1963).

[9] Fano, U., Rev Mod. Phys. **29,** 74 (1957).

[10] If the radiator is an ion in a plasma, the Coulomb interaction V_0, between this ion and the charged perturbers may be added to H_p because it does not depend on the internal structure of the radiator.

[11] There are many different ways of treating ensembles; for a more detailed discussion of the approach which we use, the reader is referred to references [9] and [12]. In reference [12], the emphasis is placed on microcanonical ensembles, for which energy is one of the fixed macroscopic constraints; the results for a canonical ensemble, which we use, are stated in section (3 4) of that reference. Reference [9] gives a very good discussion of ensembles in general.

[12] Mori, H., Oppenheim, I., and Ross, J., Studies in Statistical Mechanics, pp. 240–255, edited by J. DeBoer and G. E. Uhlenbeck (North-Holland Publishing Co., Amsterdam, 1962).

[13] It is not actually necessary that the $\varphi^{(i)}$ be energy eigenfunctions. It is necessary only that each $\varphi^{(i)}$ be an eigenfunction of some complete set of commuting operators (i.e., the $\varphi^{(i)}$ are pure states). Since there may be more than one complete set of operators, there may also be more than one set of pure states. For our purposes, it is convenient to use some set of operators which contains the Hamiltonian, H_p. Results obtained with other sets will be identical with ours, but are probably more complicated.

[14] Griem, H. R., Phys. Rev **165,** 258 (1967), footnote 17.

[15] An extensive study of relaxation functions of the autocorrelation type has been made by Kubo, R., J. Math. Phys. **4,** 175 (1963), and Lectures in Theoretical Physics, edited by W. E. Downs and J. Down (Interscience Publisher, Inc., New York, 1959), Vol **1,** p. 120. Applications to spectral line broadening in gases are discussed by Kubo in Fluctuation, Relaxation and Resonance in Magnetic Systems, edited by D. ter Haar (Plenum Press, New York, 1961), p. 49, and in sec. 2.c of Ref. 3.

[16] Margenau, H., and Lewis, M., Rev. Mod. Phys. **31,** 269 (1959).

[17] Cooper, J., Rep. Progr. Phys. (London: Institute of Physics and Physical Society) **29,** 35 (1966), sec. (11.3).

[18] Burshtein, A. I., and Naberukhin, Yu. I., Soviet Physics JETP (English trans.) **25,** 799 (1967).

[19] Schweber, S., An Introduction to Relativistic Quantum Field Theory, pp 330–334 (Harper and Row Publishers Inc., New York, 1962).

[20] Cooper, J., Phys. Rev. Letters **17,** 991 (1966).

[21] Griem, H. R., Kolb, A. C., and Shen, K. Y., Phys. Rev. **116,** 4 (1959).

[22] For various types of interactions one obtains different estimates of the impact parameter which gives rise to $V \gtrsim kT$; however the thermal wavelength estimate is within an order of magnitude for most problems of interest.

[23] Baranger, M., Phys. Rev. **112,** 855 (1958).

[24] Messiah, A., Quantum Mechanics, Vol. **1,** p. 66 (John Wiley & Sons, Inc., New York, 1961).

[25] op. cit. ch. VI.

[26] Dirac, P. A. M., Principles of Quantum Mechanics, pp. 121–125 (Claredon Press, Oxford, 1958).

[27] Mott, N. F., and Massey, H. S. W., The Theory of Atomic Collisions p. 332 and p. 350 (Claredon Press, Oxford, 1965).

[28] Merzbacher, E., Quantum Mechanics (John Wiley & Sons, Inc., New York, 1961).

[29] For hydrogenic ions the level spacing is on the order of e^2Z^2/a_0n^3 and the ionization energy is $(e^2Z^2/2n^2a_0)$.

[30] Seaton, M. J., Proc. Phys. Soc. **79,** 1105 (1962).

[31] Griem, H. R., Phys. Rev. **140,** A1140 (1965).

[32] Shen, K. Y., and Cooper, J., Ap. J. **155,** 37 (1969).

(Paper 73A4–558)

JOURNAL OF RESEARCH of the National Bureau of Standards—A. Physics and Chemistry
Vol. 73A, No. 4, July-August 1969

Classical Path Methods in Line Broadening. II. Application to the Lyman Series of Hydrogen

Earl W. Smith,* C. R. Vidal,* and J Cooper**

Institute for Basic Standards, National Bureau of Standards, Boulder, Colorado 80302

(February 28, 1969)

The use of the classical path approximation in line broadening theory is illustrated in a development of the familiar impact and one-electron theories. The one-electron theory which is presented is an improved version of the usual one-electron theory; this improved version of the theory provides a consistent description of a line profile from the halfwidth to the quasi-static wings. The validity criteria for the impact and one-electron theories are discussed in detail and a comparison of the theories is made with a view toward the development of a more general theory containing elements of both. To avoid unnecessary mathematical complications and to provide a more transparent comparison of the theories, the Stark broadening of the Lyman series in hydrogen is used as a specific example.

Key words: Classical path; impact theory; line broadening theory; one electron theory.

1. Introduction

In a previous paper [1],[1] henceforth referred to as I, a general expression for the thermal average, eq (I–47), was derived using classical path methods. In this paper we will show how this expression may be used to derive the familiar results of the impact theories [2, 3, 4] and the one-electron theories [3, 5]. Possible improvements to these theories by means of a more general treatment of the thermal average, will also be discussed.

The perturber coordinates, $\mathbf{x}$ (eigenvectors of the perturber position operator) are integrated out of the expression for the thermal average when classical path methods are used (see eq (I–36)). The only perturber variables which need to be considered in the expression for the thermal average, eq (I–47) are the coordinates $\mathbf{x}^{(i)}$, $\mathbf{v}^{(i)}$ of the perturber wave packets (which are viewed as classical particles). The superscript (i) notation, which was used in I to distinguish between these variables, is no longer needed and, for convenience in notation, this superscript will not be used in this paper.

The thermal average will be evaluated by means of statistical techniques. In order to clearly illustrate these techniques and avoid unnecessary mathematical complications, we will consider the case of the Lyman lines emitted by hydrogen atoms in a plasma.

2. Preliminary Mathematics and Approximations

2.1. The Line Shape in the Static Ion Approximation

We will make the usual quasi-static approximation [2, 3] for the ions in the plasma. The electric field, $\mathscr{E}$, produced by these ions is regarded as being static during the time of interest, and this static field is used to define the Z axis for the atom. H_a is the Hamiltonian for an isolated hydrogen atom and, for convenience, the perturbation is taken to be a dipole interaction with the atomic dipole $-e\mathbf{R}$,

$$V(t)=eZ\mathscr{E}+V_e(\mathbf{R},\mathbf{x},\mathbf{v},t) \tag{1}$$

$$V_e(\mathbf{R},\mathbf{x},\mathbf{v},t)=e\mathbf{R}\cdot\mathscr{E}_e(\mathbf{x},\mathbf{v},t), \tag{2}$$

where Z denotes the Z component of $\mathbf{R}$, and $\mathscr{E}_e(t)$ is the fluctuating electric field produced by the electrons. The classical variables $\mathbf{x}$ and $\mathbf{v}$ are $3N$-vectors describing the N electron perturbers (these were denoted by $\mathbf{x}^{(i)}$ and $\mathbf{v}^{(i)}$ in I). The average over ion fields is performed by means of the usual microfield average [2, 3, 6]. In this case, the complete line profile is given by

$$\mathscr{I}(\omega)=\int \mathscr{P}(\mathscr{E})I(\omega,\mathscr{E})d\mathscr{E}, \tag{3}$$

where $\mathscr{P}(\mathscr{E})$ is the probability of finding an ion field of magnitude $\mathscr{E}$. The function $I(\omega,\mathscr{E})$ is the same as

*Radio Standards Physics Division, Plasma Physics, National Bureau of Standards Laboratories, Boulder, Colo. 80302

**Joint Institute for Laboratory Astrophysics and Department of Physics and Astrophysics, University of Colorado, Boulder, Colo. 80302.

[1] Figures in brackets indicate the literature references at the end of this paper.

the function $I(\omega)$ discussed in I, except that we now explicitly indicate a dependence on the ion field $\mathscr{E}$. That is, we may regard the radiator as being an atom which is subjected to a static field $\mathscr{E}$: the perturbers are electrons and the resulting line shape, for a given field $\mathscr{E}$, is $I(\omega,\mathscr{E})$; the total line profile is then obtained by averaging $I(\omega,\mathscr{E})$ over all possible ion fields as shown in eq (3).

2.2. The Time Development Operator in the No-Quenching Approximation

The time development operator $T_a(t)$ (see eq (I–39)) is the solution of the differential equation

$$i\hbar\frac{\partial}{\partial t}T_a(t)=[H_a+e\mathscr{E}Z+V_e(t)]T_a(t) \tag{4}$$

$$T_a(0)=1.$$

In an interaction representation defined by

$$T_a(t)=\exp(-itH_a/\hbar)T'_a(t), \tag{5}$$

we have

$$i\hbar\frac{\partial}{\partial t}T'_a(t)=[e\mathscr{E}Z'(t)+V'_e(t)]T'_a(t) \tag{6}$$

$$Z'(t)=\exp(itH_a/\hbar)Z\exp(-itH_a/\hbar) \tag{7}$$

$$V'_e(t)=\exp(itH_a/\hbar)V_e(t)\exp(-itH_a/\hbar). \tag{8}$$

The formal solution of eq (6) may be given by

$$T'_a(t)=\mathcal{O}\exp\left\{-(i/\hbar)\int_0^t[e\mathscr{E}Z'(t')+V'_e(t')]dt'\right\} \tag{9}$$

where $\mathcal{O}$ is the time ordering operator [7] which is required since $[e\mathscr{E}Z'(t)+V'_e(t)]$ does not commute with $[e\mathscr{E}Z'(t')+V'_e(t')]$ unless $t=t'$ (cf. eq (6) of ref. [8]). Equation (9) is a very complicated expression and approximations must be employed to simplify the form of this operator. In this section we will consider the no-quenching approximation [9] which is frequently used for hydrogen lines.

To make an explicit statement of the no-quenching approximation, we must first introduce a complete set of H_a eigenstates. The H_a eigenvalues, $E_{n'}$, depend only on the principal quantum number n', hence we denote the H_a eigenstates by $|n'k'>$ where k' is some set of quantum numbers which index the degenerate states of the level $E_{n'}$. We are interested in the radiation produced when the atom makes a radiative transition from a group of initial states (degenerate states of some particular level E_n) to a group of final states which have a lower energy. For the Lyman series in hydrogen, there is only one final state (i.e., the ground state neglecting spin) which we shall denote by $|1>$; the frequency of the line of interest may then be denoted by $\omega_{n1}=(E_n-E_1)/\hbar$.

A radiationless transition which depopulates the initial level E_n may be said to quench the radiation near ω_{n1}. The probability for such an inelastic transition from an initial state $|nk>$ to some other state $|n'k'>$ (where $n\neq n'$) is given by the square of $\langle nk|T_a|n'k'\rangle$. The no-quenching approximation states that these "off-diagonal" (i.e., $n\neq n'$) terms may be neglected (see eq (12) of ref. [9]). The justification for this approximation will be given in section 7; in this section we will simply use $<nk|T_a|n'k'>=0$ to simplify the form of $T_a(t)$.

Since the "off-diagonal" matrix elements of $T_a(t)$ are assumed to be negligible, it is clear from eq (5), that the "off-diagonal" elements of $T'_a(t)$ must also be negligible. Noting that the H_a eigenvalues depend only on n, the differential equation for $T'_a(t)$, eq (6), becomes

$$i\hbar\frac{\partial}{\partial t}\langle nk|T'_a(t)|nk'\rangle$$
$$=\Sigma_{k''}\langle nk|e\mathscr{E}Z+V_e(t)|nk''\rangle\langle nk''|T'_a(t)|nk'\rangle \tag{10}$$

with the aid of eqs (7) and (8). If we define a projection operator P which picks out the part of any operator which is diagonal in n

$$\langle nk|PZ|n'k'\rangle=\delta_{nn'}\langle nk|Z|nk'\rangle,$$

then eq (10) may be written

$$i\hbar\frac{\partial}{\partial t}T'_a(t)=[e\mathscr{E}PZ+PV_e(t)]T'_a(t). \tag{11}$$

The appearance of the projection operator P in the generator $[e\mathscr{E}PZ+PV_e(t)]$ indicates that $T'_a(t)$ will be diagonal in n as required. It is interesting to note that, while $V_e(t)$ commutes with Z (they are functions of atomic position coordinates), the operators PZ and $PV_e(t)$ will *not* commute in general. The formal solution of eq (11) will therefore be a time-ordered exponential similar to eq (9). We will define an operator $\mathscr{Z}(\mathscr{E})$ by

$$\mathscr{Z}(\mathscr{E})=e\mathscr{E}PZ/\hbar \tag{12}$$

and $T'_a(t)$ will be written in an interaction representation defined by

$$T'_a(t)=\exp(-it\mathscr{Z})U_a(t) \tag{13}$$

where

$$i\hbar\frac{\partial}{\partial t}U_a(t)=\tilde{V}(t)U_a(t) \tag{14}$$

and

$$\tilde{V}(t)=\exp(it\mathscr{Z})PV_e(t)\exp(-it\mathscr{Z}). \tag{15}$$

With these new definitions, $T_a(t)$ may be written

$$T_a(t)=\exp(-itH_a/\hbar)\exp(-it\mathscr{Z})U_a(t), \tag{16}$$

where $U_a(t)$ is the (time ordered) solution of eq (14):

$$U_a(t) = \mathcal{O} \exp\left\{-(i/\hbar)\int_0^t \tilde{V}(t')dt'\right\}. \quad (17)$$

2.3. The Line Shape for the Lyman Series

The line shape function defined by eqs (I–7) and (I–11) involves a trace over atomic states hence this function will describe all spectral radiation emitted by the atom. Since we wish to study only one line (or a group of overlapping lines) at a time, we may pick out the relevant terms in this trace as discussed in section 7.2 of I (see eq (I–51)). This selection may be accomplished by restricting the atomic dipole operator $\mathbf{d}$ to have matrix elements only between the initial and final states which contribute to the line, or lines, of interest (cf. eq (12) of ref. [9]).

For the Lyman lines in hydrogen there is only one final state (neglecting spin), which we have denoted by $|1\rangle$; the initial states for any given line are the H_a eigenstates $|n\kappa\rangle$ which correspond to the given initial energy level E_n. All matrix elements of $\mathbf{R}$ vanish in the ground state, $\langle 1|\mathbf{R}|1\rangle = 0$, hence we have $\langle 1|U_a|1\rangle = 1$ (this is why we have chosen the Lyman series as an example).

For convenience we will now specify the states $|n\kappa\rangle$ to be the parabolic states which diagonalize both [10, 11] H_a and PZ. The diagonal elements of Z will be denoted by $Z_{n\kappa}$ and the diagonal elements of H_a (the energy eigenvalues) have already been denoted by E_n. There is no loss in generality in choosing parabolic states because the line shape is defined in terms of a trace over atomic states and we are free to choose any complete set of basis states when evaluating a trace (i.e., a trace is invariant under a unitary transformation of the basis states). The atomic density matrix, $\rho^a(H_a)$, is also diagonal in $|n\kappa\rangle$ and its matrix elements are denoted by $\rho^{(a)}_{n'}$.

Using eqs (I–7), (I–11), (I–47) and defining a frequency variable $\Delta\omega = (\omega - \omega_{n1})$ for the particular line of interest, the line shape function $I(\omega, \mathscr{E})$ may be written in the form

$$I(\omega, \mathscr{E}) = (\rho^{(a)}_{n'}/\pi)\ \mathrm{Re}\,\Sigma_{\kappa\kappa'}\langle n\kappa'|\mathbf{d}|1\rangle \cdot \langle 1|\mathbf{d}|n\kappa\rangle$$

$$\int_0^\infty \exp\left[it(\Delta\omega - e\mathscr{E}Z_{n\kappa}/\hbar)\right]\langle n\kappa|F(t)|n\kappa'\rangle dt \quad (18)$$

where

$$F(t) = Q^{-1}\int\int \exp[-E_p(\mathbf{x}, \mathbf{v})/kT]U_a(\mathbf{R}, \mathbf{x}, \mathbf{v}, t)d\mathbf{x}d\mathbf{v}. \quad (19)$$

$$E_p(\mathbf{x}, \mathbf{v}) = \tfrac{1}{2}mv^2 + V_p(\mathbf{x}) \quad (20)$$

$$Q = \int\int \exp[-E_p(\mathbf{x}, \mathbf{v})/kT]\mathrm{d}\mathbf{x}\mathrm{d}\mathbf{v}; \quad (21)$$

E_p represents the energy of the N electrons which are described by $\mathbf{x} = (\mathbf{x}_1, \mathbf{x}_2, \ldots, \mathbf{x}_N)$ and $\mathbf{v} = (\mathbf{v}_1, \mathbf{v}_2, \ldots, \mathbf{v}_N)$, and $V_p(\mathbf{x})$ is the potential of interaction between electrons.

The thermal average is contained entirely in $F(t)$ and the remaining sections are devoted to the evaluation of this function. When $F(t)$ is known, the line shape is readily obtained from eqs (3) and (18).

3. Further Simplification of the Time Development Operator

3.1. General Purpose

Although the time development operator was considerably simplified by the no-quenching approximation, the resulting expression, eq (16), is still quite complicated and further simplifications are necessary in order to evaluate $F(t)$. To facilitate these simplifications we note that when we use the classical trajectories discussed in section 8.4 of I, the interaction potential $V_e(t)$ in eq (2) may be written in the form

$$V_e(\mathbf{R}, \mathbf{x}, \mathbf{v}, t) = e\mathbf{R}\cdot\Sigma_j\mathscr{E}_e(\mathbf{x}_j, \mathbf{v}_j, t) = \Sigma_j V_j(t) \quad (22)$$

$$\mathscr{E}_e(\mathbf{x}_j, \mathbf{v}_j, t) = e(\mathbf{x}_j + \mathbf{v}_j t)/|\mathbf{x}_j + \mathbf{v}_j t|^3, \quad (23)$$

where $\mathscr{E}_e(\mathbf{x}_j, \mathbf{v}_j, t)$ represents the electric field at the atom produced by the jth perturber; $V_j(t)$ is simply a shorthand notation for $e\mathbf{R}\cdot\mathscr{E}_e(\mathbf{x}_j, \mathbf{v}_j, t)$, the interaction between the atom and the jth perturber. The form of the potential, $\Sigma_j V_j(t)$, suggests that it may be possible to express $U_a(t)$ in terms of a product of time development operators $U_j(t)$ for the individual electron-atom collisions. In section 3.4 it will be shown that such a product form is obtained without approximation if the time of interest is very short. For most cases however, the interaction $\tilde{V}(t)$ contains terms like

$$\tilde{V}_j(t) = \exp(it\mathscr{L})PV_j(t)\exp(-it\mathscr{L})$$

which do not in general commute with one another, and this prevents us from obtaining the product form for $U_a(t)$. Nevertheless, if the $V_j(t)$ do not overlap in time (or if this overlap is negligible) the ordered exponential in eq (17) may be expressed as an ordered product:

$$\mathcal{O}\exp\left[-(i/\hbar)\int_0^t \tilde{V}(t')dt'\right]$$

$$= \mathcal{O}\Pi_j \exp\left[-(i/\hbar)\int_0^t \tilde{V}_j(t')dt'\right] \quad (24)$$

where $\tilde{V}_j(t)$ is defined by

$$\tilde{V}_j(t) = \exp(it\mathscr{L})PV_j(t)\exp(-it\mathscr{L}). \quad (25)$$

(Equation (24) may be verified by comparing terms in the series expansions.) This result will be the basis of the following approximations.

3.2. The Impact Approximation

The purpose of the impact approximation is to disentangle the overlapping collisions [12, 13] in $U_a(t)$ and permit the use of the product form stated in eq (24).

To do this, the impact approximation assumes that, for collisions which overlap in time, the average collision is weak enough that it may be described by a perturbation series in powers of $V_j(t)$. Collisions for which $(V\tau/\hbar) < 1$ may be treated this way (cf. sec. 7 of I). Strong collisions, $(V\tau/\hbar) > 1$, for which such an expansion is not practical, are assumed to be well separated in time so that two strong collisions never occur simultaneously. If a weak collision overlaps with a strong one, the weak collision is neglected and strong collisions are thus disentangled. The entanglement between overlapping weak collisions first appears in the second order terms in the series expansion of eq (24). In footnote 7 of ref. [13] it is stated the entanglement in the second order terms vanishes because the terms involving different electrons will average to zero (recall that $U_a(t)$ appears only under an average as stated in eq (19)). This result was obtained in ref. [13] by treating the electrons as statistically independent particles (using Debye shielded fields to approximate their correlations). Although we have not made such an assumption, we note from eq (22) that the second order terms involve an electric field autocorrelation function $\langle \mathscr{E}_e(t)\mathscr{E}_e(t')\rangle$; and the use of statistically independent quasi-particles is known to be a good approximation in evaluating such functions. We may thus regard the impact approximation as being valid to second order for weak collisions.

Using eqs (17) and (24), we see that, in the impact approximation, $U_a(t)$ may be written in the form (cf. p. 497 of ref. [12])

$$U_a(t) = \mathscr{O}_0 \Pi_j U_j(t) \tag{26}$$

$$U_j(t) = \mathscr{O} \exp\left[-(i/\hbar)\int_0^t \tilde{V}_j(t')dt'\right], \tag{27}$$

where $\mathscr{O}_0$ is a time ordering operator which keeps the collisions in chronological order; that is, the $U_j(t)$ which describes the first collision must be the first operator from the right in the product $\Pi_j U_j(t)$, and the second collision must be the second from the right, etc. To state the action of $\mathscr{O}_0$ more explicitly, we note that the variables $\mathbf{x}_j$ and $\mathbf{v}_j$ in $V_j(t)$ may be transformed into the collision variables ρ_0, v_0, t_0, etc., (see appendix) where t_0 is a reference time for the collision (t_0 is the time of closest approach if the collision is completed). The operator $\mathscr{O}_0$ simply requires that t_0 for the first collision always be less than t_0 for the second collision, etc. (this ordering is necessary because the $\tilde{V}_j(t)$ for different collisions do not in general commute). It is important to note that, when the impact approximation is valid, $U_j(t)$ refers to a *single* collision which may be either weak or strong.

3.3. The Line Wings

In the wings of a line, the time of interest $1/\Delta\omega$ (cf. eq (I–52)) is relatively short and it may be possible to neglect the exponentials, $\exp(it\mathscr{Z})$, in $\tilde{V}(t)$. To show this, we write eq (14) in the form

$$i\hbar \frac{\partial}{\partial t}\langle n\mathscr{k}|U_a(t)|n\mathscr{k}'\rangle = \sum_{\mathscr{k}''} \exp[ite\mathscr{E}(Z_{n\mathscr{k}} - Z_{n\mathscr{k}''})/\hbar]$$
$$\langle n\mathscr{k}|V_e(t)|n\mathscr{k}''\rangle\langle n\mathscr{k}''|U_a(t)|n\mathscr{k}'\rangle \tag{28}$$

(recall that $U_a(t)$ is diagonal in n). If the time of interest, $(1/\Delta\omega)$, is small enough that

$$\Delta\omega > e\mathscr{E}_{av}(Z_{n\mathscr{k}} - Z_{n\mathscr{k}''})\hbar \tag{29}$$

for all $\mathscr{k}$ which pertain to the initial level, then the exponential in eq (28) may be neglected for $\mathscr{E} \lesssim \mathscr{E}_{av}$, where $\mathscr{E}_{av}$ denotes the average ion field strength. For $\mathscr{E} > \mathscr{E}_{av}$, the electron broadening is negligible (as we will discuss in sec. 7), thus, if eq (29) is satisfied, we may neglect the exponentials involving Z. In this case, the solution of eq (28) is

$$U_a(t) = \mathscr{O} \exp\left\{-(i/\hbar)\int_0^t PV_e(t')dt'\right\} \tag{30}$$

and the time ordering is still necessary because $PV_e(t)$ will not in general commute with $PV_e(t')$.

Using the impact approximation, $U_a(t)$ is again given by the product form stated in eq (26) and $U_j(t)$ is given by

$$U_j(t) = \mathscr{O} \exp\left\{-(i/\hbar)\int_0^t PV_j(t')dt'\right\}. \tag{31}$$

Again the time ordering appears because $PV_j(t)$ does not commute with $PV_j(t')$.

For weak collisions the exponential is valid only to second order in $PV_j(t)$ (because of the impact approximation) and it can be shown that, to this order, the operator $\mathscr{O}$ is unnecessary. To show this we note from eq (22) that $PV_j(t)$ may be written in the form

$$PV_j(t) = e[PX\mathscr{E}_x(t) + PY\mathscr{E}_y(t) + PZ\mathscr{E}_z(t)]. \tag{32}$$

It is the orthogonal components of $P\mathbf{R}$ which do not commute: that is, $PX\mathscr{E}_x(t)$ commutes with $PX\mathscr{E}_x(t')$ but not with $PY\mathscr{E}_y(t')$ or $PZ\mathscr{E}_z(t')$. To second order the terms which do not commute will contain factors like $\langle \mathscr{E}_x(t)\mathscr{E}_y(t')\rangle$ (recall that $U_a(t)$ appears only under an average). For a spherically symmetric (about the atom) distribution of electrons these terms will average to zero. We may therefore drop the time ordering and write

$$U_j(t) = \exp\left\{-(i/\hbar)\int_0^t PV_j(t')dt'\right\} \tag{33}$$

which is valid to second order in $PV_j(t)$ for the line wings (as specified by eq (29)).

The above argument is not valid for strong collisions because the series expansion of U_j is not applicable. We will nonetheless assume that eq (33) provides a good description of the influence of strong collisions: this approximation will be discussed in section 7.

3.4. The Quasi-Static Region

In the far line wings where the time of interest, $1/\Delta\omega$, is much less than the duration time τ for a collision,

$$\tau\Delta\omega \gg 1, \tag{34}$$

an interaction which would normally be regarded as dynamic (e.g., an electron-atom interaction) will take on a quasi-static aspect because the perturber motion during the time of interest is negligible. The transition from dynamic behavior in the line center to quasi-static behavior in the far wings is not properly described by current line shape theories because these theories approximate $U_a(t)$ by the first few terms in its series expansion and, as will be shown in section 7, this approximation breaks down in the quasi-static wings. Nevertheless, it can be shown that $U_a(t)$ takes a relatively simple form in the quasi-static wings. In fact, the product form $\Pi_j U_j(t)$ may be obtained without approximation and no time ordering is necessary in the operators $U_j(t)$. To show this, we note that the time ordered exponential in eq (30) (which is valid in the wings) may be expressed as an exponential involving a series of commutators [14]:

$$U_a(t) = \exp\left\{-(i/\hbar)\int_0^t PV_e(t')dt' + \tfrac{1}{2}(i/\hbar)^2\int_0^t\int_0^{t'}[PV_e(t'), PV_e(t'')]dt'\,dt'' + \ldots\right\}. \tag{35}$$

If the commutator is negligible, $PV_e(t)$ may be regarded as an operator which commutes with itself at different times; similarly we may regard $PV_i(t)$ and $PV_j(t')$ as commuting operators for all i, j, t, and t'. In this case, $U_a(t)$ may be expressed in the product form $\Pi_j U_j(t)$ where $U_j(t)$ is given by eq (33).

To show when the commutator is negligible we expand $V_e(t)$ about $t=0$ (in the far wings t is a small parameter). To lowest order the integral over $PV_e(t')$ is given by $t\,PV_e(0)/\hbar$ and the integral over $[PV_e(t'), PV_e(t'')]$ becomes $t^3\,[PV_e(0), PV_e'(0)]/6\hbar^2$, where $V_e'(0)$ denotes $(\partial V_e(t)/\partial t)$ at $t=0$. Since the magnitude of $[PV_e(0), PV_e'(0)]$ is less than or equal to $PV_e(0)PV_e'(0)$, we need only compare the magnitude of $(t^2PV_e'(0)/6\hbar)$ with unity. To estimate this quantity we use eqs (22) and (23) and we obtain

$$(\partial V_e/\partial t) = (\partial x/\partial t)\,(\partial V_e/\partial x) \simeq v_0(\partial V_e/\partial x) \simeq (v_0 V_e/\rho_0),$$

where ρ_0 and v_0 denote the position and velocity at the time of closest approach (when PV_e' is largest). Using $\tau = (\rho_0/v_0)$ and $t = (1/\Delta\omega)$, we obtain

$$t^2PV_e'(0)/6\hbar \simeq (V_e/\hbar\Delta\omega)\,(1/\tau\Delta\omega).$$

For quasi-static interactions we have $V \simeq \hbar\Delta\omega$ (cf. p. 23 of ref. [4]) and $t^2PV_e'(0)/6\hbar \simeq 1/\tau\Delta\omega \ll 1$. Thus, if eq (34) is satisfied, the commutator in eq (35) is negligible and $U_a(t)$ may be expressed in the product form as stated.

4. Series Expansions of $F(t)$

In this section we will obtain series expansions for the function $F(t)$ defined by eq. (19). The various methods of handling these expansions give rise to different types of theories (e.g., the one-electron theory, impact theory, etc.).

The classical Hamiltonian $E_p(\mathbf{x}, \mathbf{v})$ appearing in $F(t)$ was given, in eq (20), by

$$E_p(\mathbf{x}, \mathbf{v}) = \sum_j mv_j^2/2 + V_p(\mathbf{x}_1, \ldots, \mathbf{x}_N) \tag{36}$$

where $\mathbf{x}_j$ and $\mathbf{v}_j$ refer to the jth electron and $V_p(\mathbf{x})$ represents the electron-electron interaction. We may define position and velocity distribution functions $P(\mathbf{x})$ and $W(\mathbf{v})$ by

$$P(\mathbf{x}) = \exp\{-V_p(\mathbf{x})/kT\}/\int d\mathbf{x}\exp\{-V_p(\mathbf{x})/kT\} \tag{37}$$

$$W(\mathbf{v}_j) = \exp\{-mv_j^2/2kT\}/\int d\mathbf{v}_j\exp\{-mv_j^2/2kT\} \tag{38}$$

$$W(\mathbf{v}) = \Pi_j W(\mathbf{v}_j), \tag{39}$$

and these have the property that

$$W(\mathbf{v})P(\mathbf{x}) = Q^{-1}\exp\{-E_p(\mathbf{x}, \mathbf{v})/kT\} \tag{40}$$

where Q was defined by eq (21). Using the product form for $U_a(t)$ given in eq (26), we obtain

$$F(t) = \mathcal{O}_0\int d\mathbf{x}P(\mathbf{x})\int \Pi_j d\mathbf{v}_j W(\mathbf{v}_j)U_j(t). \tag{41}$$

Following the technique used by Baranger and Mozer [15], we define a function $\varphi(\mathbf{R}, \mathbf{x}_j, t)$ (which should not be confused with the wave functions φ used in I) by

$$1 + \varphi(\mathbf{R}, \mathbf{x}_j, t) = \int d\mathbf{v}_j W(\mathbf{v}_j)U_j(\mathbf{R}, \mathbf{x}_j, \mathbf{v}_j, t). \tag{42}$$

Using $\varphi(j)$ as a shorthand notation for $\varphi(\mathbf{R}, \mathbf{x}_j, t)$ we have

$$\Pi_j[1+\varphi(j)] = 1 + \sum_j \varphi(j) + \sum_{j<k}\varphi(j)\varphi(k) + \ldots. \tag{43}$$

Substituting eqs (42) and (43) into (41) we obtain the series

$$F(t) = \mathcal{O}_0\left[1 + \sum_{M=1}^{N} F_M(t)\right] \tag{44}$$

where

$$F_M(t) = \sum_{j_1<j_2<\ldots<j_M}\int \varphi(j_1)\ldots\varphi(j_M)P(\mathbf{x})d\mathbf{x}. \tag{45}$$

Since $P(\mathbf{x}_1, \ldots, \mathbf{x}_N)$ is invariant under an interchange of particle coordinates we have

$$F_M(t) = [N!/M!(N-M)!] \int \ldots \int \varphi(1) \ldots \varphi(M) P(\mathbf{x}_1, \ldots, \mathbf{x}_N) d\mathbf{x}_1 \ldots d\mathbf{x}_N = [N!/M!(N-M)!] \int \ldots \int \varphi(1) \ldots \varphi(M) P_M(\mathbf{x}_1, \ldots, \mathbf{x}_M) d\mathbf{x}_1 \ldots d\mathbf{x}_M, \tag{46}$$

where the reduced distribution function $P_M(\mathbf{x}_1, \ldots, \mathbf{x}_M)$ is defined by

$$P_M(\mathbf{x}_1, \ldots, \mathbf{x}_M) = \int \ldots \int P(\mathbf{x}_1, \ldots, \mathbf{x}_M, \mathbf{x}_{M+1}, \ldots, \mathbf{x}_N) d\mathbf{x}_{M+1} \ldots d\mathbf{x}_N. \tag{47}$$

$P_M(\mathbf{x}_1, \ldots, \mathbf{x}_M) d\mathbf{x}_1 \ldots d\mathbf{x}_M$ represents the probability of finding the M particles labeled 1 through M in the volumes $d\mathbf{x}_1, \ldots d\mathbf{x}_M$ at the points $\mathbf{x}_1, \ldots, \mathbf{x}_M$ (for a further discussion see ref. [16]). The combinatorial factor in eq (46) represents the number of ways for choosing M electrons from the perturbing gas of N identical electrons.

The reduced distribution functions $P_M(\mathbf{x}_1, \ldots, \mathbf{x}_M)$ may be expanded in an Ursell expansion [17], the first three terms of which are given by

$$\begin{aligned} \mathcal{V} P_1(\mathbf{x}_1) &= g_1(\mathbf{x}_1), \\ \mathcal{V}^2 P_2(\mathbf{x}_1, \mathbf{x}_2) &= g_1(\mathbf{x}_1) g_1(\mathbf{x}_2) + g_2(\mathbf{x}_1, \mathbf{x}_2), \\ \mathcal{V}^3 P_3(\mathbf{x}_1, \mathbf{x}_2, \mathbf{x}_3) &= g_1(\mathbf{x}_1) g_1(\mathbf{x}_2) g_1(\mathbf{x}_3) \\ &+ g_1(\mathbf{x}_1) g_2(\mathbf{x}_2, \mathbf{x}_3) + g_1(\mathbf{x}_2) g_2(\mathbf{x}_1, \mathbf{x}_3) \\ &+ g_1(\mathbf{x}_3) g_2(\mathbf{x}_1, \mathbf{x}_2) + g_3(\mathbf{x}_1, \mathbf{x}_2, \mathbf{x}_3), \end{aligned} \tag{48}$$

where $\mathcal{V}$ is the volume of the system; the general term in the Ursell expansion is given by eq (9) of ref. [17]. The function $g_1/\mathcal{V}$ is the one-body probability function; $g_1(\mathbf{x}_1) g_1(\mathbf{x}_2)/\mathcal{V}^2$ would be the two-body probability function if there were no correlation between particles. Since there is a correlation between the particles at $\mathbf{x}_1$ and $\mathbf{x}_2$, this correlation is represented by the two-body correlation function $g_2(\mathbf{x}_1, \mathbf{x}_2)$. Similarly P_3 is expressed by a group of terms which contain no more than two-body correlations plus $g_3(\mathbf{x}_1, \mathbf{x}_2, \mathbf{x}_3)$, the three-body correlation function. The general term in the Ursell expansion expresses $P_M(\mathbf{x}_1, \ldots, \mathbf{x}_M)$ as a sum of terms which contain no more than $(M-1)$-body correlations plus $g_M(\mathbf{x}_1, \ldots, \mathbf{x}_M)$, the M-body correlation function. Following Baranger and Mozer [15] we define a function

$$h_M(t) = \int \varphi(1) \ldots \varphi(M) g_M(\mathbf{x}_1, \ldots, \mathbf{x}_M) d\mathbf{x}_1 \ldots d\mathbf{x}_M, \tag{49}$$

and, after considerable algebra, it is found that $F(t)$, as given by eqs (41) and (43), can be expanded in terms of the g_M and then resummed to yield

$$F(t) = \mathcal{O}_0 \exp\left\{ \sum_{M=1}^{\infty} (n^M/M!) h_M(t) \right\}. \tag{50}$$

In the derivation of eq (50) it was necessary to let N and $\mathcal{V}$ become infinite in such a way that the density $n = N/\mathcal{V}$ remained constant. In this new series for $F(t)$, each successive term represents a higher order correlation effect.

We now have two entirely different expressions (eqs (44) and (50)) for $F(t)$. To determine the utility of these expressions, we will briefly outline the physical significance of the terms in the series expansions involved. To understand the physical significance of $F(t)$ itself, we note that, except for multiplicative constants (e.g., $\mathbf{d}$ matrix elements), $F(t)$ is the same as the autocorrelation function $C(t)$ discussed in section 7 of I.

The $F_1(t)$ term in eq (44) describes the electron-atom interactions (collisions) as though they are completely independent of one another. From eqs. (42) and (46) we see that $F_1(t)$ is given by a sum of terms, each of which contains only one U_j operator, thus, to this order the effects of the interactions are simply additive. The terms $F_2, \ldots, F_N$ account for the fact that the effect on $F(t)$ of one interaction may be influenced by other interactions. When this influence is taken into account, the effects of the collisions are no longer simply additive. This influence of one interaction on another comes about in basically two ways. The most obvious influence is due to the correlation between the perturbing electrons which are described by the correlation functions g_M for $M \geq 2$. However, even when these correlations are ignored (by setting $g_M = 0$ for $M \geq 2$), the $F_2, \ldots, F_M$ terms do not vanish and it is still possible for the outcome of one collision to be influenced by other collisions. This remaining influence comes about when a collision, or a series of collisions, produces a large change in the state of the radiator thereby reducing the autocorrelation function $F(t)$. If the state of the radiator is thus materially altered from its original value, the effect of subsequent collisions will be correspondingly modified. For example, there is a high probability that a strong collision will cause an inelastic transition between states having different principal quantum numbers and it is obvious that such a transition cannot be neglected when calculating the effect of the next collision. Since it takes several weak collisions to build up such an influence, we expect that $F_1(t)$ will provide a good approximation to $F(t)$ for times which are shorter than the mean free time between strong collisions (for those cases where a strong collision does occur during this time, the effects of subsequent weak collisions are negligible in comparison). For longer times of interest it is necessary to consider all of the terms $F_1, \ldots, F_N$, and in this case eq (50) is more appropriate than eq (44).

In eq (50), the $h_1(t)$ term describes the electron-atom interactions as though the position of an electron is not influenced by the presence of the other electrons. That is, the electron-electron correlations are neglected in this term (although the remaining influence of one collision on the effects of subsequent collisions is properly included). The h_2 term accounts for pair correlations between electrons, and subsequent terms describe higher order correlations. Since it is usually not necessary to consider more than pair correlations, it would seem that eq (50) is much more useful than eq (44). This would indeed be the case if we could always make calculations based on eq (50); as we will show in the following sections, the calculations based on eq (50) become quite difficult for short times of interest and in this case eq (44) is of more practical value.

As a further comparison of eq (44) and (50), it is interesting to note that, in the microfield theory [15], the approximation $F \simeq \exp(nh_1)$ gives rise to the Holtsmark distribution function (no correlation approximation) whereas the approximation $F \simeq 1+F_1$ gives the asymptotic Holtsmark function (or nearest neighbor approximation). This indicates that the approximation $F(t) \simeq \mathcal{O}_0[1+F_1(t)]$ is just the small t limit of $F(t) \simeq \mathcal{O}_0 \exp\{nh_1(t)\}$. To verify that this is the case, we note from eqs (42) and (49) that as $t \to 0$, $h_1(t) \to 0$ and $\exp\{nh_1(t)\} \to 1+nh_1(t)$; substituting the functions [16] $P_1(x_1) = n/N$ and $g_1(x_1) = 1$ into eqs (45) and (49) we see that $F_1(t) = nh_1(t)$, thus $1+F_1(t)$ is indeed the small t limit of $\exp\{nh_1(t)\}$.

5. The One-Electron Theory

The one-electron theory is designed to provide a description of the wings of a line profile. The version of this theory presented in this section will be shown (in sec. 7) to provide a consistent description of a line profile from the half width to the quasi-static wings. This theory is based on the approximation $F(t) \simeq \mathcal{O}_0[1+F_1(t)]$ which is valid for small times of interest or large $\Delta\omega$. Since $F_1(t)$ is given by a sum of terms each of which contains a single $U_j(t)$ operator (rather than products of the U_j), the chronological ordering operator $\mathcal{O}_0$ will have no effect on F_1. Using [16] $P_1(x_1) = n/N$ in eq (45), we obtain

$$F(t) = 1 + n\int \varphi(\mathbf{R}, \mathbf{x}_1, t)\, d\mathbf{x}_1. \tag{51}$$

Notice that this expression involves the average of the time development operator for a *single* collision; this is the origin of the name "one-electron" theory.

The first term in $F(t)$ (i.e., the constant 1) will give rise to a delta function, $\delta(\Delta\omega - e\mathcal{E}Z_{nk}/\hbar)$, when it is substituted into eq (18). Performing the ion microfield average, as required by eq (3), it is clear that the contribution to $\mathcal{I}(\omega)$ resulting from this term will be proportional to $\mathcal{P}(\hbar\Delta\omega/eZ_{nk})$. This represents the line shape which would be produced by the ions alone.

The influence of the electrons (as well as some electron-ion coupling) is contained in the second term in eq (51):

$$F_1(t) = n\int \varphi(\mathbf{R}, \mathbf{x}_1, t)\, d\mathbf{x}_1. \tag{52}$$

Using eqs (33) (which is valid only in the line wings) and (42), and noting that $\int W(v_1)dv_1 = 1$, we obtain

$$F_1(t) = n\int d\mathbf{v}_1 W(v_1) \int d\mathbf{x}_1 \left[\exp\left\{-(i/\hbar)\int_0^t PV_1(\mathbf{R}, \mathbf{x}_1 + \mathbf{v}_1 t')dt'\right\} - 1\right]. \tag{53}$$

As discussed in the appendix, we may transform to the more familiar collision variables ($\boldsymbol{\rho}_0$, $\mathbf{v}_0$, t_0) where $\boldsymbol{\rho}_0$ and $\mathbf{v}_0$ denote the impact parameter and electron velocity while t_0 is some reference time in the collision (the time of closest approach in a completed collision). In terms of these variables we have

$$F_1(t) = n\int d\Omega \int_0^\infty v_0^3 W(v_0)dv_0 \int_0^\infty \rho_0 d\rho_0 \int_{-\infty}^{+\infty} dt_0 \left[\exp\left\{-(i/\hbar)\int_0^t PV_1(\mathbf{R}, \boldsymbol{\rho}_0, \mathbf{v}_0, t'+t_0)dt'\right\} - 1\right] \tag{54}$$

where

$$V_1(\mathbf{R}, \boldsymbol{\rho}_0, \mathbf{v}_0, t'+t_0) = e^2\mathbf{R} \cdot [\boldsymbol{\rho}_0 + \mathbf{v}_0(t'+t_0)]/[\rho_0^2 + v_0^2(t'+t_0)^2]^{3/2}. \tag{55}$$

The Euler angles Ω denote the orientation of the "collision axes" relative to the direction of $\mathbf{R}$, the atomic dipole. We may therefore interpret the integral over Ω as an average over all possible orientations of the electron trajectory [5] relative to the direction of $\mathbf{R}$.

To make full use of the collision axes, we take the matrix elements of $F_1(t)$ as required by eq (18). These matrix elements are given by

$$\langle nk|F_1(t)|nk'\rangle = n\int d\Omega \int_0^\infty v_0^3 W(v_0)dv_0 \int_0^\infty \rho_0 d\rho_0 \int_{-\infty}^{\infty} dt_0 \left\langle nk\left|\left[\exp\left\{-(i/\hbar)\int_0^t PV_1(\mathbf{R}, \boldsymbol{\rho}_0, \mathbf{v}_0, t'+t_0)dt'\right\} - 1\right]\right|nk'\right\rangle. \tag{56}$$

We may now perform a rotation of the "atomic axes," through the Euler angles Ω, so that $\mathbf{R}$ will point in the same direction as $\boldsymbol{\rho}_0$, and $\mathbf{v}_0$ defines the x direction. The rotated wave functions will be given by [18] $\mathscr{D}(\Omega)|\nu k\rangle$, where $\mathscr{D}(\Omega)$ is a rotation operator. The interaction potential referred to collision axes is

$$V_c(X, Z, \rho_0, v_0, t'+t_0) = e^2[Z\rho_0 + Xv_0(t'+t_0)]/[\rho_0^2 + v_0^2(t'+t_0)^2]^{3/2}, \quad (57)$$

where X and Z denote the x and z components of $\mathbf{R}$, and we have the identity

$$\left\langle \nu k \left| \left[\exp\left\{ -(i/\hbar)\int_0^t PV_1(\mathbf{R}, \rho_0, v_0, t'+t_0)dt' \right\} - 1 \right] \right| \nu k' \right\rangle = \left\langle \nu k \left| \mathscr{D}^{-1}(\Omega) \left[\exp\left\{ -(i/\hbar)\int_0^t PV_c(X, Z, \rho_0, v_0, t'+t_0)dt' \right\} - 1 \right] \mathscr{D}(\Omega) \right| \nu k' \right\rangle. \quad (58)$$

Substituting this identity into eq (56), we obtain

$$\langle \nu k|F_1(t)|\nu k'\rangle = \int \langle \nu k|\mathscr{D}^{-1}(\Omega)F_1^c(t)\mathscr{D}(\Omega)|\nu k'\rangle d\Omega, \quad (59)$$

where

$$F_1^c(t) \equiv n\int_0^\infty v_0^3 W(v_0)dv_0 \int_0^\infty \rho_0 d\rho_0 \int_{-\infty}^\infty dt_0 \left[\exp\left\{ -(i/\hbar)\int_0^t PV_c(X, Z, \rho_0, v_0, t'+t_0)dt' \right\} - 1 \right]. \quad (60)$$

The average over Ω in eq (59) may be readily performed by transforming to spherical wave functions [19] and using the properties of $\mathscr{D}(\Omega)$ as given by Edmonds [18]. The function $F_1^c(t)$ may be evaluated by numerical methods, and the line shape is then obtained by substituting the result into eq (18) and performing the transform. Further details of such a calculation together with numerical results will be reported in a future paper.

6. The Impact Theory

To obtain the results of the impact theories we use the $U_j(t)$ which were obtained by the impact approximation, eq (27), and the approximate calculation of $F(t)$ is based on its expansion in terms of correlation functions, eq (50). For most plasma broadening problems one is interested in a temperature-density range where three-body correlations are negligible, hence it is necessary to consider only $h_1(t)$ (no correlations) and $h_2(t)$ (two-body correlations). In the impact theories, electron correlations are not treated with correlation functions (such as $g_2(\mathbf{x}_1, \mathbf{x}_2)$ which appears in $h_2(t)$). Instead, in these theories the electron correlations are approximated by impact parameter cutoffs. Shielded field arguments are used to derive a cutoff of approximately λ_D, the Debye length, in the range of the electron-atom interaction [20], and the frequency dependent Lewis cutoff [21] $(v_{av}/\Delta\omega)$ is used in place of λ_D when $(v_{av}/\Delta\omega) < \lambda_D$ (this will be discussed in sec. 7). A similar cutoff behavior has also been obtained, by means of correlation functions, within the framework of a quantum mechanical theory [22]. However a more accurate treatment of the electron correlations [23] has shown that, while the cutoff at $(v_{av}/\Delta\omega)$ is valid for $\Delta\omega > \omega_p$, the cutoffs in the line center are in error. The cutoff at the Debye length (or at 1.1 λ_D in some theories) should be multiplied by $(2.718)^{-1/2} \simeq 0.6$ resulting in a change on the order of 20 percent in the broadening function Φ_{ab} used by Griem et al. [2, 9, 13, 20]. For $\Delta\omega \simeq \omega_p$, there is a possibility of further corrections due to dynamic correlation effects.

To derive the results obtained by the impact theory, we will assume that the effect of electron correlations may be represented by some correctly chosen impact parameter cutoffs. We thus need to consider only the function $h_1(t)$ as given by eq (49):

$$F(t) \simeq \mathscr{O}_0 \exp\{nh_1(t)\}. \quad (61)$$

For a fluid [16] such as a plasma, $g_1(\mathbf{x}_1) = 1$ and h_1 is given by

$$h_1(t) = \int\int d\mathbf{x}_1 d\mathbf{v}_1 W(\mathbf{v}_1)[U_1(\mathbf{R}, \mathbf{x}_1, \mathbf{v}_1, t) - 1]. \quad (62)$$

We note in passing that if the exponential in eq (61) is expanded, the first two terms in the series are identical with the approximate expression for $F(t)$, eq (51), which is used in the one-electron theory. A further discussion of this correspondence is given in the following sections.

Using eqs (25) and (27), $h_1(t)$ is given by

$$h_1(t) = \int\int d\mathbf{x}_1 d\mathbf{v}_1 W(\mathbf{v}_1)[\mathscr{O} \exp\{-(i/\hbar)\int_0^t e^{it'\mathscr{L}} PV_1(\mathbf{R}, \mathbf{x}_1, \mathbf{v}_1, t')e^{-it'\mathscr{L}}dt'\} - 1]. \quad (63)$$

Transforming to collision variables (see appendix) and denoting the average over ρ_0, v_0, and Ω by a subscript av, this becomes

$$h_1(t)=\int_{-\infty}^{\infty}dt_0\left[\mathcal{O}\exp\left\{-(i/\hbar)\int_0^t e^{it'\mathcal{L}}PV_1(t'+t_0)e^{-it'\mathcal{L}}dt'\right\}-1\right]_{\rm av}. \tag{64}$$

Changing variables from t' to $s=t'+t_0$ and using the identity $\exp[e^{-A}B_e^A]=e^{-A}e^Be^A$, we obtain

$$h_1(t)=\int_{-\infty}^{\infty}dt_0\exp(-it_0\mathcal{L})\left[\mathcal{O}\exp\left\{-(i/\hbar)\int_{t_0}^{t_0+t}e^{is\mathcal{L}}PV_1(s)e^{-is\mathcal{L}}ds\right\}-1\right]_{\rm av}\exp(it_0\mathcal{L}). \tag{65}$$

We assume that a collision time τ exists such that $V_1(s)=0$ unless $0\leq s\leq\tau$. The completed collision assumption, which is an important part of most impact theories, states that if a collision occurs, it can be completed. That is, if some value of s in the interval $[t_0,\ t_0+t]$ satisfies $0\leq s\leq\tau$, then the completed collision assumption states that the collision should be completed in that interval, i.e., $t_0\leq 0\leq s\leq\tau\leq(t_0+t)$. Using this restriction on t_0 and extending the limits $(t_0,\ t+t_0)$ on the s integral to $(-\infty,+\infty)$ (since $V_1(s)=0$ outside the range $0\leq s\leq\tau$ anyway), eq (65) becomes

$$h_1(t)=\int_{-(t-\tau)}^{0}dt_0\exp(-it_0\mathcal{L})[S-1]_{\rm av}\exp(it_0\mathcal{L})$$

$$=\int_0^{(t-\tau)}dt_0\exp(it_0\mathcal{L})[S-1]_{\rm av}\exp(-it_0\mathcal{L}), \tag{66}$$

where S is an S-matrix for a single collision (weak or strong) defined by

$$S=\mathcal{O}\exp\left\{-(i/\hbar)\int_{-\infty}^{\infty}e^{is\mathcal{L}}PV_1(s)e^{-is\mathcal{L}}ds\right\}. \tag{67}$$

The completed collision assumption will provide a good approximation to $h_1(t)$ since τ is usually very small (i.e., $t\gg\tau$), however, if $t<\tau$, the collision cannot be completed and this approximation breaks down. Using the time of interest $1/\Delta\omega$ from eq (I-52), we may state that the completed collision assumption will be valid when

$$\tau\Delta\omega\ll 1, \tag{68}$$

where τ is some "representative" collision time [3]. This inequality is sometimes used as the validity criterion for the impact approximation [3]; this point will be discussed further in section 7.

Substituting eq (66) in eq (61) and using the operator identity

$$\mathcal{O}_0\exp\left[\int_0^t\exp(-t_0A)B\exp(t_0A)dt_0\right]=e^{-tA}e^{t(A+B)}, \tag{69}$$

we obtain

$$F(t)=e^{i(t-\tau)\mathcal{L}}\exp[-i(t-\tau)\mathcal{L}+(t-\tau)\Phi_a]$$

$$=e^{i(t-\tau)\mathcal{L}}\exp[+i\tau\mathcal{L}-\tau\Phi_a]\exp[-it\mathcal{L}+t\Phi_a], \tag{70}$$

where (cf. eq (42) of ref. [3] or eq (28) of ref. [12])

$$\Phi_a=n[S-1]_{\rm av}. \tag{71}$$

If we use

$$\tau\Phi_a\ll 1 \tag{72}$$

which is simply a statement that the impact approximation is valid (as we will show in sec. 7), then eq (70) becomes (cf. eq (39) in ref. [3] or eq (30) of ref. [12])

$$F(t)=e^{it\mathcal{L}}\exp[-it\mathcal{L}+t\Phi_a]. \tag{73}$$

Substituting this $F(t)$ into eq (18), we obtain

$$I(\omega,\mathscr{E})=(\rho_{aa}^{(a)}/\pi)\ {\rm Re}\sum_{kk'}\langle nk|\mathbf{d}|1\rangle\cdot\langle 1|\mathbf{d}|nk'\rangle$$

$$\int_0^\infty\langle nk|\exp[i(\Delta\omega-e\mathscr{E}PZ/\hbar)t+t\Phi_a]|nk'\rangle dt, \tag{74}$$

Comparing with eqs (9) and (32) of ref. [13], we see that this result is formally identical with the results obtained by the impact theory for the Lyman series.

It is important to note that, in most calculations of hydrogen line broadening, the exponentials $\exp(is\mathcal{L})$ in the integrand of the S-matrix (eq 67)) are either ignored or approximated by a cutoff [24]. To show how this cutoff is obtained, we note that when $e\mathscr{E}\tau(Z_{nk}-Z_{nk'})/\hbar\ll 1$ the exponentials may be replaced by unity. When $e\mathscr{E}\tau(Z_{nk}-Z_{nk'})/\hbar\gg 1$, the exponentials oscillate rapidly and there will be only a negligible contribution from this region of the integral. Defining a frequency

$$\omega(\mathscr{E})_{nk,\ nk'}=e\mathscr{E}(Z_{nk}-Z_{nk'})/\hbar \tag{75}$$

and noting that $\tau=\rho_0/v_0$, we define an impact parameter cutoff $\rho_{\rm max}=v_0/\omega_{nk,\ nk'}$ (in ref. [24] $\omega_{nk,\ nk'}$ is called $\Delta\omega_n$). When this cutoff is used, the exponentials $\exp(is\mathcal{L})$ in eq (67) are replaced by unity; this cutoff reduces the integrand to zero when $\tau\omega_{nk,\ nk'}>1$, thus approximating the effect of the rapidly oscillating exponentials, and when $\tau\omega_{nk,\ nk'}<1$ the exponentials are effectively replaced by unity. This cutoff is used simply as a method of simplifying the numerical calculations and it could be corrected without any modification of the theory itself.

7. Discussion of Approximations

7.1. General

In the preceding sections we have derived the familiar results of the impact and one-electron theories using the classical path formalism developed in I. The advantage of these theories lies in their simple classical description of the perturber dynamics; their disadvantage with respect to more recent quantum theories [6, 22, 25], is in the large number of approximations which are necessary to achieve this classical description. Since an understanding of these approximations plays an important role in the application and improvement of classical path theories, these approximations will be discussed in some detail in this section.

7.2. Preliminary Approximations

In our treatment of both the impact and the one-electron theories we have used a dipole approximation to the perturbation potential, a static treatment of the ion field, and the no-quenching approximation. It should also be mentioned that we have not considered any perturbation of the final state in the radiative transition because there is no linear Stark effect in the ground state of hydrogen and any higher order ground state perturbations (e.g., quadratic Stark effect) are unimportant [26]. For lines other than those in the Lyman series, lower state perturbations may have to be considered.

To show that the static approximation provides a good description of the ions, we consider the change $\delta\mathscr{E}$ in an electric field $\mathscr{E}=e/r^2$ during a time δt. Using $\delta\mathscr{E}\simeq\delta t(\partial\mathscr{E}/\partial t)\simeq v\delta t(\partial\mathscr{E}/\partial r)\simeq(v\mathscr{E}\delta t/r)$, we see that $(\delta\mathscr{E}/\mathscr{E})$ may be estimated by $(\delta t/\tau)$ where τ is the duration of a collision. If δt is replaced by the time of interest $(1/\Delta\omega)$, we see that $(\delta\mathscr{E}/\mathscr{E})$ will be negligible when

$$\tau\Delta\omega\gg 1, \tag{76}$$

as mentioned earlier. If a perturber is quasi-static it produces a Stark splitting $\hbar\Delta\omega$ given by $\hbar\Delta\omega=V$ (see p. 23 of ref. [4]). Using $V\simeq Ze^2R_0/\rho_0^2$ for an ion of charge Ze, this means that $\rho_0^2\simeq Ze^2R_0/\hbar\Delta\omega$. Since the velocity distribution is sharply peaked about $v_{\rm av}$, we estimate τ by $(\rho_0/v_{\rm av})$ and eq (76) becomes

$$\Delta\omega\gg\Delta\omega_c=(\hbar v_{\rm av}^2/e^2R_0). \tag{77}$$

The critical frequency $\Delta\omega_c$ is sometimes referred to as the Weisskopf frequency. Since $\Delta\omega_c$ for ions lies almost at the center of most lines, the static ion approximation is usually justified over most of the line profile (however see also ref. [27]). In section 3.E of ref. [6], it is shown that the effect of a static ion field may be described by the microfield average stated in eq (3).

In the no-quenching approximation it was assumed that the $T_a'(t)$ matrix elements between states having different principal quantum numbers could be neglected when calculating $C(t)$. These "off-diagonal" matrix elements represent collision induced transitions which transfer the excitation of the atom from one energy level to another. In section 7.2 of I, it was shown that collision induced transitions between excited states correspond to switching the mode of oscillation in a classical oscillator. It was also shown that this mode switching effect could be neglected if the energy separation of the excited states is much larger than the halfwidth of the lines being studied. In hydrogen, states having the same n are degenerate (or nearly degenerate in the presence of an ion field) and collision induced transitions between these states are very important; this is the reason for regarding all states with the same n as a group of initial states. Low-lying states with different n are well separated in energy (much more than the halfwidths of the lines) hence the transitions described by $\langle nk|T_a'(t)|nk'\rangle$ may usually be neglected. However, for large n the levels are closer together and some of the higher series members may overlap; in this case it may be necessary to include states with different n in the group of initial states.

In section (2.2) the no-quenching assumption was made by setting $\langle nk|T_a'(t)|n'k'\rangle$ to zero. This neglects the quenching terms which would be added to eq (18) as discussed above, however, it also neglects the influence which $\langle nk|T_a'(t)|n'k'\rangle$ has on $\langle nk|T_a'|nk'\rangle$. That is, even if a line is isolated in the sense that the quenching terms which would be added to eq (18) are negligible, it may still be necessary to consider the influence of the inelastic transitions $|nk\rangle\rightarrow|n'k'\rangle$ when calculating $\langle nk|T_a'|nk'\rangle$. To show when this influence is also negligible we consider the differential equation for $T_a'(t)$, eq (6). This equation may be written in the form

$$\begin{aligned}i\hbar\frac{\partial}{\partial t}\langle nk|T_a'(t)|nk'\rangle&=\sum_{k''}\langle nk|e\mathscr{E}Z+V_e(t)|nk''\rangle\langle nk''|T_a'(t)|nk'\rangle\\&\quad+\sum_{n''\neq n}\sum_{k''}\exp\{it\omega_{nn''}\}\langle nk|e\mathscr{E}Z\\&\quad+V_e(t)|n''k''\rangle\langle n''k''|T_a'(t)|nk'\rangle,\end{aligned} \tag{78}$$

where $\omega_{nn''}=(E_n-E_{n''})/\hbar$. From this equation we see that setting $\langle nk|T_a|n'k'\rangle$ to zero simply neglects the influence which the "off-diagonal" matrix elements of $[e\mathscr{E}Z+V_e(t)]$ may have on $\langle nk|T_a|nk'\rangle$. If eq (78) is solved in the usual iterative manner [7] by integrating over t, the term $\exp(it\omega_{nn''})$ will oscillate rapidly and contribute essentially nothing for $t>(1/\omega_{nn''})$. This indicates that the $\langle nk|Z|n''k''\rangle$ terms will be negligible compared with the $\langle nk|Z|nk'\rangle$ terms unless $t<(1/\omega_{nn''})$. Since the time of interest, $1/\Delta\omega$, is much larger than $(1/\omega_{nn''})$ for isolated lines, we may neglect the terms involving "off-diagonal" Z matrix elements. The same results apply for the terms involving "off-diagonal" elements of $V_e(t)$ unless $t>\tau$. If $t>\tau$, a similar argument indicates that the "off-diagonal" $V_e(t)$ terms are negligible only when

$\tau\omega_{\nu\nu'} > 1$. In this case we use $\tau \simeq \rho_0/v_{av}$ (the velocity distribution is sharply peaked about v_{av}) and we see that the condition $\tau\omega_{\nu\nu'} > 1$ is violated only when $\rho_0 \lesssim (\hbar v_{av}/\Delta E_{\nu\nu'})$ where $\Delta E_{\nu\nu'} = (E_\nu - E_{\nu'})$. Substituting this value of ρ_0 into $(V\tau/\hbar) \simeq (e^2R_0/\hbar\rho_0 v_{av})$ (recall that $V \simeq e^2R_0/\rho_0^2$ for a hydrogen plasma) we find $(V\tau/\hbar) \simeq (e^2R_0\Delta E_{\nu\nu'}/\hbar^2 v_{av}^2)$. Using $v_{av}^2 \simeq (3kT/m)$ and $R_0 \simeq (3n^2a_0/2)$, where $a_0 = \hbar^2/me^2$, this becomes $(V\tau/\hbar) \gtrsim (n^2\Delta E_{\nu\nu'}/2kT)$. If we use $\Delta E_{\nu\nu'} = E_\infty|(1/\nu)^2 - (1/\nu')^2|$, where $E_\infty = 13.6$ *ev.* is the ionization energy of hydrogen, we find that the off diagonal-terms are important only when

$$(V\tau/\hbar) \gtrsim (E_\infty/2kT)|1 - (\nu/\nu')^2|. \tag{79}$$

Since $E_\infty \gg kT$ one usually has $(E_\infty/2kT)|1 - (\nu/\nu')^2| > 1$ and, in this case, eq (79) indicates that the $\langle \nu''k''|T_a'|\nu k'\rangle$ terms in eq (78) are important only during strong collisions (in which case T_a' averages to zero, as discussed in sec. 7 of I, so no error results). For some higher series members (very large ν and ν'') it can happen that $(E_\infty/2kT)|1 - (\nu/\nu')^2| < 1$, and eq (79) can be satisfied even for weak collisions. In this case, the "off-diagonal" terms in eq (78) must be retained when calculating $\langle \nu k|T_a'|\nu k'\rangle$. To see when this occurs, we consider the case where $\nu'' = \nu \pm 1$ and $\nu \gg 1$. In this case the quantity $(E_\infty/2kT)|1 - (\nu/\nu'')^2|$ will be less than unity when

$$\nu > (E_\infty/kT). \tag{80}$$

Thus, for lines involving $\nu > (E_\infty/kT)$, we may not be able to neglect the influence of inelastic transitions between states having different principal quantum numbers when calculating $\langle \nu k|T_a'|\nu k'\rangle$. This effect is usually negligible for hydrogen lines from laboratory plasmas because, for these plasmas, the lines generally begin to merge (overlap) when eq (80) is satisfied. For some astrophysical applications [27] (and for lines other than hydrogen lines) this effect may be very important.

When the differential equation for the matrix elements of $T_a'(t)$ in the no-quenching approximation, eq (10), was written as an operator equation, eq (11), it was necessary to introduce a projection operator P that picks out the part of an operator which is "diagonal" in ν. Although P operates on Z and $V_e(t)$, this does not imply that the "off-diagonal" elements of these operators are small (indeed they are about the same order of magnitude as the "diagonal" elements). The appearance of P in eq (11) merely indicates that the "off-diagonal" parts of Z and $V_e(t)$ have a negligible influence on T_a' in the no-quenching approximation. The influence of this projection operator is implicit in most line broadening theories since matrix elements of Z and V are usually taken only between states having the same principal quantum numbers; we have introduced P explicitly in order to avoid errors in handling $T_a'(t)$ and to clarify subsequent approximations. For example, the only operator in $V_e(t)$ is the atomic position operator $\mathbf{R}$ and one may therefore commute Z with $V_e(t)$: this commutation is not possible with PZ and $PV_e(t)$, in fact, the matrix elements of the commutator $[PZ, PV_e(t)]$ are about the same order of magnitude as the matrix elements of PZ and $PV_e(t)$. If the influence of P is only implicit, it is possible to make serious errors by commuting Z with $V_e(t)$ when these operators appear in $T_a'(t)$.

Since PZ does not commute with $PV_e(t)$, the formal solution, $T_a'(t)$, of eq (11) is a complicated time-ordered exponential. Although this operator has a rather simple form for the quasi-static region of the line wings (see sec. 3.4), it was necessary to introduce simplifying approximations in order to evaluate the rest of a line profile. The first of these was the impact approximation which assumes that most collisions can be described by a second order perturbation expansion of $U_a(t)$. Strong collisions $(V\tau/\hbar) > 1$, for which this expansion breaks down, are treated by some other method such as an impact parameter cutoff. With this approximation, it is possible to write $U_a(t)$ in the product form $\mathcal{O}_0\Pi_j U_j(t)$ where each $U_j(t)$ is the time development operator for a single electron-atom collision. It is difficult to give a useful validity criterion for the impact approximation; the validity criterion which is usually given [3], $\tau\Delta\omega < 1$, is based on the completed collision assumption which often accompanies the impact approximation when it is used in the impact theory (see secs. 6 and 7.3). Since the impact approximation is also used in the one-electron theory, we have drawn a distinction between the impact *approximation* and the impact *theory*. The impact approximation, as we have stated it, will be valid when strong collisions are well separated in time. If we define a strong collision frequency, ν_s, and a maximum duration for a strong collision, τ_s, this condition may be given by

$$\tau_s\nu_s \ll 1. \tag{81}$$

If all collisions were strong, ν_s would be on the order of the halfwidth, $\Delta\omega_{1/2}$, of the spectral line. For hydrogen plasmas we have $\nu_s < \Delta\omega_{1/2}$. The duration of a strong collision may be estimated by using $(V\tau/\hbar) \simeq (e^2R_0/\hbar\rho_0 v_{av}) \gtrsim 1$ or $\rho_0 \lesssim (e^2R_0/\hbar v_{av})$ which gives $\tau_s \simeq (\rho_0/v_{av}) \lesssim (e^2R_0/\hbar v_{av}^2) = (1/\Delta\omega_c)$, where $\Delta\omega_c$ is the Weisskopf frequency for electrons. Using $v_{av}^2 \simeq (3kT/m)$ and $R_0 = (3n^2a_0/2)$ where $a_0 = (\hbar^2/me^2)$, we have $\tau_s \lesssim (n^2\hbar/kT)$ and $\tau_s\nu_s < n^2(\hbar\Delta\omega_{1/2}/kT)$. Since $n^2(\hbar\Delta\omega_{1/2}/kT) \ll 1$ for most hydrogen plasmas, we expect the impact approximation to be valid for the electrons.

7.3. Discussion of the Impact Theory

In the usual derivation of the impact theory [2, 3] one calculates the change in $\langle U_a(t|0)\rangle$ during some time Δt (recall that $U_a(t) \equiv U_a(t|0)$). This change is given by

$$\begin{aligned}\Delta\langle U_a(t|0)\rangle &= \langle U_a(t+\Delta t|0) - U_a(t|0)\rangle \\ &= \langle [U_a(t+\Delta t|t) - 1]U_a(t|0)\rangle. \end{aligned}\tag{82}$$

It is assumed that: (1) Δt is large enough that the two factors on the right are statistically independent and

may thus be averaged separately, and (2) Δt is small enough that the difference equation, eq (82), may be replaced by the differential equation (see eq (4.30) of ref. [2], eq (38) of ref. [3] or eq (2.8) of ref. [20])

$$\frac{d}{dt}\langle U_a(t)\rangle = [\exp(itH_a/\hbar)\Phi_a \exp(-itH_a/\hbar)]\langle U_a(t)\rangle \tag{83}$$

which is then solved for $\langle U_a(t)\rangle$ (Φ_a is given in eq (71)). In this derivation, assumption (1) requires $\Delta t > \tau$ and assumption (2) requires $\Delta t \ll t$ (as well as the average collision being weak; cf. pp. 508 and 529 of ref. [3]); together these assumptions require $t \gg \tau$ which is a mathematical statement of the completed collision assumption (cf. eq (68)). Thus we see that the completed collision assumption is an integral part of the *usual* derivation of the impact theory and the removal of this approximation would require a complete revision of the derivation. This is the reason one frequently sees the condition $t \gg \tau$ or $\tau\Delta\omega \ll 1$ given as the validity criterion for the impact approximation [3].

In our derivation of the impact theory we first used the impact approximation to write $U_a(t)$ in the product form $\mathcal{O}_0\Pi_j U_j(t)$ and we obtained a consistent correlation function expansion, eq (50), for $\langle U_a(t)\rangle \equiv F(t)$. To obtain the *usual* results of the impact theory, we assumed that the electron-electron correlations could be approximated by impact parameter cutoffs, we used the completed collision assumption and we assumed that $\tau\Phi_a < 1$. It was also noted that numerical calculations are frequently simplified by approximating the influence of the ion field splitting on the electron broadening (i.e., the factors $\exp(is\mathscr{Z})$ in eq (67)) with an impact parameter cutoff $\rho_{\max} = v_0/|\omega_{ab}, \omega_{cd}|$ which depends on the ion field strength. While this approximation does not affect the region of validity of the *theory*, it would nonetheless be desirable to improve on this approximation to insure more accurate *calculations*. It is also interesting to note that the condition $\tau\Phi_a < 1$ is simply a manifestation of the requirement that the impact approximation is satisfied (this was discussed in sec. 7.2). To show this, we use eq (71) and estimate the magnitude of Φ_a by

$$\Phi_a = n[S-1]_{\text{av}} \simeq n(V\tau/\hbar)_{\text{av}}$$

where the subscript av refers to an integral over the collision variables ρ_0, v_0, and Ω (cf. eqs (64) and (A.5)). Since $2\pi n\rho_0 d\rho_0 v_0^3 W(v_0)dv_0 d\Omega = d\nu$ where ν denotes the frequency of collisions described by ρ_0, v_0, and Ω, we see that $n(V\tau/\hbar)_{\text{av}} = \int (V\tau/\hbar)d\nu = (\bar{V}/\hbar)$ where $\bar{V}$ denotes the average value of V. The statement $\tau\Phi_a < 1$ now becomes $(\bar{V}\tau/\hbar) < 1$, which is satisfied if the average collision is weak and if strong collisions $(V\tau/\hbar > 1)$ are well separated in time. This shows that the condition $\tau\Phi_a < 1$ is always satisfied when the impact approximation is valid.

One potentially useful feature of our approach is that it permits a consistent improvement of the impact theory within the framework of the classical path methods. That is, the impact parameter cutoffs, the completed collision assumption and the second order expansion of $U_j(t)$ were needed only to simplify the calculation of eq (50) and it would be possible to correct these approximations without having to rewrite the theory. In fact, the impact parameter cutoffs have already been corrected to some extent by means of a more consistent treatment of correlation functions [22, 23].

The correction of the completed collision assumption is a matter of some importance because, if we estimate the collision duration time by $(\lambda_D/v_{\text{av}}) = (1/\omega_p)$, the region of validity for this approximation, eq (66), is given by

$$\Delta\omega < \omega_p . \tag{84}$$

That is, an impact theory with a completed collision assumption can be used only for values of $\Delta\omega$ smaller than the electron plasma frequency. It has been shown that the completed collision assumption may be corrected, *in the line wings*, by means of the Lewis cutoff [21]. This cutoff may be obtained from eqs (61) and (62) by expanding $F(t)$ to second order in $V(t)$ and performing the Fourier transform as stated in eq (18) (cf. eqs (6) and (17) of ref. [21]).

Since the derivation of the Lewis cutoff is based on an expansion of $F(t)$ which is valid only in the line wings, the use of this cutoff in the impact theory raises some doubts as to the validity of such a "modified" impact theory in the line center. These doubts may be dispelled to some extent by means of a comparison with the results of the quantum mechanical relaxation theory which does not make a completed collision assumption. In reference [22] it is shown that the results of the relaxation theory essentially reproduce the behavior of a Lewis cutoff, and these results are *not* restricted to the line wings. In spite of this useful comparison, it would nonetheless be desirable to confirm this behavior within the framework of a classical path theory. In this regard, it is important to note that the completed collision assumption is not an inherent part of *our* derivation of the impact theory. This approximation was introduced simply to compare with the results of the *usual* derivation. It would thus be possible, in principle, to calculate $F(t)$ from eqs (61) and (62) without making a completed collision assumption. This has in fact been done, to second order, [28], and it is found that the results are identical with the results of the relaxation theory. It thus appears that a "modified" impact theory which does not make a completed collision assumption (such as ref. [28]), or a theory which corrects this assumption by means of a Lewis cutoff, will have a wider range of applicability than that stated in eq (84).

If the completed collision assumption is not made (or if it can be corrected by some approximation such as the Lewis cutoff), the only serious limitation on the applicability of such a "modified" impact theory comes from the second order expansion of $U_j(t)$. This expansion should be valid whenever the quantity $(i/\hbar)\int V(t')dt'$ is small compared with unity. For completed collisions this quantity was estimated (cf. eq (I–68)) by $(V\tau/\hbar)$ and the expansion was justified

except for strong collisions. For collisions which cannot be completed during the time of interest (i.e., collisions for which $\tau\Delta\omega > 1$), we have $(1/\hbar)\int V(t')dt \simeq (V/\hbar\Delta\omega)$ and it remains to be seen whether this is small or not. This situation may arise in the far wings of a line where the electron-atom collisions take on a quasi-static aspect (cf. sec. 3.4). In this region, the intensity at a point $\Delta\omega$ is primarily determined by those interactions which produce a Stark splitting $\hbar\Delta\omega$; that is, by those interactions for which $V \simeq \hbar\Delta\omega$ (see p. 23 of ref. [4]). For these quasi-static interactions we have $(1/\hbar)\int V(t')dt' \simeq (V/\hbar\Delta\omega) \simeq 1$ and the series expansion of $U_j(t)$ breaks down [29]. To determine where this breakdown occurs, we use $\tau \simeq (\rho_0/v_{av})$ ($v_0 \simeq v_{av}$ for neutral radiators) and $\tau\Delta\omega \gtrsim 1$ to obtain $\rho_0 \gtrsim (v_{av}/\Delta\omega)$; substituting this result in $\hbar\Delta\omega \simeq V \simeq e^2R_0/\rho_0^2$, we obtain $\Delta\omega \simeq (\hbar v_{av}^2/e^2R_0) = \Delta\omega_c$ where $\Delta\omega_c$ is the Weisskopf frequency for electrons. Using $v_{av} = (3kT/m)^{1/2}$ and $a_0 = (\hbar^2/me^2)$, we have $\Delta\omega_c = (3kT/\hbar)(a_0/R_0)$; thus we see that the second order expansion of $U_j(t)$ limits the application of the impact theory to the region

$$0 \lesssim \Delta\omega \ll \Delta\omega_c = (3kT/\hbar)(a_0/R_0). \tag{85}$$

In principle this range of applicability could be extended by using the full exponential for $U_j(t)$ rather than its series expansion. In this regard it should be noted that the derivation of the Lewis cutoff is based on the second order expansion and, if this expansion is to be improved, it may be necessary to improve the Lewis cutoff as well.

7.4. Discussion of the One-Electron Theory

In the previous section it was shown that the impact theory is limited to the center region of a line profile because of the second order expansion of $U_j(t)$. The one-electron theory is designed to be valid in the line wings and it is expected that its region of validity will overlap with that of the impact theory so that the complete line profile may be described without ambiguity. To insure that the one-electron theory will be valid in the line wings, we used the exponential form of $U_j(t)$ which is valid in the wings. In the derivation of this exponential form it was assumed that both the ion field splitting and the time ordering operator could be neglected.

In section 3.3 it was shown that the time ordering operator is not necessary if the second order expansion of $U_j(t)$ is justified, and in section 3.4 it was shown that time ordering is not necessary for quasi-static interactions. It thus appears that the only errors resulting from the neglect of time ordering will come from the strong collisions. Since the average effect of strong collisions is to reduce $U_j(t)$ to zero (see sec. 7 of I), the errors made in these collisions should have a negligible effect on $\langle U_j(t)\rangle$.

To find out when we may neglect the exponential $\exp[ite\mathscr{E}(Z_{n'k'} - Z_{nk})/\hbar]$ which appears in the operator $U_n(t)$ used by the one-electron theory, eq (28), we consider a cutoff that is similar to the cutoff $v/\omega_{nk,n'k'}$ which approximates this exponential in the impact theory (see eq (75)). Using $t = 1/\Delta\omega$ and $\omega_{nk,n'k'}(\mathscr{E}) = e\mathscr{E}(Z_{n'k'} - Z_{nk})/\hbar$, we note that this exponential is essentially unity when $(\omega_{nk,n'k'}/\Delta\omega) < 1$; when $(\omega_{nk,n'k'}/\Delta\omega) \gg 1$ the exponentials oscillates rapidly and there is only a negligible contribution from $U_n(t)$. Since $U_n(t)$ appears under a microfield average, we will consider a cutoff $\mathscr{E}_c = \hbar\Delta\omega/e(Z_{n'k'} - Z_{nk})$ in the range of this microfield average. We replace the exponential by unity and average over ion field strengths $\mathscr{E} < \mathscr{E}_c$; this cutoff replaces the integrand by zero when $(\omega_{nk,n'k'}/\Delta\omega) > 1$, thus approximating the effect of the rapidly oscillating exponentials, and when $(\omega_{nk,n'k'}/\Delta\omega) < 1$, the exponentials are effectively replaced by unity. This cutoff has no effect on the static ion broadening because, in the one-electron theory, the line shape is a sum of two terms (cf. eq (51)) and the term which describes the ion broadening (the $\mathscr{P}(\hbar\Delta\omega/Z_{nk})$ term) is not affected by the microfield average of the electron broadening term (the $F_1(t)$ term) where the cutoff is applied. If it should happen that $\mathscr{E}_c \gg \mathscr{E}_{av}$, we may as well ignore the cutoff and average over $0 \leq \mathscr{E} \leq \infty$ because $\mathscr{P}(\mathscr{E})$ will be negligibly small for $\mathscr{E} > \mathscr{E}_c$. That is, the exponential may be replaced by unity for all $\mathscr{E}$ whenever $\mathscr{E}_c = \hbar\Delta\omega/e(Z_{n'k'} - Z_{nk}) > \mathscr{E}_{av}$ or, as it was stated in eq (29), whenever

$$\Delta\omega > e\mathscr{E}_{av}(Z_{n'k'} - Z_{nk})/\hbar. \tag{86}$$

It should be noted that, as a practical estimate of the region of validity for neglecting the effect of the ion field on electron broadening, eq (86), is usually too restrictive. For higher lines (large n) which have a large number of Stark components (allowed $|nk\rangle \rightarrow |1\rangle$ transitions) a more realistic estimate is obtained by considering the average Stark splitting

$$\Delta\omega > e\mathscr{E}_{av}Z_{av}/\hbar \tag{87}$$

which is usually on the order of the halfwidth [30]. The use of Z_{av} rather than the maximum value of $(Z_{n'k'} - Z_{nk})$ is more appropriate for the higher lines because, for the larger values of Z_{nk}, the quantity $e\mathscr{E}_{av}Z_{nk}/\hbar$ corresponds to a very large frequency and the electron broadening is negligible for some values of $\Delta\omega$ less than $e\mathscr{E}_{av}Z_{nk}/\hbar$ (for large Z_{nk}, $\mathscr{P}(\hbar\Delta\omega/eZ_{nk})$ is much larger than the electron broadening term for a wide range of $\Delta\omega$ which are less than $e\mathscr{E}_{av}Z_{nk}/\hbar$).

Since we wish to use a classical potential in $U_j(t)$ to describe the quasi-static interactions, it is necessary to justify the use of the classical wavepackets which give rise to a classical potential (in sec. 8.3 of I, we justified the use of classical wavepackets only for dynamic perturbers). In section 8.3 of I, it was shown that we may represent the perturbers by nonoverlapping classical wavepackets of width Δx and momentum uncertainly $\Delta p \ll p$ if

$$\lambda_{av} \ll \Delta x \ll n^{-1/3}. \tag{88}$$

Since we have $\lambda_{av} \ll n^{-1/3}$ for most problems of interest, this criterion is easily met. We thus need only

show that the radiator and perturber wave functions do not overlap during the time of interest. Using the notation of section 8.3 in I, this criterion may be written

$$[\Delta x + (t\Delta p/m) + R_0] < \rho_0 \tag{89}$$

where $R_0 \simeq \nu^2 a_0 = \nu^2\hbar^2/me^2$ denotes the effective extent of the radiator wave function. Using $\Delta p \ll p$ and $t < \tau = (\rho_0/v_0)$, we see that $(t\Delta p/m) \ll \rho_0$ hence the $(t\Delta p/m)$ term in eq (89) may be dropped. Using $V \simeq \hbar\Delta\omega$ (for quasi-static interactions) and $V \simeq e^2R_0/\rho_0^2$ we obtain $\rho_0^2 \simeq (e^2R_0/\hbar\Delta\omega) = R_0^2\,(e^2/\nu^2 a_0)\ (1/\hbar\Delta\omega) = R_0^2\ (2E_\infty/\nu^2\hbar\Delta\omega)$ where $E_\infty = e^2/2a_0$ is the ionization energy. Since $\hbar\Delta\omega \ll E_\infty/\nu^2$, we see that $R_0 \ll \rho_0$ hence the R_0 term in eq (89) may also be dropped and we need only show that

$$\Delta x < \rho_0. \tag{90}$$

Again using the value $\rho_0^2 \simeq (e^2R_0/\hbar\Delta\omega)$ given above, as well as $\lambda_{\mathrm{av}}^2 = (\hbar^2/3mkT)$ and $a_0 = \hbar^2/me^2$, we find that $\rho_0^2 = \lambda_{\mathrm{av}}^2\ (kT/\hbar\Delta\omega)\,(R_0/a_0)$. Since $R_0 > a_0$ and $\hbar\Delta\omega \ll kT$, we see that $\rho_0 \gg \lambda_{\mathrm{av}}$ hence it is possible to find a Δx which will satisfy both eq (90) and eq (88). The use of a classical potential function is thus justified for quasi-static electron-atom interactions.

The results of the one-electron theory are based on the approximation $F(t) \simeq 1 + F_1(t)$ which treats the electron-atom interactions as though they are independent of one another. In section 4 it was argued that this is probably a good approximation, if the times of interest are shorter than the mean free time between strong collisions. To obtain a validity criterion for this approximation one sometimes identifies the collision frequency with the halfwidth $\Delta\omega_{1/2}$ for the line under consideration; the requirement that the time of interest, $1/\Delta\omega$, be less than the mean free time between collisions is then written [3]

$$\Delta\omega > \Delta\omega_{1/2} \tag{91}$$

Although this argument is somewhat loose, it will be shown that eq (91) actually does provide a useful statement of the region of validity for the one-electron theory.

To derive a validity criterion for the one-electron theroy, we note that the approximate $F(t)$ used in this theory, eq (51), is formally the same as an expansion to lowest order in $h_1(t)$ of the approximate $F(t)$ used in the impact theory, eq (61). That is, the single particle approximation is simply a small $h_1(t)$ approximation which is valid when $n|h_1(t)| < 1$. From the definition of $h_1(t)$ (see eq (62)) it is clear that $n|h_1(t)| < 1$ for small t. For large t the impact theory is valid and we use eqs (66) and (71) to obtain $n|h_1(t)| \leq t\Phi_a$. Replacing t by the time of interest, $1/\Delta\omega$, the validity criterion $n|h_1(t)| < 1$ becomes

$$\Delta\omega > \Phi_a. \tag{92}$$

Thus the one-electron theory should be valid when both eqs (86) and (92) are satisfied (or, for higher lines, when eqs (87) and (92) are satisfied).

If the average ion field splitting is small, $(e\mathscr{E}_{\mathrm{av}}Z_{\nu\kappa}/\hbar) < \Phi_a$, or if the linear Stark effect due to the ion field does influence the line shape (e.g., isolated lines), the halfwidth is determined [30] by the matrix elements of Φ_a (see sec. 4.7 of ref. [2]). In this case, the region of validity is given by eq (91) as $\Delta\omega > \Delta\omega_{1/2}$.

For lines where the average ion field splitting is large, $(e\mathscr{E}_{\mathrm{av}}Z_{\mathrm{av}}/\hbar) > \Phi_a$ (e.g., higher hydrogen lines) the halfwidth is determined primarily by ion broadening [30] and $\Delta\omega_{1/2} \simeq (e\mathscr{E}_{\mathrm{av}}Z_{\mathrm{av}}/\hbar)$. In this case eq (87) is more restrictive than eq (92) and the region of validity is again given by $\Delta\omega > \Delta\omega_{1/2}$.

The low lying hydrogen lines are determined by a small number of Stark components and, for many of these lines, a discussion of the halfwidth is of little value; lines such as Ly-β and H-β do not even have a well-defined halfwidth. Lines such as Ly-α and H-α have a very intense Stark component which is not shifted by linear Stark effect and the halfwidths of these lines are determined primarily by the electron broadening of this unshifted component. In such a case, eq (92) gives $\Delta\omega > \Delta\omega_{1/2}$. However, the remaining Stark components are very important in determining the line profile outside of the relatively narrow central component and, for these shifted components, eq (86) becomes more restrictive than the condition $\Delta\omega > \Delta\omega_{1/2}$ obtained from eq (92). It should be noted that eq (86) is probably not very much more restrictive than the condition $\Delta\omega > \Delta\omega_{1/2}$; for example, in the cases where Ly-α has been studied experimentally [31, 32], eq (86) gives approximately $\Delta\omega > \omega_p/10$ and $\omega_p/10$ differs very little from $\Delta\omega_{1/2}$.

From the above discussion we conclude that the one-electron theory will be valid in the region $\Delta\omega > \Delta\omega_{1/2}$ for isolated lines and for overlapping lines which have a large number of Stark components. For overlapping lines with only a few Stark components, the condition $\Delta\omega > \Delta\omega_{1/2}$ may no longer be applicable and one should consider eqs (86) and (92) for each Stark component.

8. Comparison of the Impact and One-Electron Theories

The calculations in both the impact and one-electron theories are based on binary collisions. The one-electron theory treats the electron-atom interactions as though their effects are additive and for this reason the one-electron theory is limited to the line wings (short times of interest) whereas the impact theory is not. In principle, the impact theory (with a Lewis cutoff) should be valid over most of the line profile; however, in practice it is usually necessary to expand the time development operator, $U_j(t)$, in order to make practical calculations, and it is this expansion which limits the impact theory to the center region of a line profile.

It was shown that the series expansion of $U_j(t)$ could not adequately describe either the strong collisions, $(V\tau/\hbar) \gtrsim 1$, or the quasi-static interactions, $(i/\hbar)\int V(t)\,dt \simeq 1$, which are important in the line wings. In our version of the one-electron theory this

difficulty is avoided through the use of an exponential expression for $U_j(t)$ (previous versions of the one-electron theory have used either a completed collision assumption [5] or a series expansion [3] of $U_j(t)$ hence they cannot be valid in the quasi-static wings). While this exponential form is not rigorously correct for strong collisions it does have the following useful properties:

(1) It is correct for weak collisions, $(V\tau/\hbar) < 1$, since it reproduces the series expansion for such interactions.

(2) It is correct for quasi-static interactions whereas the series expansion is not.

(3) For strong collisions, $(V\tau/\hbar) \gtrsim 1$, the exponential would give a much more realistic approximation to the exact $U_j(t)$ than the series expansion because the exponential retains unitarity (i.e., no transition probability can exceed unity). Thus, if one chose to use classical path methods for calculating $U_j(t)$, the strong collision cutoff discussed in section 7 of I, would be essentially reproduced (i.e., the exponential would oscillate rapidly and contribute essentially nothing for strong collisions). The errors resulting from this treatment of strong collisions should be negligible because the averaged $U_j(t)$ for strong collisions is essentially zero.

It is interesting to note that if we use a second order expansion of $U_j(t)$ in the one-electron theory, we obtain the asymptotic wing expansion which is used in deriving the Lewis cutoff [21]. That is, the Lewis cutoff, which is applied to the impact theory in an ad hoc manner, is an integral part of the one-electron theory.

Since the Weisskopf frequency, $\Delta\omega_c$, for electrons is generally much greater than the halfwidth, there should be a broad range of overlap between the regions of validity $0 \leq \Delta\omega < \Delta\omega_c$ and $\Delta\omega_{1/2} < \Delta\omega$ for the impact and one-electron theories. Nevertheless, in our derivation of the impact and one-electron theories we have tried to stress the formal connection between the two in order to provide a better understanding of their similarities as well as their differences. We feel that this is particularly important since it would be desirable to formulate a classical path theory which is valid in the line center as the impact theory is, and which makes a smooth transition to the line wings as the one-electron theory does. It is hoped that the present approach will make it possible to remove some of the approximations which currently limit these classical path theories.

9. Appendix. Collision Variables

We wish to use the natural collision coordinates in evaluating the integral

$$F_1(t) = n \int d\mathbf{v}_1 W(v_1) \int d\mathbf{x}_1 \left[\exp\left\{ -(i/\hbar) \int_0^t PV_1(\mathbf{R}, \mathbf{x}_1 + \mathbf{v}_1 t') dt' \right\} - 1 \right] \quad \text{(A.1)}$$

where

$$V_1(\mathbf{R}, \mathbf{x}_1 + \mathbf{v}_1 t') = e^2 \mathbf{R} \cdot (\mathbf{x}_1 + \mathbf{v}_1 t) / |\mathbf{x}_1 + \mathbf{v}_1 t|^3. \quad \text{(A.2)}$$

For fixed values of $\mathbf{x}_1$ and $\mathbf{v}_1$, we note that the head of the vector $(\mathbf{x}_1 + \mathbf{v}_1 t')$ traces out a straight line if t' is varied from $-\infty$ to $+\infty$. We shall call this line $L(\mathbf{x}_1, \mathbf{v}_1)$. The integral over t', in eq (A.1), will cover a segment of this line. For fixed $\mathbf{x}_1$ and $\mathbf{v}_1$, we can define a vector $\boldsymbol{\rho}_0$ from the origin of coordinates to the closest point on L; this vector will be perpendicular to $\mathbf{v}_1$. We can also define a scalar t_0 by

$$\mathbf{x}_1 = \boldsymbol{\rho}_0 + \mathbf{v}_1 t_0. \quad \text{(A.3)}$$

For a fixed $\mathbf{v}_1$, we see that, as $\mathbf{x}_1$ varies over all space, $|\mathbf{v}_1| t_0$ varies on the range $(-\infty, +\infty)$ and $\rho_0 = |\boldsymbol{\rho}_0|$ varies on the range $(0, \infty)$. We may thus change variables from $\mathbf{x}_1$ to the cylindrical coordinates (ρ_0, t_0, α) where $\mathbf{v}_1$ defines the polar direction and α is an angle which ranges from 0 to 2π. The Jacobian for this transformation is such that $\mathbf{dx}_1 \rightarrow |v_1| \rho_0 d\rho_0 dt_0 d\alpha$. In these coordinates the potential function becomes

$$V_1(\mathbf{R}, \boldsymbol{\rho}_0, \mathbf{v}_1, t' + t_0) = e^2 \mathbf{R} \cdot [\boldsymbol{\rho}_0 + \mathbf{v}_1 (t' + t_0)] / [\rho_0^2 + v_1^2 (t' + t_0)^2]^{3/2}. \quad \text{(A.4)}$$

We may express $d\mathbf{v}_1$ in spherical coordinates, $v_0^2 dv_0 \sin\beta \, d\beta \, d\gamma$, where the angles β and γ denote the orientation of $\mathbf{v}_1$ relative to the direction of $\mathbf{R}$. Since $\boldsymbol{\rho}_0$ is defined to be orthogonal to $\mathbf{v}_1$, the integrals over the Euler angles α, β, and γ average over all possible orientations of the $(\boldsymbol{\rho}_0, \mathbf{v}_1)$ frame of reference (collision axes) relative to the direction of $\mathbf{R}$. Equation (A.1) may now be written

$$F_1(t) = n \int d\Omega \int_0^\infty v_0^3 W(v_0) dv_0 \int_0^\infty \rho_0 d\rho_0 \int_{-\infty}^\infty dt_0 \left[\exp\left\{ -(i/\hbar) \int_0^t PV_1(\mathbf{R}, \boldsymbol{\rho}_0, \mathbf{v}_0, t' + t_0) dt' \right\} - 1 \right], \quad \text{(A.5)}$$

where $d\Omega = \sin\beta \, d\alpha d\beta \, d\gamma$.

It is clear that the line L represents the trajectory of a perturbing electron, v_0 is the speed of the electron, ρ_0 is the impact parameter, and t_0 is some starting time for the collision (or, if the t' limits of integration are $(-\infty, +\infty)$ in a completed collision, t_0 may be regarded as the time of closest approach). The orthogonal "collision axes" to which this collision is referenced are $\boldsymbol{\rho}_0$ and $\mathbf{v}_1$. The Euler angles Ω denote the orientation of the collision plane relative to the direction of $\mathbf{R}$; the integral over Ω may therefore be interpreted as an average over all possible orientations of the electron trajectory.

10. References and Notes

[1] Smith, E. W., Vidal, C. R., and Cooper, J., J. Res. Nat. Bur. Stand. (U.S.), **73A** (4) 389–404 (1969).

[2] Griem, H. R., Plasma Spectroscopy, chap. 4 (McGraw-Hill Book Co., Inc., New York, 1964).

[3] Baranger, M., Atomic and Molecular Processes, chap. 13, edited by D. Bates (Academic Press, Inc., New York, 1962).

[4] Baranger, M., Rand Corporation Report No. (RM-2118-AEC) ASTIA Document No. (AD-150692) (Feb. 1958).
[5] Cooper, J., Phys. Rev. Letters **17,** 991 (1966).
[6] Smith, E. W., and Hooper, C. F., Jr., Phys. Rev. **157,** 126 (1967).
[7] Schweber, Silvan S., An Introduction to Relativistic Quantum Field Theory, pp. 330–334 (Harper and Row Publishers, New York, 1962).
[8] Callaway, J., and Bauer, E., Phys. Rev. **140,** A1072 (1965).
[9] Kolb, A. C., and Griem, H. R., Phys. Rev. **111,** 514 (1962).
[10] If H_a is to remain diagonal in $|n\mathcal{A}\rangle$, it is possible to diagonalize Z only "within a principal quantum number"; that is, one may simultaneously diagonalize both H_a and PZ but not H_a and Z.
[11] Bethe, H., and Salpeter, E., Quantum Mechanics of One- and Two-Electron Atoms (Academic Press Inc., New York, 1957).
[12] Baranger, M., Phys. Rev. **111,** 494 (1958).
[13] Griem, H. R., Kolb, A. C., and Shen, K. Y., Phys. Rev. **116,** 4 (1959).
[14] Magnus, W., Comm. Pure and Appl. Math. **7,** 649 (1954) and Robinson, D. W., Helv. Phys. Acta. **36,** 140 (1963).
[15] Baranger, M., and Mozer, B., Phys. Rev. **115,** 521 (1959).
[16] Hill, T. L., Statistical Mechanics, chap. 6. (McGraw-Hill Book Co., Inc., New York, 1963).
[17] Ursell, H. D., Proc. Cambridge Phil. Soc. **23,** 685 (1927); see also eq. (9) of ref. [15]).
[18] Edmonds, A. R., Angular Momentum in Quantum Mechanics (Princeton University Press, Princeton, New Jersey, 1960).
[19] Hughes, J. W. B., Proc. Phil. Soc. **91,** 810 (1967).
[20] Griem, H. R., Baranger, M., Kolb, A. C., and Oertel, G. K., Phys. Rev. **125,** 177 (1962).
[21] Lewis, M., Phys. Rev. **121,** 501 (1960).
[22] Smith, E. W., Phys. Rev. **166,** 102 (1968).
[23] Chappell, W. R., Cooper, J., and Smith, E. W., J. Quant. Spectry. Radiative Transfer **9,** 149 (1969).
[24] Kepple, P., and Griem, H. R., Phys. Rev. **173,** 317 (1968).
[25] Bezzerides, B., J. Quant. Spectry. Radiative Transfer **7,** 353 (1967).
[26] Griem, H. R., Phys. Rev. **140,** A1140 (1965).
[27] Griem, H. R., Ap. J. **148,** 547 (1967).
[28] Smith, E. W., unpublished notes.
[29] It should be noted that some authors use the term strong collision to describe any interaction for which $(1/\hbar)\int V(t)dt \gtrsim 1$ and, for this reason, quasi-static interactions are sometimes referred to as strong collisions.
[30] From eq (4–35) of ref. [2] we see that the line shape in the impact theory (which is valid in the line center) is roughly given by the real part of $[\Delta\omega - eZ\mathscr{E}_{av}/\hbar - i\Phi_a]^{-1}$. Thus, if the matrix elements of Φ_a are larger than $(eZ_{av}\mathscr{E}_{av}/\hbar)$ the halfwidth is on the order of Φ_a. If $\Phi_a < (eZ_{av}\mathscr{E}_{av}/\hbar)$ as is usually the case, the halfwidth is determined by the average ion field splitting $(eZ_{av}\mathscr{E}_{av}/\hbar)$.
[31] Elton, R. C., and Griem, H. R., Phys. Rev. **135,** A1550 (1964).
[32] Boldt, G., and Cooper, W. S., Z. Naturforsch. **19a,** 968 (1964).

(Paper 73A4–559)

JOURNAL OF RESEARCH of the National Bureau of Standards—A. Physics and Chemistry
Vol. 73A, No. 4, July–August 1969

The Second Virial Coefficient for the Realistic Pair Potential*

Harold W. Woolley

Institute for Basic Standards, National Bureau of Standards, Washington, D.C. 20234

(April 8, 1969)

An analytical formulation for the second virial coefficient is given for a spherically symmetric potential function of a simple form which has been called a realistic pair potential. This potential, given as an inverse relationship with r as a function of U, is capable of being much softer than a Lennard-Jones in the extreme of close approach. Differing forms of the result are given, including an expression by means of the generalized hypergeometric series. The result is also expressed in terms of the second virial coefficient for the (12, 6) potential.

Key words: Hypergeometric series; London interaction; pair potential function; realistic potential; second virial coefficient; spherical potential.

One of the uses of a pair potential function is for the representation or prediction of the second virial coefficient contribution to the equation of state due to the two molecules having the specified interaction potential energy. Various potential functions have been used with some success, the most notable of which may be the Lennard-Jones (especially the 12, 6), the Morse function, and the exp-6.

In spite of the varied nature of the different functions, it is sometimes pointed out that there is so much similarity in second virial behavior for them that it is difficult to select one in preference to another on the basis of second virials alone. Even if this be true, there still may be some interest in yet another potential for which the second virial may be formulated explicitly, particularly since this formulation can be made in terms of already tabulated second virial coefficients for the (12, 6) function.

A potential function has been introduced earlier [1][1] in which the value of r/r_m is given as a function of energy for the usual $1/r^6$ type of London interaction according to the relation

$$(r/r_m)^3=\phi^{-1/2}\exp\left[-3e_1(\phi-1)-3e_2(\phi-1)^2\ldots\right]. \tag{1}$$

The quantity ϕ is related to the energy U according to the equation

$$U/\epsilon=(\phi-1)^2-1. \tag{2}$$

The range of values of ϕ is from zero for very large r where U is zero, through $\phi=1$ for $r=r_m$ where U has the value $-\epsilon$, and to very large values where U becomes very large as r becomes very small, according to the expected pattern of behavior.

The second viral coefficient may for the present simple case of a spherical potential function be written as

$$B=N_0\int_0^\infty (1-\exp(-U/kT))\,.\,2\pi r^2 dr \tag{3}$$

if the pair is composed of like molecules. Integration by parts transforms the integral to

$$B=(2\pi/3)\,(N_0/kT)\int_0^\infty [r^3]\exp(-U/kT)\,dU, \tag{4}$$

where the quantity $[r^3]$ is a function of U and represents the simple r^3 value in the positive energy region but represents the difference of r^3 for the repulsion side of the potential valley minus r^3 for the attractive side if the potential energy is negative. This double-valued character is removed if the variable ϕ is introduced, since the integral then is

$$B=(2\pi/3)N_0(2\epsilon/kT)\int_0^\infty r^3\exp[-(\phi^2-2\phi)\epsilon/kT](\phi-1)\,d\phi \tag{5}$$

with ϕ advancing simply from zero to infinity and with r^3 having its ordinary algebraic meaning.

If we now introduce the present potential in the form

*This research was supported in part by the United States Air Force.

[1] Figures in brackets indicate the literature references at the end of this paper.

$$(r/r_m)^3=\phi^{-1/2}\exp(-a\phi^2-b\phi+c) \tag{6}$$

where $a=3e_2$, $b=3e_1-6e_2$, and $c=3e_1-3e_2$, we have, with T^* for kT/ϵ,

$$B=(2\pi/3)N_0r_m^3(2/T^*)\int_0^\infty \exp[c-(b-2/T^*)\phi - (a+1/T^*)\phi^2](\phi-1)\phi^{-1/2}d\phi \tag{7}$$

Expansion of the exponential involving the first power of ϕ using $\beta=b+2/T^*$ and $\alpha=a+1/T^*$ gives

$$B=(2\pi/3)N_0r_m^3(2/T^*)\int_0^\infty \exp[c-\alpha\phi^2] \sum_{n=0}^{\infty}\frac{\beta^n\phi^n}{n!}(\phi-1)\phi^{-1/2}d\phi. \tag{8}$$

The substitution of x for ϕ^2 puts the result in the form

$$B=(2\pi/3)N_0r_m^3(e^c/T^*)\sum_{n=0}^{\infty}\frac{\beta^n}{n!} \int_0^\infty e^{-\alpha x}(x^{n/2-1/4}-x^{n/2-3/4})dx \tag{9}$$

or

$$B=(2\pi/3)N_0r_m^3(e^c/T^*)\sum_{n=0}^{\infty}\frac{\beta^n}{n!} [\alpha^{-n/2-3/4}\Gamma(n/2+3/4)-\alpha^{-n/2-1/4}\Gamma(n/2+1/4)]. \tag{10}$$

This can be written as $B=b_m$. (B/b_m) with $b_m=(2\pi/3)N_0r_m^3$, and

$$B/b_m=(e^c/T^*)\left[\alpha^{-3/4}\sum_{n=0}^{\infty}\Gamma(n/2+3/4)(4/T^{**})^{n/2}/n! -\alpha^{-1/4}\sum_{n=0}^{\infty}\Gamma(n/2+1/4)(4/T^{**})^{n/2}/n!\right] \tag{11}$$

where T^{**} is an abbreviation for $4\alpha/\beta^2$.

Another formulation can be given by which the summations may be avoided by various relationships according to which the first summation is equal to

$$-(\sqrt{2})(T^{**})^{5/4}[(3/8)B^*(T^{**})+4B_1^*(T^{**})+2B_2^*(T^{**})]$$

and the second is

$$-\frac{\sqrt{2}}{2}(T^{**})^{3/4}[B^*(T^{**})+4B_1^*(T^{**})],$$

where B^*, B_1^*, and B_2^* are the usually tabulated second virial coefficients and dimensionless derivatives for the Lennard-Jones (12, 6) potential function.

Using these, (11) can be written

$$\frac{B}{b_m}=-\frac{e^c}{T^*}\alpha^{-1/4}(T^{**})^{3/4}\sqrt{2}\{(1/2+\tfrac{3}{8}\alpha^{-1/2}T^{**1/2})B^*(T^{**})+(2+4\alpha^{-1/2}T^{**1/2})B_1^*(T^{**})+2\alpha^{-1/2}T^{**1/2}B_2^*(T^{**})\} \tag{12}$$

or as

$$B/b_m=-\frac{e^c}{[2-bT^*]^2}\sqrt{\frac{1+aT^*}{2-bT^*}} \{[4+(3-2b)T^*]B^*(T^{**}) +8[2+(4-b)T^*]B_1^*(T^{**})+16T^*B_2^*(T^{**})\} \tag{13}$$

Another arrangement of the result can be arrived at in the following way. If the second sum in the expression for B/b_m is written out in detail through several terms, it is possible to recognize that there is a relation to the generalized hypergeometric function and the confluent hypergeometric function in particular. With τ representing $(4/T^{**})^{1/2}$, the summation becomes

$$\Gamma(1/4)[{}_1F_1(1/4;1/2;\tau^2/4)] +\Gamma(3/4)[{}_1F_1(3/4;3/2;\tau^2/4)]. \tag{14}$$

which also has a relationship to Bessel functions [2] We further note that if the ordinary hypergeometric function $F(\alpha,\beta;\gamma;\xi)$ with $\xi=\eta/\beta$ is considered and the limit taken as $\beta^{-1}\to 0$, the result is found to be ${}_1F_1(\alpha;\gamma;\eta)$. A function equivalent to the original hypergeometric function according to a standard relation is $(1-\xi)^{\gamma-\alpha-\beta}F(\gamma-\alpha,\gamma-\beta;\gamma;\xi)$. A similar use of $\xi=\eta/\beta$ and a passing to the limit $\beta^{-1}\to 0$ produces an equivalent form $e^{\eta}{}_1F_1\ (\gamma-\alpha;\gamma;-\eta)$. Then for the case with $\alpha=\frac{1}{2}\gamma$ the equating of the two expressions leads to

$$e^{-\eta/2}{}_1F_1(\tfrac{1}{2}\gamma;\gamma;\eta)=e^{\eta/2}{}_1F_1(\tfrac{1}{2}\gamma;\gamma;-\eta); \tag{15}$$

from which it is evident that both expressions, on either side of the equation, are even functions of η. It would appear plausible that a series involving even powers only would need half as many terms to attain a given quality of approximation as a related one with both odd and even powers. Thus, we would presume that a more rapidly convergent form for the result should exist and might be looked for. For this purpose we examine the differential equation [2]

$$\alpha y=(\gamma-x)y'+xy'', \tag{16}$$

for which $y={}_1F_1(\alpha;\gamma;x)$ is known to be a solution. For the special case with $\alpha=\frac{1}{2}\gamma$, if we use $z=e^{-x/2}y$ or $y=e^{x/2}z$ and substitute into the differential equation, we obtain

$$xz''+\gamma z'-\tfrac{1}{4}xz=0 \tag{17}$$

Solution in series by the method of Frobenius gives

$$z=1+\frac{1}{1\cdot\delta}\left(\frac{x}{4}\right)^2+\frac{1}{1\cdot2\cdot\delta(\delta+1)}\left(\frac{x}{4}\right)^4+\frac{1}{1\cdot2\cdot3\cdot\delta(\delta+1)(\delta+2)}\left(\frac{x}{4}\right)^6+\cdots \quad (18)$$

or

$$z={}_0F_1\left(\delta;\left(\frac{x}{4}\right)^2\right), \quad (19)$$

where $\delta=(1+\gamma)/2$, according to the notation [3] for the generalized hypergeometric series.

In summary, the final series obtained may be substituted into the earlier expressions with the result that the second virial coefficient may be obtained from

$$B/b_m=e^c T^{**-1}[\alpha^{-3/4}Y_1(\tau)-\alpha^{-1/4}Y_0(\tau)] \quad (20)$$

where

$$Y_0(\tau)=[\Gamma(1/4)\,{}_0F_1(3/4;\tau^4/256)+\Gamma(3/4)\tau\,{}_0F_1(5/4;\tau^4/256)]\exp(\tau^2/8) \quad (21)$$

with $Y_1(\tau)$ obtainable by differentiation according to $Y_1(\tau)=dY_0(\tau)/d\tau$, and with $\tau=(4/T^{**})^{1/2}$.

It may be seen that this particular hypergeometric function has a simple rule for differentiation; namely,

$$d[{}_0F_1(a;x)]/dx=a^{-1}\,{}_0F_1(a+1;x). \quad (22)$$

Thus a procedure may be found to evaluate B/b_m and any of its derivatives which are of interest.

References

[1] Woolley, H. W., J. Chem. Phys. **37**, 1307 (1962).

[2] Ince, E. L., Ordinary Differential Equations [Longmans, Green and Co., 1926] (Dover Publications, Inc., p. 180, 1956).

[3] Bateman Manuscript Project, Higher Transcendental Functions, Vol. 1, p. 182, A. Erdely, Ed. (McGraw-Hill Book Company, Inc., New York, 1953).

(Paper 73A4–560)

JOURNAL OF RESEARCH of the National Bureau of Standards—A. Physics and Chemistry
Vol. 73A, No. 4, July-August 1969

Synthesis of Barium Ferrates in Oxygen

Taki Negas and Robert S. Roth

Institute for Materials Research, National Bureau of Standards, Washington, D.C. 20234

(April 9, 1969)

Phase relations in the system BaO—Fe_2O_3—"FeO_2" at 1 atm (1 atm = 1.013×10^5 N/m^2) oxygen and between 800 to 1050 °C are shown in the vicinity (high Ba portion) of the 1:1 cation-cation ratio composition. A hexagonal $BaTiO_3$-like phase, $BaFeO_{3-X}$ ($a = 5.676$ Å, $c = 13.934$ Å), exists below 960 °C. A perovskite-like phase $BaFeO_{3-X'}$ occurs between 960 and 1050 °C. Single-phase tetragonal perovskite can be obtained at room temperature by quenching compositions with Ba-Fe ratios of 67:66 ($a = 3.985$ Å, $c = 4.005$ Å, 1000 °C) and 27:26 ($a = 3.988$ Å, $c = 4.003$ Å, 1000 °C) from above 960 °C. At the 17:16 ratio, single phase cubic perovskite ($a = 3.994$ Å, 1000 °C), can be synthesized. Influence of temperature, additions of barium, and use of Pt-containers on phase relations are discussed.

Key words: Ferrates; hexagonal barium ferrate; perovskite; phase equilibria; tetravalent iron.

1. Introduction

Mixed alkaline earth-transition metal oxides are of particular importance because of their interesting electrical and magnetic properties. Characterization of such materials through phase equilibrium and x-ray diffraction studies is complicated by the tendency of the transition metal to exist in disproportioned oxidation states within a single phase. Variable oxygen stoichiometries, controlled by temperature and oxygen pressure result. The 1:1 cation-cation barium ferrates are excellent examples of this phenomenon. Tetravalent iron has been confirmed in phases within the $BaFeO_{2.5-3.0}$ compositional range by MacChesney et al. [1][1], and Gallagher et al. [2], using magnetic studies and the Mössbauer technique. Some inconsistencies, however, exist concerning the nature of the phases within this compositional range. Erchak et al. [3], reported the compound $BaFeO_{2.62}$ ($Ba_8Fe_2^{4+}Fe_6^{3+}O_{21}$) which was thought to be a cubic perovskite ($a = 8.05$ Å). Subsequently, Malinofsky and Kedesdy [4] showed that this phase is not cubic, but is actually analogous to the hexagonal polymorph of $BaTiO_3$ [5] with $a = 5.68$ Å and $c = 13.86$ Å. They also reported a tetragonal perovskite polymorph, admixed with the hexagonal form, with $a = 3.98$ Å and $c = 4.01$ Å. This mixture was prepared by heating the hexagonal form at 1275 °C in oxygen and slow-cooling. MacChesney, et al. [1], and Gallagher, et al. [2], prepared hexagonal forms in the $BaFeO_{2.74-2.95}$ range using oxygen pressures from 0.2 to 2400 atm and generally below 850 °C. Gushee et al. [6], reported a $BaFeO_{2.72}$ hexagonal form with $a = 5.76$ Å and $c = 13.9$ Å while Goto and Takada [7] synthesized a $2BaO \cdot Fe_2O_3$ phase with a melting point at 1370 °C in 1 atm O_2. The latter phase was reported as cubic ($a = 8.07$ Å) but is most likely a hexagonal barium ferrate similar to that reported by Erchak et al. [3], and originally thought to be a cubic perovskite with $a' = 2a_{cub}$.

Mori [8, 9] reported a number of $BaFeO_{3-X}$ phases with X values ranging from 0.50 to 0.10. These were prepared in air and 1 atm oxygen using quenching and slow-cooling techniques within the 25 to 1080 °C range. A hexagonal $BaTiO_3$-like phase was found by quenching from below 950 °C in oxygen. Above this temperature a transitory cubic form was obtained after a ½-hr heating time. With longer heating times this form converted to a triclinic form through a rhombohedral form. Heating a $2BaCO_3$:Fe_2O_3 mixture at 1080 °C in oxygen for ½-hr and quenching also produced a cubic form, $BaFeO_{2.75}$, which upon further heating converted to a tetragonal phase, $BaFeO_{2.81}$, through a series of tetragonal phases with lower oxygen contents. The $BaFeO_{2.81}$ phase was not of the simple tetragonal perovskite type as its powder pattern gave evidence of superstructure lines. Final equilibration products were not indicated and difficulty was encountered in reproducing each phase, in terms of symmetry and oxygen content, by the quenching method.

Although the existence of the hexagonal form is well documented, synthesis of a stable single-phase tetragonal perovskite or a stable, truly cubic perovskite has not been demonstrated. This study was conducted

[1] Figures in brackets indicate the literature references at the end of this paper.

to examine the latter possibility and, therefore, considers only the existence and stabilities of phases encountered. Chemical analyses establishing Fe^{4+}:Fe^{3+} ratios (oxygen concentration) and Mössbauer data will be reported in the future.

2. Experimental Procedure

Starting material was prepared from appropriately weighed (±0.1 mg) quantities of $BaCO_3$ and Fe_2O_3. These were hand mixed under acetone, packed in gold envelopes, and calcined in air at 800 °C for two weeks with periodic remixing and reheating. Gold was used as the container instead of platinum because of the tendency of uncombined $BaCO_3$ to react with the latter. Another problem with platinum will be discussed later. Calcined specimens were equilibrated at elevated temperatures in 1 atm (1 atm = 1.013×10^5 N/m^2) oxygen using the quench method. A vertical tube, resistance type, furnace, modified for vacuum and gas flow capability with end-closures and "O"-ring seals, was used for the quenching experiments. Oxygen was passed through the furnace at 10^{-6} m^3/s flow rate. Open gold envelopes were used as containers to 1050 °C. A few experiments were conducted above 1050 °C using platinum. Temperatures were measured with Pt-Pt 10 percent Rh thermocouples calibrated against the melting points of NaCl (801 °C) and Au (1063 °C). The furnace was controlled by an a-c Wheatstone bridge controller capable of maintaining temperature to at least ±2 °C. Specimens were quenched into an ice-cooled brass cold finger which constitutes the lower portion of the furnace. X-ray patterns were made using a high-angle Geiger counter-diffractometer and nickel-filtered Cu radiation at a 1/4° 2θ/min scanning rate. Reported unit cell data are considered accurate to about ±2 in the last decimal place listed.

3. Experimental Results

A portion of the BaO-"iron oxide" pseudobinary in the vicinity (high baria portion) of the 1:1 cation-cation compound is shown in figure 1. The diagram was constructed from the data in table 1. It is emphasized that the diagram represents stability of phases present (determined by room temperature x-ray patterns) as a function of starting Ba:Fe ratio. Absolute compositions involving Ba:Fe^{4+}:Fe^{3+} ratios belonging to the BaO—Fe_2O_3—"FeO_2" ternary are not indicated.

The 1:1 hexagonal $BaTiO_3$-like phase, $BaFeO_{3-X}$ ($a = 5.676$ Å, $c = 13.934$ Å), exists at low temperatures as previously observed by others. An indexed powder pattern is provided in table 2. MacChesney et al. [1], reported the hexagonal form, $BaFeO_{2.82}$ and $BaFeO_{2.84}$, at low temperatures in 1 atm O_2 and air, respectively. The value of X for the $BaFeO_{3-X}$ in this study is, therefore, probably within the 0.20–0.15 range. Above approximately 960° C the phase transforms to a perovskite-like form, probably by further

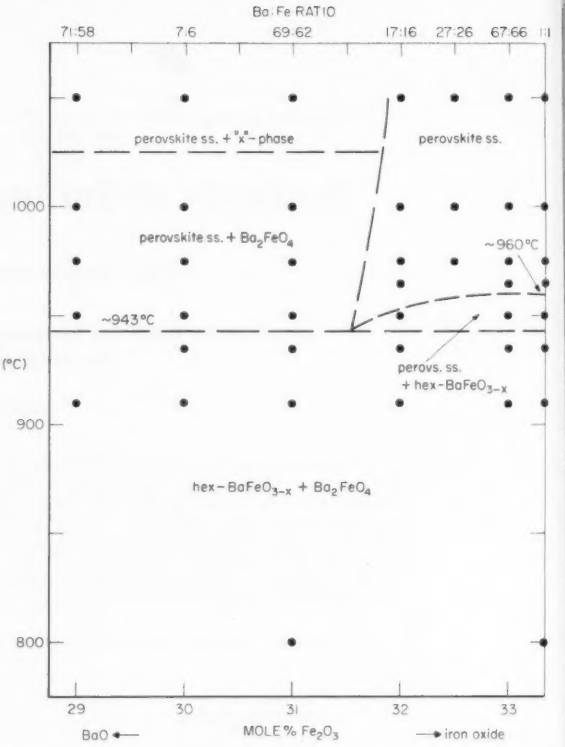

FIGURE 1. *Subsolidus relations at 1 atm O_2 for that portion of the* BaO-*"iron oxide" pseudobinary near the 1:1 barium-iron ratio.*

Absolute Ba-Fe-O concentrations are not indicated.

reduction of part of the available Fe^{4+} to Fe^{3+}. The powder pattern, given in table 3, bears a superficial resemblance to a tetragonal perovskite but is rather diffuse and contains a number of extra lines. This phase may be represented as $BaFeO_{3-X'}$, where $0.5 > X' > 0$ and $X' > X_{hex}$, where X_{hex} refers to the oxygen deficiency in the hexagonal form. It is not $Ba_2Fe_2O_5$, ($BaFeO_{2.5}$, $X' = 0.5$), a brownmillerite-like compound also reported by MacChesney et al. [1]. Within this temperature range, however, a $Ba_2Fe_2O_5$-like phase was found to exist in air. Although the transformation near 960 °C in this study correlates well with that observed by Mori [9] (> 950 °C), a definitive correlation of phases could not be made. It seems very likely, however, that Malinofsky and Kedesdy [4] observed the $BaFeO_{3-X'}$ of this study or one of the tetragonal phases reported by Mori when they heated and slow-cooled the hexagonal form from 1275 °C in oxygen.

Hexagonal $BaFeO_{3-X}$ does not appear to form solid solutions in the high baria portion of the system below 960 °C. Changes in oxygen stoichiometry may occur as a function of temperature to 960 °C. Cell parameters, however, do not change from 800 to 960 °C and it is, therefore, expected that change in oxygen concentration within this temperature range is limited. Below approximately 943 °C, the phase assemblage consists

TABLE 1. *Experimental data for compositions in the system* BaO-"*iron oxide*" *at 1 atm oxygen*

Composition	Heat treatments				X-ray diffraction analyses [a]
	Initial [b]		Final [c]		
	Temp.	Time	Temp.	Time	
Ba:Fe ratio	°C	*hr*	°C	*hr*	
1:1	800	335			
			800	70	Hex-$BaFeO_{3-x}$ $a=5.676$ $c=13.934$
			910	70	Hex-$BaFeO_{3-x}$ $a=5.676$ $c=13.934$
			935	45	Hex-$BaFeO_{3-x}$ $a=5.676$ $c=13.934$
			950	70	Hex-$BaFeO_{3-x}$ $a=5.676$ $c=13.934$
			965	45	Hex-$BaFeO_{3-x}$ + $BaFeO_{3-x'}$ [d]
			975	70	$BaFeO_{3-x'}$
			1000	70	$BaFeO_{3-x'}$
			1050	70	$BaFeO_{3-x'}$
67:66	800	335			
			910	70	Hex-$BaFeO_{3-x}$ [e]
			935	45	Hex-$BaFeO_{3-x}$ [e]
			950	70	Hex-$BaFeO_{3-x}$ + perovskite
			965	45	t. p.[f]
			975	70	t. p. $a=3.984$ $c=4.005$
			1000	70	t. p. $a=3.985$ $c=4.005$
			1050	70	t. p. $a=3.987$ $c=4.004$
27:26	800	335			
			975	70	t. p. $a=3.986$ $c=4.003$
			1000	70	t. p. $a=3.988$ $c=4.003$
			1050	70	t. p. $a=3.992$ $c=4.001$
17:16	800	335			
			910	70	Hex-$BaFeO_{3-x}$ + Ba_2FeO_4
			935	45	Hex-$BaFeO_{3-x}$ + Ba_2FeO_4
			950	70	c. p.[g] + Hex-$BaFeO_{3-x}$
			965	45	c. p.
			975	70	c. p. $a=3.993$
			1000	70	c. p. $a=3.994$
			1050	70	c. p. $a=3.997$
69:62	800	335			
			800	70	Hex-$BaFeO_{3-x}$ + Ba_2FeO_4
			910	70	Hex-$BaFeO_{3-x}$ + Ba_2FeO_4
			935	45	Hex-$BaFeO_{3-x}$ + Ba_2FeO_4
			950	70	c. p. + Ba_2FeO_4 + Hex-$BaFeO_{3-x}$ [h]
			975	70	c. p. ($a=3.992$) + Ba_2FeO_4
			1000	70	c. p. ($a=3.993$) + Ba_2FeO_4
			1050	70	c. p. ($a=3.996$) + unknown phase "*X*"
7:6	800	335			

TABLE 1. *Experimental data for compositions in the system* BaO-"*iron oxide*" *at 1 atm oxygen*—Continued

Composition	Heat treatments				X-ray diffraction analyses [a]
	Initial [b]		Final [c]		
	Temp.	Time	Temp.	Time	
Ba:Fe ratio	°C	*hr*	°C	*hr*	
			910	70	Hex-$BaFeO_{3-X}$ + Ba_2FeO_4
			935	45	Hex-$BaFeO_{3-X}$ + Ba_2FeO_4
			950	70	c. p. + Ba_2FeO_4 + Hex-$BaFeO_{3-X}$ [h]
			975	70	c. p. + Ba_2FeO_4
			1000	70	c. p. + Ba_2FeO_4
			1050	70	c. p. + unknown phase "*X*"
71:58	800	335			
			910	70	Hex-$BaFeO_{3-X}$ + Ba_2FeO_4
			950	70	c. p. + Ba_2FeO_4
			975	70	c. p. + Ba_2FeO_4
			1000	70	c. p. + Ba_2FeO_4
			1050	70	c. p. + unknown phase "*X*"

[a] Phases identified are given in the order of amount present at room temperature. The phases are not necessarily those present at the temperature to which the specimen was heated.
[b] Heated in air in Au.
[c] Heated in 1 atm oxygen in Au.
[d] Perovskite-like phase.
[e] Ba_2FeO_4 in insufficient amount to detect.
[f] t. p. = tetragonal perovskite.
[g] c. p. = cubic perovskite.
[h] Incomplete reaction.

TABLE 2. *X-ray diffraction powder data for the hexagonal* $BaTiO_3$*-like phase,* $BaFeO_{3-x}$ [a]

d_{obs} [b]	I/I_0 [c]	$\frac{1}{d^2_{calc}}$	$\frac{1}{d^2_{obs}}$	*hkl* [d]
4.017	9	0.0620	0.0620	102
3.376	23	.0877	.0878	103
2.838	100	.1238	.1242	104
		.1242		110
2.421	13	.1705	.1706	113
		.1707		201
2.322	15	.1854	.1855	006
2.318	17	.1861	.1861	202
2.173	21	.2119	.2119	203
2.009	28	.2479	.2479	204
1.8433	12	.2943	.2943	205
		.2948		211
1.7954	8	.3103	.3102	212
1.7251	7	.3361	.3361	213
1.6388	28	.3721	.3724	214
		.3725		300
1.5457	8	.4185	.4186	215
		.4188		303
1.4837	[e] 2	.4538	.4543	118
		.4549		304
1.4765	5	.4586	.4587	109
1.4209	7	.4952	.4953	208
1.4190	12	.4966	.4966	220
1.3573	5	.5429	.5428	223
1.3389	[e] 3	.5564	.5578	1, 0, 10
		.5579		306
		.5586		312
1.3084	6	.5844	.5842	313
1.2696	8	.6204	.6204	314
1.2242	3	.6673	.6673	401
1.2106	6	.6820	.6824	226
		.6828		402
1.1881	4	.7085	.7085	403
1.1589	4	.7446	.7446	404
1.1245	3	.7909	.7909	405
1.0727	8	.8691	.8691	410

[a] Prepared at 910 °C, 1 atm O_2.
[b] Interplanar spacing, A.
[c] Observed intensity.
[d] Indexed on the basis of a hexagonal cell with $a = 5.676$ Å and $c = 13.934$ Å.
[e] Broad.

TABLE 3. *X-ray diffraction powder data for the perovskite-like phase,* $BaFeO_{3-X}$ [a]

line	d [b]	I/I_0 [c]
1	4.09	[d] 2
2	4.01	6
3	3.98	7
4	2.91	[d] 9
5	2.86	[d, e] 7
6	2.82	100
7	2.31	4
8	2.30	15
9	2.02	[d] 3
10	2.00	9
11	1.989	15
12	1.789	4
13	1.781	4
14	1.633	10
15	1.627	18
16	1.413	11
17	1.408	[d] 8

[a] Prepared at 1000 °C, 1 atm O_2.
[b] Interplanar spacing, Å.
[c] Observed intensity.
[d] Broad.
[e] Appears only after long exposure to air.

of hex-$BaFeO_{3-X}$ and Ba_2FeO_4. The latter phase is extremely sensitive to moisture and tends to deteriorate when exposed to air and during x-ray analysis. The compound was made from a $4BaCO_3$:Fe_2O_3 mixture at 900 °C in air and at 900 °C in 1 atm O_2. A portion of its powder pattern, indexed by analogy with K_2SO_4 is given in table 4. The phase is orthorhombic with $a = 5.93$ Å, $b = 10.36$ Å, and $c = 7.64$ Å.

Above 943 °C, phase assemblages are quite interesting, as true perovskite-like phases appear. At the 67:66 Ba:Fe ratio single-phase tetragonal perovskites may be quenched from 960 to 1050 °C. The indexed powder

TABLE 4. *X-ray diffraction powder data for the compound,* Ba_2FeO_4 [a]

d_{obs} [b]	I/I_0 [c]	$\frac{1}{d^2_{calc}}$	$\frac{1}{d^2_{obs}}$	hkl [d]
4.279	10	0.0544	0.0546	021
		.0549		111
3.824	12	.0685	.0684	002
3.581	12	.0779	.0780	012
3.474	64	.0828	.0829	121
3.211	33	.0970	.0970	102
3.149	21	.1010	.1009	031
3.069	100	.1058	.1062	022
		.1063		112
2.985	91	.1123	.1122	130
2.964	71	.1138	.1138	200

[a] Prepared at 900 °C in air.
[b] Interplanar spacing, Å.
[c] Observed intensity.
[d] Indexed on the basis of an orthorhombic cell with $a = 5.93$ Å, $b = 10.36$ Å, $c = 7.64$ Å.

pattern of a typical tetragonal phase is given in table 5. Single-phase tetragonal perovskites can also be quenched from above 960 °C at the 27:26 Ba:Fe ratio. Tetragonal perovskites at the 67:66 ratio transform to cubic on heating near 75 °C while those at the 27:26 ratio transform near 45 °C. Single phase cubic perovskites are obtained at room temperature at the 17:16 Ba:Fe ratio. An indexed pattern of a typical cubic phase is given in table 6. Figure 2 shows the variation of room temperature-determined cell parameters with temperature and composition from 975 to 1050 °C. Compositions more BaO-rich than 17:16 yield cubic perovskite solid-solution plus Ba_2FeO_4 between

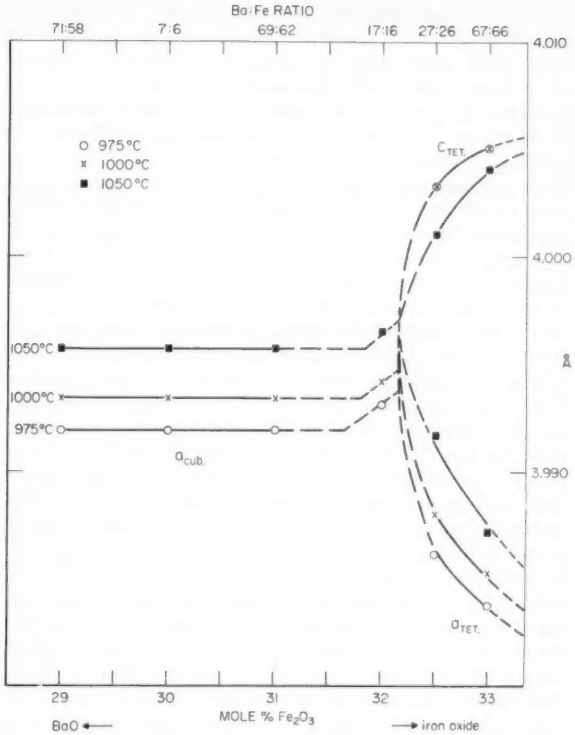

FIGURE 2. *Variation of room temperature-determined cell parameters with temperature and composition for cubic and tetragonal barium-iron perovskites.*

TABLE 5. *X-ray diffraction data for the tetragonal perovskite at the 67:66* Ba-Fe *ratio* [a]

d_{obs} [b]	I/I_0 [c]	$\frac{1}{d^2_{calc}}$	$\frac{1}{d^2_{obs}}$	hkl [d]
4.003	8	0.0624	0.0624	001
3.981	12	.0630	.0631	100
2.824	100	.1253	.1254	101
2.818	90	.1259	.1259	110
2.304	29	.1883	.1884	111
2.002	13	.2494	.2494	002
1.9922	26	.2519	.2520	200
1.7892	4	.3124	.3124	102
1.7836	7	.3142	.3143	201
1.7823	5	.3148	.3148	210
1.6321	18	.3754	.3754	112
1.6281	35	.3772	.3772	211
1.4124	13	.5013	.5013	202
1.4090	14	.5037	.5038	220
1.3349	4	.5612	.5612	003
1.3284	4	.5667	.5667	300
1.2657	6	.6242	.6242	103
1.2606	10	.6290	.6293	301
		.6296		310
1.2064	4	.6871	.6872	113
1.2021	5	.6920	.6921	311
1.1524	7	.7531	.7531	222
1.0684	6	.8760	.8760	213
1.0666	10	.8791	.8791	312
1.0655	8	.8809	.8809	321

[a] Prepared at 1000 °C, 1 atm O_2.
[b] Interplanar spacing, Å.
[c] Observed intensity.
[d] Indexed on the basis of a tetragonal cell with $a = 3.985$ Å, $c = 4.005$ Å.

TABLE 6. *X-ray powder diffraction data for the cubic perovskite at the 17:16* Ba-Fe *ratio* [a]

d_{obs} [b]	I/I_0 [c]	$\frac{1}{d^2_{calc}}$	$\frac{1}{d^2_{obs}}$	hkl [d]
3.994	13	0.0627	0.0627	100
2.824	100	.1254	.1253	110
2.306	23	.1880	.1880	111
1.9972	34	.2507	.2507	200
1.7862	8	.3134	.3134	210
1.6308	37	.3761	.3760	211
1.4122	17	.5014	.5015	220
1.3315	4	.5641	.5641	300
1.2631	12	.6268	.6268	310
1.2043	5	.6895	.6895	311
1.1530	6	.7522	.7522	222
1.0675	13	.8775	.8775	321
0.99858	3	1.0029	1.0029	400
.96875	3	1.0656	1.0656	410/322
.94146	5	1.1283	1.1282	411/330
.91635	3	1.1910	1.1909	331
.89313	5	1.2536	1.2537	420

[a] Prepared at 1000 °C, 1 atm O_2.
[b] Interplanar spacing, Å.
[c] Observed intensity.
[d] Indexed on the basis of a cubic cell with $a = 3.994$ Å.

943° and about 1025 °C. Above 1025 °C an unknown phase exists with the perovskite and is characterized by the appearance of lines with $d = 4.19$, 3.84, 3.66, 3.23, 3.12, and 2.97 Å in the low angle region. Variation of cell parameters as a function of cation-cation

ratio and temperature in the limited homogeneity region is a complex feature which can be deciphered only with knowledge of accurate Fe^{4+}:Fe^{3+} ratios. At a fixed ratio, cell expansion with increasing temperature is probably a result of increased reduction of Fe^{4+} to Fe^{3+} with a corresponding decrease in oxygen content. Changes with cation-cation ratio at fixed temperature may be much more complicated than merely being due to variation in barium content. Increasing barium appears to cause expansion of a_{tet} and contraction of c_{tet} and a_{cubic} at fixed temperature in the single-phase region. Furthermore, it is highly unlikely that a stable perovskite structure can accommodate interstitial barium. At 1000 °C, the single-phase cubic perovskite, for example, contains an excess of about 1.3 mol percent BaO (in terms of BaO:Fe_2O_3) and its composition might be described as $Ba_{17}Fe_{16}O_N$ where $N=49-X$. This may be more appropriately written as $BaFe_{16/17}O_{N/17}$ which now indicates iron and oxygen vacancies rather than barium interstitials. The value of X will, of course, depend on the Fe^{4+}:Fe^{3+} ratio in the phase. Starting at the $BaFeO_{3-X'}$ phase, increasing amounts of barium at constant temperature will tend to increase the concentration of iron and oxygen vacancies. Increasing iron and $O^{=}$ vacancies should tend to expand the structure. Although unit cell volumes increase initially with increasing barium content, the apparent a cubic contraction associated with single phases from near the 17:16 ratio to the two phase region suggests a second mechanism operating simultaneously. A plausible hypothesis involves the general equilibrum

$$2Fe^{3+}+\tfrac{1}{2}O_2 \rightarrow 2Fe^{4+}+O^{2-}.$$

Physically, this mechanism would operate in the following manner. As iron and $O^{=}$ vacancies are created by addition of barium, the concentration level of the $O^{=}$ vacancies would be decreased if some of the available Fe^{3+} is oxidized to Fe^{4+}. The total number of iron vacancies would not be affected but the Fe^{4+}:Fe^{3+} ratio, and consequently $O^{=}$ concentration, would increase. Cell contraction, as observed, might result.

Data pertinent to temperatures above 1050 °C could not be obtained in this study because of problems with container materials. Above the melting point of Au, platinum tubes were used as containers for equilibration runs. In gold, hex-$BaFeO_{3-X}$ is not stable above 960 °C and 1 atm O_2. In platinum, however, a hexagonal $BaFeO_{3-X}$-like phase does exist above 960 °C and persists at elevated temperatures to at least 1300 °C. The phase is normally admixed with perovskite-like material but tends to predominate with increasing firing time. Consistent and reproducible equilibria data are difficult to obtain. It is hardly likely that hex-$BaFeO_{3-X}$ converts at 960 °C to perovskite-like $BaFeO_{3-X'}$ which in turn transforms at some temperature > 1050 °C back to a hex-$BaFeO_{3-X''}$ phase. This is apparent, especially in view of the data of MacChesney et al. [1], suggesting the existence of an orthorhombic brownmillerite-like $Ba_2Fe_2O_5$ which might be expected to form at sufficiently elevated temperatures in O_2. Goto and Takada [7] using Pt containers and 1 atm O_2 reported a cubic $2BaO \cdot Fe_2O_3$ phase with a melting point near 1370 °C. As pure $Ba_2Fe_2O_5$ is not cubic and the reported $a=8.07$ Å parameter is approximately $2 \times a_{cubic}$ perovskite, a value which may be used to index a hexagonal $BaTiO_3$-like phase, the compound was probably erroneously identified. It is likely that the phase observed was of the hex-$BaFeO_{3-X}$ type. More interesting, however, is the stability of the compound to a congruent melting point in 1 atm O_2 and the exclusion of a stability range for a perovskite-like $BaFeO_{3-X'}$. These reported data and the inconsistent data above 1050 °C in this study have but one common denominator, platinum containers. It is, therefore, suggested that in the presence of Pt, a reaction occurs resulting in the stabilization of a hexagonal $BaTiO_3$-like phase containing Pt^{4+}. Hexagonal phases containing Pt^{4+} are not unusual and have been reported by Dickinson et al. [10], Blattner et al. [11], and Stratton [12]. If platinum does indeed tend to stabilize the hexagonal form, it is not surprising that the cubic and tetragonal high temperature perovskites herein reported have not been previously observed, as most experiments involving synthesis of materials are conducted using Pt-containers. Furthermore, chemical analyses for Fe^{4+}:Fe^{3+} ratios, when Pt is present, would lead to erroneous oxygen ion concentrations.

4. Summary

Phase relations in the BaO-"iron oxide" pseudobinary in the vicinity of the 1:1 cation-cation ratio were determined in 1 atm 0_2 and between 800 to 1050 °C. Below 960 °C a hex-$BaTiO_3$-like phase, $BaFeO_{3-X}$ exists. Above 960 °C, this phase transforms to a perovskite-like $BaFeO_{3-X'}$. Specimens quenched from the 960 to 1050 °C range and having Ba:Fe ratios of 67:66 and 27:26 yield single-phase tetragonal perovskite at room temperature. Single-phase cubic perovskite can be quenched from this temperature range at the 17:16 ratio. Hex-$BaTiO_3$-like phases were observed in specimens heated above 1050 °C in Pt-containers. These are considered to be products of a Pt-specimen reaction.

5. References

[1] MacChesney, J. B., Potter, J. F., Sherwood, R. C., and Williams, H. J., J. Chem. Phys. **43,** 3317 (1965).
[2] Gallagher, P. K., MacChesney, J. B., and Buchanan, D. N. E., J. Chem. Phys. **43,** 516 (1965).
[3] Erchak, M., Fankuchen, T., and Ward, R., J. Am. Chem. Soc. **68,** 2085 (1946).
[4] Malinofsky, W. W., and Kedesdy, H., J. Am. Chem. Soc. **76,** 3090 (1954).
[5] Burbank, R. D., and Evans, H. T., Acta Cryst. **1,** 330 (1948).
[6] Gushee, B. E., Katz, L., and Ward, R., J. Am. Chem. Soc. **79,** 5601 (1957).
[7] Goto, Y., and Takada, T., J. Am. Ceram. Soc. **43,** 150 (1960).
[8] Mori, S., J. Am. Ceram. Soc. **48,** 165 (1965).
[9] Mori, S., J. Am. Ceram. Soc. **49,** 600 (1966).
[10] Dickinson, J. G., Katz, L., and Ward, R., J. Am. Chem. Soc. **83,** 3026 (1961).
[11] Blattner, H., Gränicher, H., Kanzig, W., and Merz, W., Helv. Phys. Acta **21,** 341 (1948).
[12] Stratton, W. O., J. Chem. Phys. **19,** 33 (1951).

(Paper 73A4–561)

JOURNAL OF RESEARCH of the National Bureau of Standards—A. Physics and Chemistry
Vol. 73A, No. 4, July-August 1969

The System SrO— "Chromium Oxide" in Air and Oxygen

Taki Negas and Robert S. Roth

Institute for Materials Research, National Bureau of Standards, Washington, D.C. 20234

(April 25, 1969)

Phase relations in the system SrO-"chromium oxide" were determined in air and 1 atm O_2 (1 atm = 1.013×10^5 N/m^2) and are shown as isobaric projections on the SrO—Cr_2O_3 pseudobinary. At both oxygen pressures, the system consists of three joins in the SrO—Cr_2O_3-oxygen ternary, (1) SrO—$Sr_3Cr_2O_8$, (2) $Sr_3Cr_2O_8$—$SrCrO_4$, and (3) $SrCrO_4$—Cr_2O_3. The former is binary from 1065 °C to liquidus temperatures in air and includes a eutectic near 79 mol percent SrO (in terms of SrO—Cr_2O_3 starting materials). $Sr_3Cr_2O_8$ melts congruently at 1453 °C. Below 1065 °C in air, phase relations are complicated by reactions with atmospheric water vapor resulting in the formation of $Sr_{10}Cr_6O_{24}(OH)_2$ which decomposes to SrO and $Sr_3Cr_2O_8$ above 1065 °C. In air, below 775 °C, $Sr_3Cr_2O_8$ reacts with water vapor and oxygen to form $Sr_{10}Cr_6O_{24}(OH)_2$ and $SrCrO_4$. Water vapor reactions are restricted in 1 atm O_2. The $Sr_3Cr_2O_8$—$SrCrO_4$ join contains a binary eutectic between 69–70 mol percent SrO but liquidus relations are ternary below 69 (air) and 68 (oxygen) mol percent SrO, as reduction of Cr^{6+} occurs. Likewise, the $SrCrO_4$—Cr_2O_3 join is not binary at solidus and liquidus temperatures. In air, $SrCrO_4$ melts at 1251 °C to Cr_2O_3 plus liquid with release of oxygen. In oxygen, the compound melts at 1283 °C with evolution of oxygen.

Key words: Chromium oxide; phase equilibria; strontium chromates; strontium-"chromium oxide" system, $SrCrO_4$, $Sr_3Cr_2O_8$.

1. Introduction

Investigation of phase relations in the system SrO-"chromium oxide" was initiated as part of a program of phase equilibrium studies involving the high temperature oxidation-reduction behavior of the first-row transition series metals. Although a number of mixed oxide compounds of strontium and chromium are reported in the literature [1–6],[1] systematic attempts to deduce phase relations as a function of temperature and controlled oxygen pressure were not made. This paper presents two oxygen isobaric sections, air (0.21 atm O_2) and 1 atm O_2 (1 atm = 1.013×10^5 N/m^2), through the SrO—Cr_2O_3-oxygen ternary which is a subsystem of the Sr—Cr-oxygen ternary. X-ray diffraction and gravimetric data together with determinations of the melting points of compounds and of solidus and liquidus temperatures for various compositions in the system were used to construct the two isobaric sections. For convenience, phase relations in the ternary are depicted as projections on the SrO—Cr_2O_3 preudobinary but do not necessarily reflect equilibria for compositions confined to the pseudobinary. Although ternary in nature, the SrO—Cr_2O_3 pseudobinary may be interpreted in the normal binary manner because of the assignment of a fixed P_{O_2}.

[1] Figures in brackets indicate the literature references at the end of this paper.

2. Sample Preparation and Experimental Procedure

Strontium carbonate was used as the source for the alkaline earth metal and highly reactive Cr_2O_3, prepared from $Cr(NO_3)_3 \cdot 9H_2O$ by gentle ignition, for chromium. Compositions were calculated to ± 0.01 percent and included a weight loss factor for $SrCO_3$. Starting materials in sufficient quantities to yield 3.0 g batches were weighed to the nearest 0.1 mg. Each batch was mixed in a mechanical shaker, dry mixed by hand, and pressed into a disk in a $\frac{5}{8}$-in diam mold at 10,000 lb/in^2. The disks were fired, with periodic remixing and pressing, at 850 °C in air in a horizontal muffle furnace for 100 hr.

Melting point and subsolidus data were obtained by the quenching method from calcined samples equilibrated at constant temperature and pressure in open platinum tubes. In some cases, open gold envelopes or Vycor tubes were used. A vertical tube resistance-type furnace wound with 80 percent Pt–20 percent Rh wire was used for equilibrations in air. Specimens were equilibrated at 1 atm O_2 in a similar furnace modified for vacuum and gas flow capability with end-closures and "O"-ring seals. High purity oxygen was passed at a flow rate of 60 cm^3/min through a kerosene-solid CO_2 cold trap into the furnace and out to the atmosphere through a second cold trap followed by a glass "bubbler" containing a 1-in water column.

The furnace was twice evacuated to 3×10^{-4} atm and flushed with oxygen before each experiment.

Temperatures were measured with Pt-Pt 10 percent Rh thermocouples calibrated against the melting points of NaCl (801 °C), Au (1063 °C), and Pd (1552 °C) [7]. The furnaces were controlled by an a–c Wheatstone bridge controller capable of maintaining temperature to at least ±2 °C.

Air-heated specimens were quenched onto a cold metal tray while those equilibrated in oxygen were quenched into a "dry ice" cooled brass cold-finger that constitutes the lower portion of the furnace. After quenching, specimens were examined under a binocular microscope for physical appearances of melting and x-ray powder patterns were made. Glazing accompanied by direct, but limited, specimen to Pt-container-surface contact was interpreted as the first experimental evidence for solidus temperatures. High chromium content specimens (>33 mol percent Cr_2O_3) also displayed small cavities indicative of gas release at solidus temperatures as well as minor changes in x-ray powder patterns. Liquidus temperatures were more difficult to deduce but were generally characterized by the development of a deeply concave meniscus indicative of a highly mobile material. Chromium-rich specimens were particularly difficult to retain in their containers as high fluidity was enhanced by gas release. The overall reproducibility of the temperature measurements for the experimental data points is within ±2 °C and the overall accuracy of the reported temperatures is within ±5 °C.

Equilibrium was considered to have been attained when the x-ray diffraction patterns of specimens heated successively for longer times and/or at higher temperature did not change. X-ray powder patterns were made using a high-angle Geiger counter-diffractometer at 1/4° 2θ/min scanning rate and nickel-filtered Cu radiation. Reported unit cell data are considered accurate to about ±2 in the last decimal place given.

The air and 1 atm O_2 liquidus isobars were determined by weight regain measurements. One-half to 1½ g specimens were equilibrated within 5 °C above their liquidus temperature and quenched. After weighing at room temperature they were reoxidized by heating at a subsolidus temperature in air where phase assemblage and bulk composition were known from previous experiments. These were reweighed at room temperature after sufficient heating to permit complete reversal. Weight gain at the subsolidus temperature, therefore, represented weight loss for an equivalent amount of specimen at the liquidus temperature.

3. Compounds

The system SrO-"chromium oxide" contains few compounds in air or 1 atm O_2. The phase $Sr_3Cr_2O_8$ has been reported [2,3,8,9,10,11] and is trigonal with s.g. (space group) $R\bar{3}m$. It is isostructural with $Ba_3P_2O_8$ [12] and contains the unusual Cr^{5+} state. The hexagonal cell dimensions for the compound in this study, $a=5.569$ Å and $c=20.17$ Å, are in accord with those of Scholder and Schwarz [2] and Wilhelmi and Jonsson [3].

Pistorius and Pistorius [1] reported $SrCrO_4$ (monoclinic, s.g. $P2_1/n$, $a=7.083$ Å, $b=7.388$ Å, $c=6.771$ Å, $\beta=103.43°$) which is isostructural with $PbCrO_4$. Cell parameters for the $SrCrO_4$ in this study, $a=7.09$ Å, $b=7.40$ Å, $c=6.74$ Å, $\beta=103.3°$, are in good agreement with the above.

The compounds $SrCr_2O_7$ [4], $Sr_2Cr^{4+}O_4$ [5], and $SrCr^{4+}O_3$ [6] do not appear in the system at 0.21 and 1 atm O_2. The former is probably a higher P_{O_2}-low temperature phase. Sr_2CrO_4 was prepared in this laboratory at 1215 °C (44 hr) and 2×10^{-5} atm and is, therefore, a low P_{O_2} phase with Cr^{4+} in tetrahedral coordination while $SrCrO_3$ is a high pressure cubic perovskite with Cr^{4+} in octahedral coordination.

Phase relations at low temperatures in air of compositions within the SrO-rich portion of the system are severely influenced by atmospheric water vapor. The compound $Sr_{10}Cr_6O_{24}(OH)_2$, a hydroxyapatite, readily develops and persists to elevated temperatures before decomposing with H_2O evolution at about 1065 °C to SrO and $Sr_3Cr_2O_8$. Scholder and Schwarz [2] and Banks and Jaunarajs [13] prepared a Sr—Cr hydroxyapatite (*hex*, s.g. $P6_3/m$, $a=10.009$ Å, $c=7.435$ Å and $a=9.98$ Å, $c=7.40$ Å, respectively). According to Scholder and Suchy [14] magnetochemical analysis yielded data indicating that pentavalent Cr exists in the compound, as well as in Ba and Ca analogs, instead of a 2:4 disproportionation of Cr^{3+} and Cr^{6+}. The apatite phase found in this study is hexagonal with $a=10.009$ Å and $c=7.427$ A. To investigate the possibility that this compound might be of the oxyapatite-type, $Sr_{10}Cr_6{}^{5+}O_{24}O$, rather than a hydroxyl phase which, more appropriately, belongs to the SrO—Cr_2O_3—O_2—H_2O quaternary, a qualitative analysis

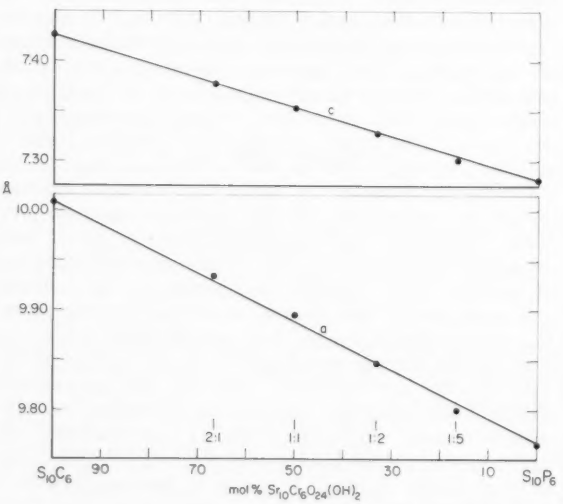

FIGURE 1. *Unit cell parameters of* $Sr_{10}(CrO_4)_{2\times}(PO_4)_{6-2\times}(OH)_2$ *solid solutions prepared at 900 °C in air.*
($S_{10}C_6$=$Sr_{10}Cr_6O_{24}(OH)_2$, $S_{10}P_6=Sr_{10}P_6O_{24}(OH)_2$)

was made for protons on material made at 1000 °C on gold using broadline nuclear magnetic resonance. The analysis suggested a large concentration of protons. Furthermore, the possible reactions

(a) $3Sr_3Cr_2O_8 + SrO + H_2O \rightarrow Sr_{10}Cr_6O_{24}(OH)_2$
(b) $3Sr_3Cr_2O_8 + SrO \rightarrow Sr_{10}Cr_6O_{24}O$

were tested gravimetrically by heating $Sr_3Cr_2O_8 + SrO$ at 850 °C in air. Equation (a) suggests a theoretical weight gain of 1.13 percent while (b) involves no weight change. A measured value of 1.08 percent suggested reaction (a). A specimen decomposed to $SrO + Sr_3Cr_2O_8$ at 1225 °C, sealed in a Pt tube, and reheated at 825 °C, did not reverse, also suggesting reaction (a). Additional evidence for the existence of a Cr^{5+} hydroxyapatite is the isotypism with $Sr_{10}P_6O_{24}(OH)_2$ as demonstrated by the formation of ideal solid solutions, $Sr_{10}(CrO_4)_{2x}(PO_4)_{6-2x}(OH)_2$, at 900 °C in air (fig. 1).

4. Discussion of Phase Equilibria

Phase relations in air (0.21 atm O_2) and 1 atm O_2 are shown in figures 2, 3, 4, and 5. The data from which these diagrams were constructed are given in tables 1 and 2. The system is not truly binary in its entirety because of reactions with oxygen but consists of a number of ternary elements (figs. 2 and 4) which may be projected onto the $SrO—Cr_2O_3$ pseudobinary (figs. 3 and 5), or any other convenient compositional reference join, through lines of constant cation-cation ratio but variable oxygen content (oxygen reaction lines).

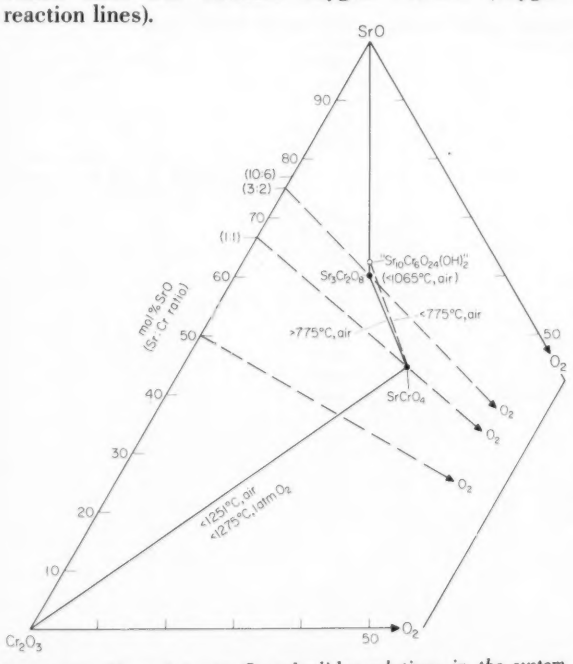

FIGURE 2. *Air and 1 atm O_2 subsolidus relations in the system $SrO—Cr_2O_3—O_2$.*

4.1. Air Equilibria

a. The $SrO—Sr_3Cr_2O_8$ Join and Related Equilibria

The 0.21 atm isobar coincides at subsolidus temperatures (> 1065 °C) and liquidus temperatures with the $SrO—Sr_3Cr_2O_8$ join; the join is a true binary in air at all temperatures above 1065 °C to at least the liquidus. Apatite, $Sr_{10}Cr_6O_{24}(OH)_2$, does not belong to this join but lies in the $SrO—Sr_3Cr_2O_8—H_2O$ subternary of the $SrO—Cr_2O_3—O_2—H_2O$ quanternary but is nevertheless indicated, because of its influence on phase relations, as a projection onto the $SrO—Sr_3Cr_2O_8$ join in figure 2 and with dashed lines at the 10:3 $SrO:Cr_2O_3$ ratio in figure 3. Between 1065 and 775 °C phase relations for compositions between SrO and the 3:2 cation-cation ratio actually consist of:

(a) $SrO—Sr_{10}Cr_6O_{24}(OH)_2$: a tie line extending above the plane of the ternary toward a hypothetical H_2O apex and connecting SrO and the composition of apatite.
(b) $Sr_{10}Cr_6O_{24}(OH)_2—Sr_3Cr_2O_8$; a tie line extending from the composition of apatite to that of $Sr_3Cr_2O_8$.

Above 1065 °C, the apatite phase decomposes to $Sr_3Cr_2O_8$ plus SrO with H_2O evolution thereby establishing the $SrO—Sr_3Cr_2O_8$ tie line. An unusual reaction not indicated in figures 2 and 3 but involving the apatite, occurs below approximately 635 °C. The reaction is very sluggish because of the low temperature. Dehydroxylation of apatite proceeds not because of instability due to high temperature but as a result of low temperature oxidation of Cr^{5+} to Cr^{6+} according to

$$Sr_{10}Cr_6^{5+}O_{24}(OH)_2 + 1\tfrac{1}{2}O_2 \rightarrow 6SrCr^{6+}O_4 + 4SrO + H_2O.$$

The available SrO reacts with CO_2 at low temperatures and is readily identified in x-ray powder patterns as $SrCO_3$.

$Sr_3Cr_2O_8$ melts congruently at 1453 °C and a binary eutectic occurs between 79–80 mol percent SrO and 1365 °C. The liquidus curve delimiting the primary field of SrO shows a pronounced "flattening" which could not be followed using compositions more SrO-rich than 85 mol percent. These tend to react with the platinum container to form Sr_4PtO_6 [15]. In fact, the "flattening" tendency and the magnitude of the solidus temperature are probably the result of traces of Sr_4PtO_6. Materials more SrO-rich than $Sr_3Cr_2O_8$ could be prepared free of Sr_4PtO_6 only by heating multiple disks of specimens resting on two strands of fine Pt wire wrapped about an alumina dish. The disks were located at the open end of the dish to prevent contact with the alumina.

$Sr_3Cr_2O_8$ has a "minimum" at approximately 775 °C below which it reacts with atmospheric oxygen and water vapor according to:

$$4Sr_3Cr_2O_8 + \tfrac{1}{2}O_2 + H_2O \rightarrow Sr_{10}Cr_6O_{24}(OH)_2 + 2SrCrO_4$$

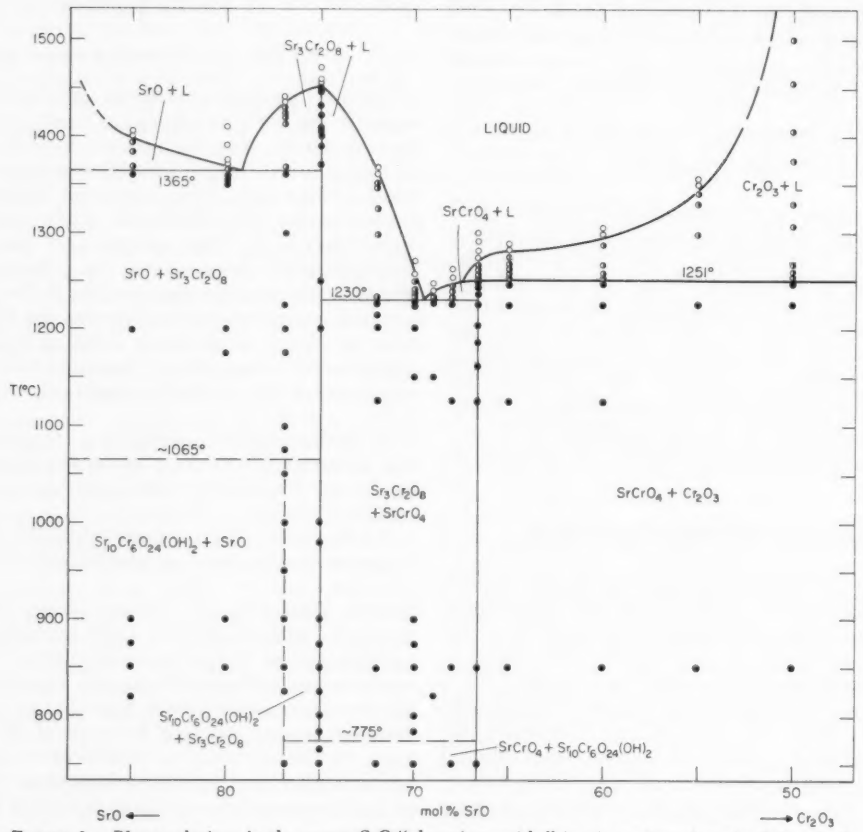

FIGURE 3. *Phase relations in the system* **SrO-"chromium oxide," in air, projected on the SrO—Cr_2O_3 pseudobinary.**
(●—solid; ◑—partly melted; ○—liquid.)

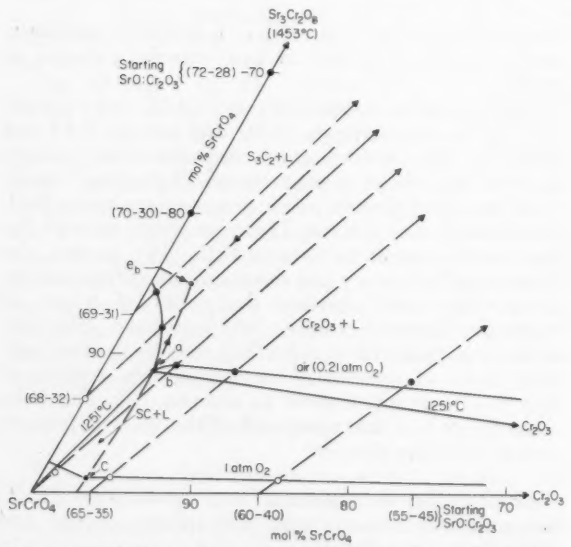

FIGURE 4. *The air and 1 atm O_2 liquidus isobars in the* **$Sr_3Cr_2O_8$—$SrCrO_4$—Cr_2O_3** *subternary of the system* **SrO-"chromium oxide."**
(●—air; ○—1 atm O_2; dashed straight lines with arrows are lines of constant Sr—Cr ratio; e_b is a binary eutectic; dashed curved lines with arrows are boundary curves; S_3C_2=$Sr_3Cr_2O_8$; SC=$SrCrO_4$.)

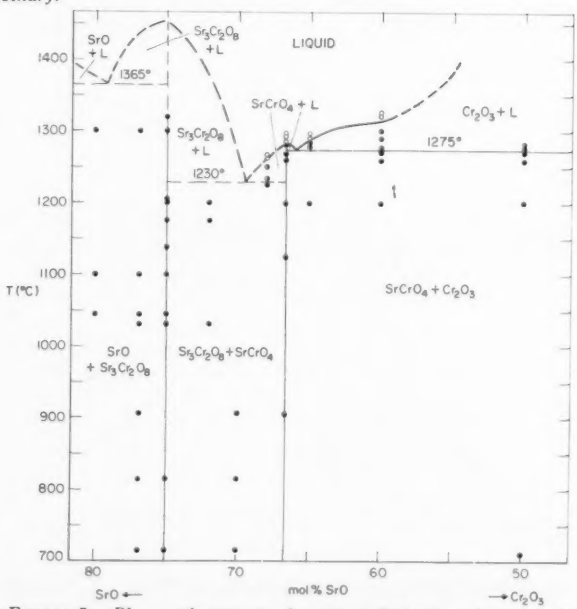

FIGURE 5. *Phase relations in the system* **SrO-"chromium oxide" at 1 atm O_2,** *projected on the* **SrO—Cr_2O_3** *pseudobinary.*
(●—solid; ◑—partly melted; ○—liquid.)

TABLE 1. *Experimental data for the system* SrO-"*chromium oxide*"

Heat treatments [a]								Results	
Composition		Initial		Final (air)		Final (O_2)[b]		Physical State	X-ray analysis [c]
SrO	Cr_2O_3	Temp.	Time	Temp.	Time	Temp.	Time		
mol %	*mol %*	*°C*	*hr*	*°C*	*hr*	*°C*	*hr*		
85	15	850	100						$S_{10}C_6 + SrCO_3$
				820	22				$S_{10}C_6 + SrCO_3$
				875	60				$S_{10}C_6 + SrCO_3$
		1200	60						$S_3C_2 + S$
				900	60				$S_{10}C_6 + S$
				1363	1			No melting	$S_3C_2 + S$
				1367	1			Partial melting	$S_3C_2 + S$
				1384	1			Partial melting	$S_3C_2 + S$
				1394	1			Partial melting	$S_3C_2 + S$
				1399	0.75			Completely melted (?)	$S_3C_2 + S$
				1404	1			Completely melted	$S_3C_2 + S$
80	20	850	100						
				900	60				$S_{10}C_6 + SrCO_3$
						1045	20		$S_3C_2 + S + tr \cdot S_4P$
						1100	20		$S_3C_2 + S + tr \cdot S_4P$
						1300	5		$S_3C_2 + S + tr \cdot S_4P$
		1200	60						$S_3C_2 + S$
				1175	4				$S_3C_2 + S$
				1351	1			No melting	$S_3C_2 + S$
				1357	1			No melting	$S_3C_2 + S$
				1361	1			No melting	$S_3C_2 + S$
				1364	1			No melting	$S_3C_2 + S$
				1366	1			Partial melting	$S_3C_2 + S$
				1367	1			Partial melting	$S_3C_2 + S$
				1371	1			Completely melted	$S_3C_2 + S$
				1375	1			Completely melted	$S_3C_2 + S$
				1391	1			Completely melted	$S_3C_2 + S$
				1410	1			Completely melted	$S_3C_2 + S$
76.92	13.08	850	100						$S_{10}C_6$
				[d]500	48				$S_{10}C_6 + SC + SrCO_3$
				[d]600	120				$S_{10}C_6 + SC + SrCO_3$
				[d]625	96				$S_{10}C_6 + SC + SrCO_3$
				[d]650	122				$S_{10}C_6$
				[d]700	100				$S_{10}C_6$
				[d]750	100				$S_{10}C_6$
				[d]900	60				$S_{10}C_6$
				[d]950	70				$S_{10}C_6$
				[d]1000	70				$S_{10}C_6$
				[d]1050	70				$S_{10}C_6$
				[e]1075	4				$S_{10}C_6 + S_3C_2 + S$
				[e]1100	25				$S_3C_2 + S$
				1175	4				$S_3C_2 + S$
				1225	19				$S_3C_2 + S$
						[d]714	120		$S_3C_2 + S$
						[d]1032	120		$S_3C_2 + S$
		1200	60						$S_3C_2 + S$
				[f]825	65				$S_3C_2 + S$
				[d]900	60				$S_{10}C_6$
				[d]950	70				$S_{10}C_6 + tr \cdot S_3C_2$
				[d]1000	70				$S_{10}C_6 + tr \cdot S_3C_2$
				[d]1050	70				$S_{10}C_6 + tr \cdot S_3C_2$
				[e]1075	4				$S_3C_2 + S$

TABLE 1. *Experimental data for the system* SrO-"*chromium oxide*" —Continued

Heat treatments [a]								Results	
Composition		Initial		Final (air)		Final (O_2) [b]		Physical State	X-ray analysis [c]
SrO	Cr_2O_3	Temp.	Time	Temp.	Time	Temp.	Time		
mol %	*mol %*	*°C*	*hr*	*°C*	*hr*	*°C*	*hr*		
				[e] 1100	25				$S_3C_2 + S$
				1300	50			No melting	$S_3C_2 + S$
				1363	1			No melting	$S_3C_2 + S$
				1367	1			Partial melting	$S_3C_2 + S$
				1413	1			Partial melting	$S_3C_2 + S$
				1419	1			Partial melting	$S_3C_2 + S$
				1425	1			Partial melting	$S_3C_2 + S$
				1430	1			Partial melting	$S_3C_2 + S$
				1435	1			Completely melted	$S_3C_2 + S$
				1442	1			Completely melted	$S_3C_2 + S$
						[d] 714	120		$S_3C_2 + S$
						[d] 815	70		$S_3C_2 + S$
						[d] 906	120		$S_3C_2 + S$
						[d] 1032	120		$S_3C_2 + S$
						1045	20		$S_3C_2 + S + tr \cdot S_4P$
						1100	20		$S_3C_2 + S + tr \cdot S_4P$
						1300	5		$S_3C_2 + S + tr \cdot S_4P$
75	25	850	100						
		750	100						
				750	24				$S_{10}C_6 + SC$
				765	65				$S_{10}C_6 + SC$
				785	40				$S_{10}C_6 + S_3C_2 + SC$
				800	90				$S_3C_2 + tr \cdot S_{10}C_6 + tr \cdot SC$
				825	25				$S_3C_2 + tr \cdot S_{10}C_6 + tr \cdot SC$
				850	18				$S_3C_2 + tr \cdot S_{10}C_6 + tr \cdot SC$
				875	18				$S_3C_2 + tr \cdot S_{10}C_6 + tr \cdot SC$
				900	16				S_3C_2
				980	18				S_3C_2
				1000	18				S_3C_2
						[d] 714	120		S_3C_2
						[d] 815	70		S_3C_2
						1045	20		$S_3C_2 + tr \cdot S_4P$
						1100	20		$S_3C_2 + tr \cdot S_4P$
						1138	70		$S_3C_2 + tr \cdot S_4P$
						1200	4		S_3C_2
						1205	49		S_3C_2
						1300	5		S_3C_2
						1320	72		S_3C_2
		1200	60						S_3C_2
				750	24				$S_{10}C_6 + S_3C_2 + SC$
				765	65				$S_{10}C_6 + S_3C_2 + SC$
				785	40				S_3C_2
				800	90				S_3C_2
				900	16				S_3C_2
				1250	15			No melting	S_3C_2
				1370	1			No melting	S_3C_2
				1390	1			No melting	S_3C_2
				1400	2			No melting	S_3C_2
				1404	1			No melting	S_3C_2
				1409	1			No melting	S_3C_2
				1425	1			No melting	S_3C_2
				1432	1			No melting	S_3C_2
				1449	1			No melting	S_3C_2
				1452	1			Partial melting (?)	S_3C_2
				1455	1			Completely melted	S_3C_2
				1459	1			Completely melted	S_3C_2
				1471	1			Completely melted	S_3C_2
						1032	120		S_3C_2
						1175	120		S_3C_2

TABLE 1. *Experimental data for the system* SrO-"*chromium oxide*" —Continued

Heat treatments [a]								Results	
Composition		Initial		Final (air)		Final (O_2) [b]		Physical State	X-ray analysis [c]
SrO	Cr_2O_3	Temp.	Time	Temp.	Time	Temp.	Time		
mol %	*mol %*	*°C*	*hr*	*°C*	*hr*	*°C*	*hr*		
72	28	850	100						
				750	100				$S_{10}C_6 + SC$
						1032	120		$S_3C_2 + SC$
						1175	3		$S_3C_2 + SC$
						1200	4		$S_3C_2 + SC$
		1125	60						$S_3C_2 + SC$
				1202	2			No melting	$S_3C_2 + SC$
				1215	2			No melting	$S_3C_2 + SC$
				1227	1			No melting	$S_3C_2 + SC$
				1232	1			Partial melting	$S_3C_2 + SC$
				1299	1			Partial melting	$S_3C_2 + SC$
				1326	1			Partial melting	$S_3C_2 + SC$
				1349	1			Partial melting	$S_3C_2 + SC$
				1351	1			Partial melting	$S_3C_2 + SC$
				1362	1			Completely melted	$S_3C_2 + SC$
				1369	1			Completely melted	$S_3C_2 + SC$
70	30	850	100						
				750	100				$SC + S_{10}C_6$
				785	40				$SC + S_3C_2 + tr \cdot S_{10}C_6$
				800	90				$SC + S_3C_2 + tr \cdot S_{10}C_6$
				850	18				$SC + S_3C_2 + tr \cdot S_{10}C_6$
						714	120		$SC + S_3C_2$
						815	70		$SC + S_3C_2$
						906	120		$SC + S_3C_2$
		1150	48						$SC + S_3C_2$
				750	24				$SC + S_{10}C_6 + tr \cdot S_3C_2$
				785	40				$SC + S_3C_2$
				800	90				$SC + S_3C_2$
				900	16				$SC + S_3C_2$
				1202	2			No melting	$SC + S_3C_2$
				1225	1			No melting	$SC + S_3C_2$
				1228	1			No melting	$SC + S_3C_2$
				1232	1			Partial melting	$SC + S_3C_2$
				1236	1			Partial melting	$SC + S_3C_2$
				1240	1			Partial melting	$SC + S_3C_2$
				1249	1			Partial melting (?)	$SC + S_3C_2$
				1257	1			Completely melted	$SC + S_3C_2$
				1273	1			Completely melted	$SC + S_3C_2$
69	31	820	20						
		1150	50						$SC + S_3C_2$
				1228	1			No melting	$SC + S_3C_2$
				1233	1			Partial melting	$SC + S_3C_2$
				1240	1			Completely melted (?)	$SC + S_3C_2$
				1247	1			Completely melted	$SC + S_3C_2$
68	32	850	100						
				750	24				$SC + S_{10}C_6 + tr \cdot S_3C_2$
		1125	60						$SC + S_3C_2$
				1227	1			No melting	$SC + S_3C_2$
				1232	1			Partial melting	$SC + S_3C_2$
				1239	1			Partial melting	$SC + S_3C_2$

349-367 O-69—4

TABLE 1. *Experimental data for the system* SrO-"*chromium oxide*" – Continued

Heat treatments [a]								Results	
Composition		Initial		Final (air)		Final (O_2) [b]		Physical State	X-ray analysis [c]
SrO	Cr_2O_3	Temp.	Time	Temp.	Time	Temp.	Time		
mol %	*mol %*	*°C*	*hr*	*°C*	*hr*	*°C*	*hr*		
				1246	1			Partial melting	SC + S_3C_2
				1256	1			Completely melted	SC + S_3C_2
				1263	1			Completely melted	SC + S_3C_2
						1228	5	No melting	SC + S_3C_2
						1234	5	Partial melting	SC + S_3C_2
						1252	5	Partial melting	SC + S_3C_2
						1262	16	Completely melted	SC + S_3C_2
						1266	5	Completely melted	SC + S_3C_2
66.67	33.33	850	100						
				750	100				SC
				1125	60			No melting	SC
				1162	16			No melting	SC
				1186	15			No melting	SC
				1204	1			No melting	SC
				1227	1			No melting	SC
				1238	16			No melting	SC
				1243	5			No melting	SC
				1245	1			No melting	SC
				1249	1			No melting	SC
				1252	1			Partial melting	SC + tr · S_3C_2
				1255	1			Partial melting	SC + tr · S_3C_2
				1263	1			Partial melting	SC + tr · S_3C_2
				1269	1			Partial melting	SC + tr · S_3C_2 + tr · C
				1274	1			Completely melted	SC + tr · S_3C_2 + tr · C
				1282	1			Completely melted	SC + tr · S_3C_2 + tr · C
				1292	1			Completely melted	SC + tr · S_3C_2 + tr · C
				1301	1			Completely melted	SC + tr · S_3C_2 + tr · C
						906	120	No melting	SC
						1125	70	No melting	SC
						1200	4	No melting	SC
						1260	2	No melting	SC
						1270	2	No melting	SC
						1281	2	No melting	SC
						1285	1	Completely melted	SC + tr · S_3C_2
						1294	1.25	Completely melted	SC + tr · S_3C_2
						1296	1	Completely melted	SC + tr · S_3C_2
65	35	850	100						
				1125	60				SC + C
				1225	15			No melting	SC + C
				1247	1			No melting	SC + C
				1253	1			Partial melting	SC + C + tr · S_3C_2
				1257	1			Partial melting	SC + C + tr · S_3C_2
				1261	1			Partial melting	SC + C + tr · S_3C_2
				1266	1			Partial melting	SC + C + tr · S_3C_2
				1274	1			Partial melting	SC + C + tr · S_3C_2
				1284	1			Completely melted	SC + C + tr · S_3C_2
				1288	1			Completely melted	SC + C + tr · S_3C_2
						1200	3	No melting	SC + C
						1278	1.25	Partial melting	SC + C
						1285	1.25	Partial melting	SC + C + tr · S_3C_2
						1290	1.25	Completely melted	SC + C + tr · S_3C_2
						1297	1.25	Completely melted	SC + C + tr · S_3C_2
60	40	850	100						
				1125	60				SC + C
				1225	15			No melting	SC + C
				1248	1			No melting	SC + C
				1253	1			Partial melting	SC + C + tr · S_3C_2
				1257	1			Partial melting	SC + C + tr · S_3C_2

TABLE 1. *Experimental data for the system* SrO-"*chromium oxide*"—Continued

Heat treatments [a]								Results	
Composition		Initial		Final (air)		Final (O_2)[b]		Physical State	X-ray analysis [c]
SrO	Cr_2O_3	Temp.	Time	Temp.	Time	Temp.	Time		
mol %	*mol %*	*°C*	*hr*	*°C*	*hr*	*°C*	*hr*		
				1268	1			Partial melting	SC + C + tr · S_3C_2
				1287	1			Partial melting	SC + C + tr · S_3C_2
				1298	1			Completely melted	SC + C + tr · S_3C_2
				1306	1			Completely melted	SC + C + tr · S_3C_2
						1200	3	No melting	SC + C
						1259	1.25	No melting	SC + C
						1273	1.25	No melting	SC + C
						1277	1.25	Partial melting	SC + C
						1290	1.25	Partial melting	SC + C + tr · S_3C_2
						1300	1.25	Partial melting	SC + C + tr · S_3C_2
						1321	1.25	Completely melted	SC + C + tr · S_3C_2
						1325	1.25	Completely melted	SC + C + tr · S_3C_2
55	45	850	100						
				1225	15			No melting	SC + C
				1298	1			Partial melting	SC + C + tr · S_3C_2
				1328	1			Partial melting	SC + C + tr · S_3C_2
				1341	1			Partial melting (?)	SC + C + tr · S_3C_2
				1351	1			Completely melted	SC + C + tr · S_3C_2
				1355	1			Completely melted	SC + C + tr · S_3C_2
50	50	850	100						
				1225	15			No melting	SC + C
				1247	1			No melting	SC + C
				1254	1			Partial melting	SC + C + tr · S_3C_2
				1258	1			Partial melting	SC + C + tr · S_3C_2
				1267	1			Partial melting	SC + C + tr · S_3C_2
				1307	1			Partial melting	SC + C + tr · S_3C_2
				1330	1			Partial melting	SC + C + tr · S_3C_2
				1374	1			Partial melting	SC + C + tr · S_3C_2
				1405	1			Partial melting	SC + C + tr · S_3C_2
				1455	1			Partial melting	SC + C + tr · S_3C_2
				1500	1			Partial melting	SC + C + tr · S_3C_2
						710	46		SC + C
						1200	3	No melting	SC + C
						1259	1.25	No melting	SC + C
						1273	1.25	No melting	SC + C
						1277	1.25	Partial melting	SC + C
						1281	1	Partial melting	SC + C + tr · S_3C_2

[a] After the initial heat treatment(s) all specimens were reheated in open Pt tubes, unless otherwise indicated.
[b] 1 atmosphere.
[c] Phases identified are given in the order of amount present at room temperature. They are not necessarily those present at the temperature at which the specimen was heated.
[d] Open gold envelope.
[e] Open Vycor tube.
[f] Sealed Pt tube.
(?)—interpretation uncertain. S = SrO $S_3C_2 = Sr_3Cr_2O_8$ $S_{10}C_6 = Sr_{10}Cr_6O_{24}(OH)_2$ SC = $SrCrO_4$ C = Cr_2O_3 $S_4P = Sr_4PtO_6$, formed by reaction with Pt tube

This reaction is represented in figure 3 by the 775 °C horizontal. For compositions between apatite and $SrCrO_4$ the apatite-$SrCrO_4$ tie line, therefore, exists below 775 °C.

b. $Sr_3Cr_2O_8$—$SrCrO_4$—Cr_2O_3 Equilibria

Above 775 °C, to liquidus temperatures, compositions between $Sr_3Cr_2O_8$ and $SrCrO_4$ behave in a binary fashion at least to about 70 mol percent SrO. The $Sr_3Cr_2O_8$—$SrCrO_4$ tie line in figure 2 suggests binary behavior in the subsolidus. The invariant point between 70–69 mol percent SrO at 1230 °C is a true binary eutectic. Compositions more Cr-rich than $SrCrO_4$ behave in a binary manner only below the 1251 °C solidus as suggested by the $SrCrO_4$—Cr_2O_3 tie line in figure 2. The 0.21 atm O_2 liquidus isobar coincides only with a portion of the $Sr_3Cr_2O_8$—$SrCrO_4$ join and lies entirely off the $SrCrO_4$—Cr_2O_3 tie line within the $Sr_3Cr_2O_8$—$SrCrO_4$—Cr_2O_3 subternary (fig. 4.). This situation is created by the "incongruent" melting behavior of $SrCrO_4$ at 1251 °C. The compound melts to Cr_2O_3 plus liquid with evolution of oxygen as the result of reduction of Cr^{6+} to Cr^{3+} and Cr^{5+}. The

TABLE 2. *Summary of gravimetric experiments for the location of the air and 1 atm O_2 liquidus isobars in the $Sr_3Cr_2O_8$—$SrCrO_4$—Cr_2O_3 subternary*

Initial composition					Heat treatments [a]						
					Air		Oxygen				
SrO	Cr_2O_3	Subsolidus phases			Temp.	Time	Temp.	Time	Liquidus composition [b]		
mol %	*mol %*	*Bulk*		*mol %*	*°C*	*hr*	*°C*	*hr*	*Bulk* [c]	*Ternary phases* [d]	*mol %*
72	28	$Sr_{16}Cr_{13}O_{52}$	S_3C_2	30	1360	5			no change		
			SC	70							
70	30	$Sr_{14}Cr_{12}O_{48}$	S_3C_2	20	1256	5			no change		
			SC	80							
69	31	$Sr_{69}Cr_{62}O_{248}$	S_3C_2	12.73	1242	5			$Sr_{69}Cr_{62}O_{246.25}$	S_3C_2	14.27
			SC	87.27						SC	85.08
										C	0.65
68	32	$Sr_{85}Cr_{80}O_{320}$	S_3C_2	6.67	1255	5			$Sr_{85}Cr_{80}O_{312}$	S_3C_2	11.76
			SC	93.33						SC	85.92
										C	2.32
							1262	16	no change		
66.67	33.33	$SrCrO_4$	SC	100	1275	6			$SrCrO_{3.8}$	S_3C_2	9.10
										SC	86.36
										C	4.54
							1284	5	$SrCrO_{3.97}$	S_3C_2	1.36
										SC	97.96
										C	0.68
65	35	$Sr_{26}Cr_{28}O_{107}$	SC	96.29	1283	5			$Sr_{26}Cr_{28}O_{101.84}$	S_3C_2	8.57
			C	3.71						SC	82.97
										C	8.56
							1290	4	$Sr_{26}Cr_{28}O_{106.29}$	S_3C_2	1.05
										SC	94.66
										C	4.29
60	40	$Sr_6Cr_8O_{27}$	SC	85.71	1297	5			$Sr_6Cr_8O_{25.60}$	S_3C_2	8
			C	14.29						SC	72
										C	20
							1320	5	$Sr_6Cr_8O_{26.84}$	S_3C_2	1
										SC	84
										C	15

[a] Melted within 5 °C above liquidus temperature.
[b] Compositions melted in air and oxygen were reversed by reheating at 1125 °C in air.
[c] Calculated from the weight gains of melted specimens when reversed to their initial bulk composition (phase assemblage) at 1125 °C in air.
[d] Liquidus bulk compositions recalculated on the basis of mol percent $Sr_3Cr_2O_8$, $SrCrO_4$, and Cr_2O_3.
S_3C_2=$Sr_3Cr_2O_8$ SC=$SrCrO_4$ C=Cr_2O_3.

composition of the liquid lies at point *a* (fig. 4) which is within the $Sr_3Cr_2O_8$—$SrCrO_4$—Cr_2O_3 subternary and is represented by the "peritectic" between 68–67 mol percent SrO in figure 3. The "peritectic" is not binary but is merely the projection of point *a* which is the intersection of the 0.21 atm liquidus isobar and the boundary curve delimiting the primary fields of $SrCrO_4$ and Cr_2O_3 in the $Sr_3Cr_2O_8$—$SrCrO_4$—Cr_2O_3 subternary as shown in figure 4. Triangle $SrCrO_4$—*a*—Cr_2O_3 represents the univariant equilibria among $SrCrO_4$, liquid, Cr_2O_3, and O_2 at 1251 °C and is represented by the 1251 °C "peritectic" horizontal in figure 3. As liquid *a* is not binary, specimens between $SrCrO_4$ and Cr_2O_3, quenched from solidus temperatures and above, show $Sr_3Cr_2O_8$ in their x-ray powder patterns. This manifestation of reduction was of particular importance in the determination of the 1251 °C solidus. The compound $PbCrO_4$, isostructural with $SrCrO_4$, decomposes in the solid state at low temperatures in air to Pb_2CrO_5 plus Cr_2O_3 with O_2 evolution without intervention of melting [16]. Hexavalent Cr in the presence of Sr is thus more stable, requiring temperatures to 1251 °C before reduction proceeds.

The 0.21 atm liquidus isobar is shown in figure 4. Commencing at the 1453 °C melting point of $Sr_3Cr_2O_8$, it follows the $Sr_3Cr_2O_8$—$SrCrO_4$ join through the eutectic (e_b). This portion of the system is strictly binary. Between the eutectic and 69 mol percent SrO, it migrates into the subternary across the primary field of $SrCrO_4$ to the $SrCrO_4$—Cr_2O_3 boundary curve (point a) from where it crosses the primary field of Cr_2O_3. Assuming that Cr_2O_3 melts congruently without oxygen loss in air at elevated temperatures, it terminates at the sesquioxide apex. It is, therefore, obvious that in figure 3, the liquidus curves (< 69 mol

% SrO) shown represent the described isobar in projection but only indicate the temperature at which a given phase assemblage melts. Compositions corresponding to each liquidus temperature can be deduced only with aid of the ternary.

Interpretation of figure 4 may be facilitated by two appropriate examples.

(a) Starting with a raw compositon of 68–32 mol percent SrO and Cr_2O_3, respectively, and heating in air at subsolidus temperatures results in the oxidation of available Cr^{3+} and the formation of a two phase mixture, $Sr_3Cr_2O_8 + SrCrO_4$, whose bulk composition lies on the $Sr_3Cr_2O_8$—$SrCrO_4$ tie line. At 1230 °C, initial melting occurs. Phases present are $Sr_3Cr_2O_8$, $SrCrO_4$, and binary eutectic liquid. As temperature is raised $Sr_3Cr_2O_8$ dissolves in the liquid and the phase assemblage consists of $SrCrO_4$ + binary liquid. Further elevation of temperature results in increased solubility of $SrCrO_4$ in the liquid which begins to evolve O_2 (reduce). As this occurs, the composition of the liquid follows the isobar into the ternary while bulk composition follows the 68 mol percent SrO oxygen reaction line. At about 1247 °C complete melting occurs in the primary field of $SrCrO_4$ and liquid composition and bulk composition (intersection of the isobar and the pertinent oxygen reaction line) coincide.

(b) Starting with a 2:1 mixture of SrO and Cr_2O_3 and heating in the subsolidus results in the complete oxidation of Cr^{3+} to Cr^{6+} and the formation of $SrCrO_4$. At 1251 °C, $SrCrO_4$ melts "incongruently" with O_2 evolution to Cr_2O_3 + liquid. Composition of the liquid is at point *a* in figure 4 while the bulk composition is located in the $SrCrO_4$—*a*—Cr_2O_3 triangle on the $SrCrO_4$ oxygen reaction line. The exact position has not been determined but at maximum heat content point *b* is representative. As temperature is raised, reduction in the liquid proceeds and its composition follows the air isobar as bulk composition continues along the oxygen reaction line. The equilibrium assemblage is Cr_2O_3 + liquid during this process. At about 1292 °C complete melting occurs and liquid and bulk composition coincide, again at the intersection of the air isobar and the pertinent oxygen reaction line.

4.2. 1 Atm O_2 Equilibria

Phase relations at 1 atm O_2 shown in figure 5, are not signifigantly different from those in air. Decrease of P_{H_2O}, inherent in the oxygen experiments, prevents the formation of apatite. Initially, it was anticipated that $Sr_3Cr_2O_8$ would show a low temperature minimum indicative of the possible oxidation reaction:

$$Sr_3Cr_2O_8 + \tfrac{1}{2}O_2 \rightarrow SrO + 2SrCrO_4$$

The compound, however, is stable to at least 715 °C in oxygen. The 775 °C minimum in air, therefore, is apparently due solely to the influence of water vapor. Melting relations in the SrO-rich portion of the system were not determined as they are expected to be identical to those in air. Confirmation of the 1230 °C solidus in air between $Sr_3Cr_2O_8$ and $SrCrO_4$ was made using the 68 mol percent SrO composition. The binary nature of the solidus is further validated, as this temperature does not increase in oxygen.

The 1 atm O_2 liquidus isobar (fig. 4) between $Sr_3Cr_2O_8$ and $SrCrO_4$ coincides with that join beyond 69 and 68 mol percent SrO. The join is, therefore, almost entirely binary in oxygen. $SrCrO_4$ melts sharply at 1283 °C but some reduction at the melting point was indicated by small amounts of $Sr_3Cr_2O_8$ found in diffraction patterns. Gravimetric experiments confirmed this observation. The compound melts in a "congruent" manner although melting is accompanied by O_2 evolution from the liquid. This indicates that the 1 atm O_2 isobar and the $SrCrO_4$ oxygen reaction line intersect in the primary field of $SrCrO_4$. Figure 6 schematically demonstrates the influence of oxygen pressure on the melting behavior of $SrCrO_4$.

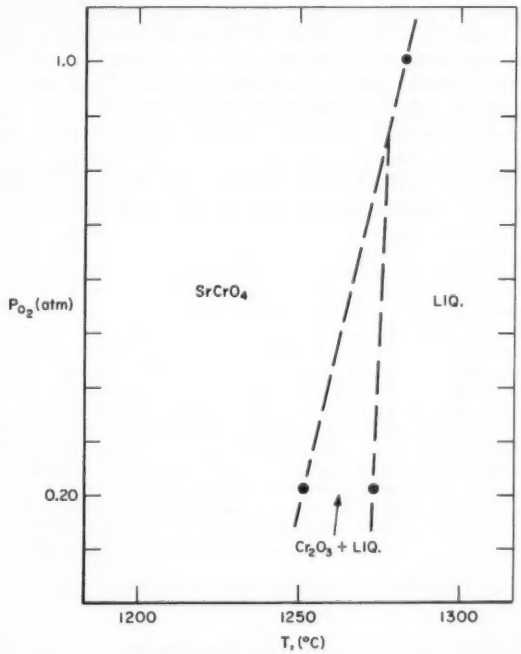

FIGURE 6. *Schematic representation of the melting behavior of* $SrCrO_4$ *between* 0.21 *and* 1 atm O_2.

Compositions of liquids are not indicated.

From a value of 1251 °C in air, the solidus temperature between $SrCrO_4$ and Cr_2O_3 is raised to 1275 °C and a "eutectic" appears to exist between 65 and 66 mol percent SrO. As $SrCrO_4$ and the 65 and 60 mol percent SrO compositions evolve O_2 at liquidus temperatures, the two segments of the 1 atm O_2 isobar may be extrapolated to an intersection on an oxygen reaction line pertinent to a composition initially between 65 to 66 mol percent SrO but within the ternary. This intersection delimits to within at least 1 mol percent the location (point *c*) of the $SrCrO_4$—Cr_2O_3 boundary curve at 1 atm O_2. In projection

(fig. 5) point c is the "eutectic" between 65 to 66 mol percent SrO. The 1 atm O_2 liquidus isobar coincides with the $Sr_3Cr_2O_8$—$SrCrO_4$ join to at least 68 mol percent SrO. Between this composition and $SrCrO_4$ it must migrate into the ternary (it cannot coincide with $SrCrO_4$ since the phase melts with O_2 loss), cross the primary field of $SrCrO_4$ to the boundary curve, and eventually terminate at Cr_2O_3.

The approximate position of the $SrCrO_4$—Cr_2O_3 boundary curve in figure 4 may be extrapolated toward the $Sr_3Cr_2O_8$ apex beyond point a. Similarly, the binary eutectic on the $Sr_3Cr_2O_8$—$SrCrO_4$ join must be a temperature maximum on that join (Alkemade theorum) and can, therefore, be extrapolated into the ternary. The resulting line, the $Sr_3Cr_2O_8$—$SrCrO_4$ boundary curve, where it intersects the $SrCrO_4$—Cr_2O_3 boundary curve, approximates the position of the $Sr_3Cr_2O_8$—$SrCrO_4$—Cr_2O_3 ternary eutectic. Another boundary curve, that between $Sr_3Cr_2O_8$ and Cr_2O_3, must, of course, converge at this point. A possible position is, therefore, indicated. It should be emphasized that the ternary invariant point is an integral portion of the system but is experimentally realized only at a fixed P_{O_2} and temperature. Similarly, for every P_{O_2}, a corresponding liquidus isobar exists within the ternary (as long as new phases do not appear). It is, therefore, obvious that every point on a boundary curve is characterized by a specific temperature and P_{O_2}. Having determined two such points (a, c) for the $SrCrO_4$—Cr_2O_3 boundary curve and the 1230 °C maximum on the $Sr_3Cr_2O_8$—$SrCrO_4$ boundary (e_b), values of < 0.1 atm O_2 and about 1210 to 1220 °C are not too improbable for the position of the ternary eutectic.

5. References

[1] Pistorius, C. W. F. T., and Pistorius, M. C., Zeit. Krist. **117**, 259 (1962).
[2] Scholder, V. B., and Schwarz, H., Z. anorg. allgem. Chem. **326**, 11 (1963).
[3] Wilhelmi, K. A., and Jonsson, O., Acta Chem. Scand. **19**, 177 (1965).
[4] Wilhelmi, K. A., Arkiv für Kemi **26**, 149 (1966).
[5] Wilhelmi, K. A., Arkiv für Kemi **26**, 157 (1966).
[6] Chamberland, B. L., Solid State Communications **5**, 663 (1967).
[7] Stimson, H. F., J. Res. NBS **65A** (Phys. and Chem.) No. 3, 139 (1961).
[8] Klemm, W., Angew. Chem. **63**, 396 (1951).
[9] Scholder, R., Angew. Chem. **65**, 240 (1953).
[10] Scholder, R., Angew. Chem. **70**, 583 (1958).
[11] Scholder, R. and Klemm, W., Angew. Chem. **66**, 461 (1954).
[12] Zachariasen, W. H., Acta Cryst. **1**, 263 (1946).
[13] Banks, E. and Jaunarajs, K. L., Inorg. Chem. **4**, **78** (1965).
[14] Scholder, R. and Suchy, E., Z. anorg. allgem. Chem. **308**, 295 (1961).
[15] Randall, Jr., J. J. and Katz, L., Acta Cryst. **12**, 519 (1959).
[16] Negas, T., J. Am. Ceram. Soc., December (1968).

(Paper 73A4–562)

JOURNAL OF RESEARCH of the National Bureau of Standards—A. Physics and Chemistry
Vol. 73A, No. 4, July–August 1969

Publications of the National Bureau of Standards*

Selected Abstracts

Causes of variation in chemical analyses and physical tests of portland cement, Bean, B. L., Dise, J. R., *Nat. Bur. Stand. (U.S.), Bldg. Sci. Ser. 17, 32 pages (March 1969), 40 cents.*
Variations in testing that could lead to the rejection of a material fully conforming to specification requirements, or the acceptance of a material with undesirable chemical or physical properties, are apparent in the results reported by laboratories participating in comparative tests of portland cements. Many of the causes for variation in chemical analyses and physical test results are listed in this discussion, and remedies for some of the more frequently encountered deficiencies in apparatus and methods are suggested. Particular consideration is given to problems which do not seem to have been covered in sufficient detail in previous discussions of cement testing procedures. Literature references are given for additional information. This publication supersedes NBS Monograph 28.

Key words: Portland cement; chemical analyses; physical tests.

Nuclear standards for chemistry and technology. Beeghly, H. F., Cali, J. P., Meinke, W. W., Editors, *Proceedings of a Symposium on Standards in Nuclear Chemistry and Technology held at the 156th National Meeting of the American Chemical Society, Atlantic City, N. J., September 8–9, 1968, Nat. Bur. Stand. (U.S.), Spec. Publ. 310, 261 pages (Dec. 1968), $1.25.*
Many diverse organizations are engaged in developing the nuclear standards needed by science, industry, and government for the rapidly growing field of nuclear technology. Often there has been inadequate communication between these groups and insufficient opportunity to get an overall picture of the needs of the country for the many different kinds of standards necessary for this new industry. The Symposium sponsored by the American Chemical Society Division of Nuclear Chemistry and Technology in cooperation with the Committee on Standardization Relations brought together most of the groups with interests in standards for nuclear chemistry and technology to identify the problems, to discuss present programs, and to outline future needs for standards in this broad field. Standards for purposes of the symposium were defined very broadly to include standard materials, standard procedures, standard specifications, standard data, and engineering standards. The mechanisms available for standardization, the "state of the art" in standardization in many areas of the nuclear field, some indications of unmet needs, and estimates of future needs were discussed in a series of papers and panel discussions which are presented here in either complete or summary form.

Key words: Activation analysis standards; isotope reference standards; nuclear fuel burn-up standards; radiation effect standards; radioactivity standards; standards for nuclear chemistry; standards for nuclear technology.

Interrelations between cement and concrete properties, Part 4, Shrinkage of neat portland cement pastes and concretes, Blaine, R. L. Arni, H. T., Evans, D. N., *Nat. Bur. Stand. (U.S.), Bldg. Sci. Ser. 15, 79 pages (March 1969), 75 cents.*
The relationship between cement properties and drying shrinkage of partially hydrated neat cement pastes of normal consistency made of a large number of portland cements of different types and composition were studied by fitting multivariable regression equations with the aid of a digital computer. The time of cracking of annular specimens restrained from shrinking by a steel core varied from 0.1 to more than 40 hours. The principal variables which appeared to have the greatest effect were the fineness and K_2O and C_4AF contents of the cements. The fineness and K_2O contents of the cements appeared to have the greatest effect on the nonrestrained shrinkage of prisms at the time of cracking of the annular specimens. The shrinkage of neat cement bars after 1, 6, 27 days, and 6 months in laboratory air differed greatly with different cements. The principal variables appeared to be the C_3A, SO_3, and C_3A/SO_3 ratios. Other commonly determined variables were associated with each of the above test values. The trace elements, other than Na_2O and K_2O, were not generally associated with the shrinkage or cracking characteristics.

Key words: Chemical composition of portland cements; cracking of portland cements; cracking resistance of cements; portland cement; shrinkage of portland cements; trace elements.

Line emission sources for concentration measurements and photochemistry, Braun, W., Carrington, T., *Nat. Bur. Stand. (U.S.), Tech. Note 476, 23 pages (March 1969), 30 cents.*
When a resonance line is absorbed in its own gas, measurements of this absorption can be used to derive a value of the product, nf, of concentration of the absorber and f value of the transition. This line absorption process is also important in the study of fluorescence and photochemistry, where it is possible to produce atoms or molecules in a single quantum state without otherwise disturbing the system. The interpretation and success of these applications of line absorption depend critically on the shape of the line emitted by the light source. This is strongly influenced by the optical depth in the emitting region, and by the inevitable presence of a reversing layer through which the light must travel on its way out of the lamp. This paper presents a simple model which can be used to estimate the effects of these properties of the light source on the threshold and sensitivity of measurements of nf, and on the power which can be delivered to absorbing atoms outside the lamp. Emphasis is on the general principles of lamp design and diagnosis, rather than on accurate description of a particular lamp.

Key words: Spectroscopy; photochemistry; analysis; gas; vacuum ultraviolet; absorption.

Methods of measurement for semiconductor materials, process control, and devices. Bullis, W. M., ed., *Quarterly report October 1 to December 31, 1968, Nat. Bur. Stand. (U.S.), Tech. Note 475, 38 pages (Feb. 1969), 45 cents.*
This second quarterly progress report in this series describes NBS activities relating to: measurement of resistivity, carrier lifetime, inhomogeneities, and Hall effect in semiconductor crystals; study of infrared measurement methods, properties of deep-lying impurities (in InSb), and high field effects; establishment of a processing facility; evaluation of aluminum metallization, wire bonds, and wafer die attachment; review of NASA measurement methods; and measurement of second breakdown in transistors, thermal properties of devices, and noise in microwave diodes. Projects on silicon nuclear radiation detectors and specification of germanium are also described. Supplementary data concerning staff, committee activities, technical services, and publications are included as appendixes.

Key words: Carrier lifetime; die attachment; electrical properties; germanium; metallization; methods of measurement; microelectronics; resistivity; semiconductor devices;

semiconductor materials; semiconductor process control; silicon; thermal resistance; thermographic measurements; wire bonds.

Incipient and developed cavitation in liquid cryogens, Edmonds, D. K., Hord, J., *Nat. Bur. Stand. (U.S.), Tech. Note 374, 31 pages (Feb. 1969), 35 cents.*
Cavitation characteristics of liquid hydrogen and liquid nitrogen flowing in a transparent plastic venturi have been determined and conventional cavitation-inception-parameter curves are given. Representative developed-cavitation data, consisting of pressure and temperature measurements within fully-developed cavities, are also given; measured temperatures and pressures within the cavities were generally not in thermodynamic equilibrium. Existing theory was used to obtain equations which correlate the experimental data for developed cavities in liquid hydrogen or liquid nitrogen. The theory is extended to include the effect of cavity thickness and the experimental data are used to evaluate the results. Some recommendations for future work are given.

Key words: Cavitation; cryogens; incipience.

Thermodynamic properties of argon from the triple point to 300 K at pressures to 1000 atmospheres, Gosman, A. L., McCarthy, R. D., Hust, J. G., *Nat. Bur. Stand. (U.S.), Nat. Stand. Ref. Data Ser. 27, 153 pages (March 1969), $1.25.*
Tabular values of density, internal energy, enthalpy, and entropy of liquid and gaseous argon are presented for temperatures from 83.8 to 300 K at pressures of 0.01 to 1000 atmospheres. Diagrams of specific heats, compressibility factor, and entropy are included. The properties presented are calculated from an equation of state which was fitted to experimental P–ρ–T data from the world literature. Extensive comparisons were made between the equation of state and the experimental data, and deviation plots are presented. The second virial coefficient and Joule-Thomson inversion curve were also calculated and comparisons made with values from other sources. A vapor pressure equation which covers the range from the triple point to the critical point is also given.

Key words: Argon; compressibility factor; enthalpy; entropy; equation of state; internal energy; Joule-Thomson coefficients; P–V–T; specific heat; vapor pressure; virial coefficient.

The performance of roofing made with Asplund felts, Greenfeld, S. H., *Nat. Bur. Stand. (U.S.), Tech. Note 477, 27 pages (March 1969), 35 cents.*
A study of the durability of roofing made with Asplund wood fibers was conducted from 1942 to 1967. Concentrations of 0 to 60 percent wood fibers (oak or pine) prepared by three variations of the Asplund process were evaluated. All the mineral-surfaced roll roofings and shingles were performing well after 25 years, with only four specimens showing more deterioration than the controls (only rags and paper in their felts). No differences in performance could be related to the felt composition.

Key words: Asphalt; Asplund; felt; mineral-surfaced roll roofing; shingles; wood fibers.

Precision measurement and calibration. Statistical concepts and procedures, Ku, H. H., Editor, *Nat. Bur. Stand. (U.S.), Spec. Publ. 300, Volume* **I,** *436 pages (Feb. 1969), $5.50.*
This volume is one of an extended series which brings together the previously published papers, monographs, abstracts, and bibliographies by NBS authors dealing with the precision measurement of specific physical quantities and the calibration of the related metrology equipment. The contents have been selected as being useful to the standards laboratories of the United States in tracing to NBS standards the accuracies of measurement needed for research work, factory production, or field evaluation.
Volume 1 deals with methodology in the generation, analysis, and interpretation of precision measurement data. It contains 40 reprints assembled in 6 sections: 1) The Measurement Process 2) Design of Experiments in Calibration 3) Interlaboratory Tests 4) Functional Relationships 5) Statistical Treatment of Measurement Data 6) Miscellaneous. Each section is introduced by an interpretive forework, and the whole is supplemented by abstracts and selected references.

Key words: Accuracy; analysis of measurement data; design of experiments; functional relationships; interlaboratory tests; measurement process; precision; statistical concepts in measurements; systematic error.

Activation Analysis Section: Summary of activities July 1967 to June 1968, LaFleur, P. D., Editor, *Nat. Bur. Stand. (U.S.), Tech. Note 458, 109 pages (March 1969), $1.00.*
The facilities used by the reactor, LINAC and neutron generator groups for activation analysis are described. Proposed installation of four new irradiation terminals and a new pneumatic transfer tube system are outlined.
A new 2.5-mA neutron generator has been installed and the biological shield, pneumatic transfer system and the detector assembly modified. Studies of blank problems for oxygen determination and self-absorption corrections in photopeak analysis have resulted in greatly improved precision for Standard Reference Materials. Halide in photographic emulsions, using 14-MeV and 2.6-MeV neutrons, have been determined.
Considerable emphasis has been placed on the development of group radiochemical separations, SRM steel and high purity zinc samples have been analyzed using this technique.
Eighteen different SRMs were analyzed for a variety of elements and a variety of service analyses were performed.
The self-absorption effects of the matrix on irradiation photons were studied and calculations of sensitivities for photon activation analysis were made. Carbon in sulfur, yttrium in rare earth oxides and oxygen in sodium were determined by photon activation.
The extraction of metals by bis(2-ethylhexyl) orthophosphoric acid has been studied, and distribution coefficients are given for many of the transition metals. The results indicate enhanced applicability of this reagent for radiochemical separations.
Updated keys for computer literature searching and a sample output are included.

Key words: Activation analysis; Cockcroft-Walton neutron generator; computer literature searching; extraction; group separations; homogeneity testing; hydrogen bis(2-ethylhexyl) phosphate; matrix effect; molybdenum, NBS LINAC, NBS reactor, photon activation analysis sensitivities; Standard Reference Materials; zinc.

Edpac: Utility programs for computer-assisted editing, copy-production, and data retrieval, Messina, C. G. Hilsenrath, J., *Nat. Bur. Stand. (U.S.), Tech. Note 470, 80 pages (Jan. 1969), 75 cents.*
A description and listings are given of EDPAC, a package of five related utility computer programs: SCRAMBLE, SUBSTITUTE, SEARCH, BLOCKSEARCH, JUSTIFY, and their subroutines. These programs perform transformations on alphanumeric data. The programs have been written in FORTRAN, with care taken to make them as system and machine-independent as possible, permitting their use on many different computers.
SCRAMBLE scans an input-file for specified characters, which it replaces by different characters. SUBSTITUTE similarly replaces strings of characters by other strings. SEARCH and BLOCKSEARCH scan for the occurrence of certain strings and list the lines or blocks, respectively, in which they occur. JUSTIFY produces text, for printing on a card-controlled typewriter or on an extended character printer, which has been left and right-justified between specified margins.
Some applications of the EDPAC programs are discussed. Emphasis is placed on computer-assisted text preparation.

Key words: Alphanumeric data files; computer-assisted text preparation; data retrieval, FORTRAN programs; free field text files; mechanized text editing.

A semi-automated single fingerprint identification system, Wegstein, J. H., *Nat. Bur. Stand. (U.S.), Tech. Note 481, 23 pages (Apr. 1969), 30 cents.*
A system is described in which a fingerprint is manually coded by tracing certain ridges and noting events such as ridge endings and ridge beginnings. This code is sent by teleprinter to a central file

where a computer identifies the fingerprint by comparing the code with codes previously entered in the file. The scheme for comparing codes is given along with some preliminary test results using typical fingerprints.

Key words: Computerized-fingerprint identification, fingerprints, pattern-recognition.

Standard Reference Materials: Homogeneity characterization of NBS spectrometric standards IV: Preparation and microprobe characterization of W–20% Mo alloy fabricated by powder metallurgical methods, Yakowitz, H., Michaelis, R. E., Vieth, D. L., *Nat. Bur. Stand. (U.S.), Spec. Publ. 260–16, 30 pages (Jan. 1969), 35 cents.*

A significant problem of the National Bureau of Standards Standard Reference Materials program is the provision of standards suitable in homogeneity for use with micro analytical techniques such as the spark source mass spectrograph and the electron probe microanalyzer. An interim approach to the problem has been the extended homogeneity characterization of selected existing standards. This paper describes the preparation and evaluation of the first NSB standard tested specifically from the beginning for application to electron probe microanalyzers. The standard designated SRM 480 is a tungsten-20 weight percent molybdenum alloy prepared by a powder metallurgy process. Based on the results of about 1500 determinations for both tungsten and molybdenum by electron probe microanalysis, the material was found to be of high homogeneity at about the micrometer level of spatial resolution. The coefficient of variation for molybdenum was 2.5% and that for tungsten 1.5%. Correction of relative intensity ratios to obtain concentrations is discussed in terms of input parameter uncertainties such as mass absorption coefficients, and electron backscatter factors. The result of studies for atomic number correction and effects on operating voltage on the microprobe absorption correction, will be given. It is concluded that SRM 480 should be a valuable addition to any microprobe laboratory doing quantitative analyses.

Key words: Electron probe analysis; metallography; powder metallurgy; spectrometric standards; Standard Reference Materials; W-Mo alloys.

Neutron damage in single crystal aluminum oxide, Barber, D. J., Tighe, N. J., *J. Am. Ceram. Soc.* **51,** *No. 11, 611–617 (Nov. 1968).*

Sunthetic aluminum oxide crystals were irradiated with fast neutrons to a dose of 1.8×10^{20} nvt and examined by transmission electron microscopy. As-irradiated crystals contained damage on a fine scale, revealed by diffraction contrast and showed a 28% increase in Knoop diamond hardness compared with un-irradiated material. Annealing above 600 °C, which decreased the hardness, caused the small defect clusters to grow, forming dislocation loops on $\{10\bar{1}0\}$ planes, with $\langle 10\bar{1}0\rangle$ Burgers vectors. Vacancy and interstitial loops occurred. High temperature annealing caused the loops to interact to give dislocation segments; these tended to align with the $\langle 10\bar{1}0\rangle$ and $\langle 11\bar{2}0\rangle$ directions. Grown-in dislocations also began to climb at high temperatures but showed evidence of impurity pinning. Isolated platelike precipitates on $\{10\bar{1}0\}$ planes were also observed at high temperatures but showed evidence of impurity pinning. Isolated platelike precipitates on $\{10\bar{1}0\}$ planes were also observed in samples annealed at high temperatures. Possible effects of the observed damage on physical properties are considered and there is qualitative agreement between predictions and existing data.

Key words: Aluminum oxide; defects; electron microscopy; neutron damage dislocations; sapphire.

Equilibrium properties of acids and bases in amphiprotic mixed solvents, Bates, R. G. *(Proc. Symp. Equilibria and Reaction Kinetics in Hydrogen Bonded Solvent Systems, University of New Castle, Upon Tyne, England, Jan 10–12, 1968), Chapter in Hydrogen-Bonded Solvent Systems, A. K. Covington and P. Jones, ed., pp. 49–86 (Taylor and Francis, London, England, 1968).*

Binary mixed solvents which contain water as one component possess the capacity to react protolytically both with hydrogen acids and with their conjugate bases. Although the acid-base behaviour of many of these solvent mixtures resembles that of water in kind, wide differences of degree are observed. Furthermore, there is evidence that solute-solvent interactions become more complex as the dielectric constant of the mixed medium is lowered. The effect of adding an organic constituent to aqueous solutions of acids and bases is examined through summaries of data for standard electromotive forces, equilibrium constants, medium effects, and thermodynamic functions for the transfer from water to mixed solvents of various compositions. Systems consisting of strong and weak electrolytes in mixed solvents are considered. An attempt is made to identify the factors on which the observed solvent effect depends. In particular, the roles of dielectric constant, solvent basicity, hydrogen bonding, sorting of the two types of solvent molecules by the ions, and the formation of ion pairs and higher aggregates are discussed. Recent proposals for the establishment of a useful scale of individual ionic transfer energies for mixed solvents are reviewed.

Key words: Acidity; medium effects; mixed solvents; solvation of ions; solvent effect; transfer energy.

Satellite geodesy using laser range measurements only, Bender, P. L., Alley, C. O., Currie, D. G., Faller, J. E., *J. Geophys. Res.* **73,** *No. 16, 5353–5358 (Aug. 15, 1968).*

We have investigated the potential accuracy with which the distances between 12 observing stations spread fairly uniformly over the earth can be determined by using laser range measurements to a high altitude satellite equipped with optical retro-reflectors. For each of 30 satellite positions, it was assumed that range measurements were made at about the same time from the 4 closest stations. For ideal distribution of the stations, the expected uncertainty in the distance between any two stations was found to be less than 45 cm, with little dependence on satellite altitude over the range of 20,000 to 110,000 km. With 12 stations chosen from the Pageos Worldwide Geometric Satellite Network, the expected accuracy for a satellite altitude of 110,000 km is 60 cm or better between any two stations.

Key words: Geodesy; laser; geodetic satellite; distance measurements; worldwide geodetic network; geophysics; continental drift.

Decay modes with coherent resonant-energy transfer between deep impurities in solids, Casella, R. C., *Phys. Rev.* **174,** *No. 3, 830–834 (Oct. 15, 1968).*

Attention is called to the existence of new decay modes for deep impurities in solids associated with coherence in the resonant-energy transfer between them. The theoretical decay rate R of the two-impurity complex is of the form,

$$R(t) = C_1 \exp(-\gamma_1 t) + C_2 \exp(-\gamma_2 t) + \exp[-\tfrac{1}{2}(\gamma_1+\gamma_2)t] \times \mathrm{Re}\, D \exp(-i\Delta t),$$

with C_n and γ_n real positive and D complex. The oscillations in time, t exhibited by the third term in the expression for R provide an experimental test for the coherence effect. The partial rate $R_r(t)$ for radiative decay is of the same form as $R(t)$. In the analysis, use is made of an analogy between the decay of the excited impurity complex and that of K° mesons in particle physics, where similar coherent oscillations have been observed experimentally.

Key words: Coherence; decay modes; impurities; resonant-energy transfer.

Search for plasmaron structure in the soft x-ray $L_{2,3}$ emission spectrum of Al, Cuthill, J. R. Dobbyn, R. C., McAlister, A. J. Williams, M. L., *Phys. Rev.* **174,** *No. 2, 515–517 (Oct. 10, 1968).*

The $L_{2,3}$ soft X-ray emission spectrum of Al has been carefully scanned for a weak low energy edge predicted by recent theoretical studies of the interacting electron gas. A very weak structure, near the predicted location, but just within the noise, is seen. An upper limit to the magnitude of such structures is established, and it is suggested that the light alkali metals should provide a better test of the theory.

Key words: Aluminum; electron gas; emission spectrum; excitations; plasmaron; soft X-ray.

Soft X-ray spectra and comparison with the theoretical density of states, Cuthill, J. R., McAlister, A. J., Williams, M. L., Dobbyn, R. C. *(Proc. Conf. Soft-X-ray Band Spectra and the Electronic Structure of Metals and Materials, Strathclyde, Scotland, Sept. 18–21, 1967), Chapter in Soft X-ray Band Spectra and the Electronic Structure of Metals and Materials. Part II. Heavy Metal and Alloy Spectra and Comparison with other Optical Methods, pp. 151–162 (Academic Press Inc., New York, N. Y., 1968).*

Emission spectra are being obtained with a 2-meter grazing incidence glass grating (30,000 lines/inch) spectrometer with photoelectron detection and digital recording. The long range objective is information pertaining to the changes in the density of states with alloying and intermetallic compound formation. However, most of the effort to date has been on the determination of the nickel-$M_{2,3}$ spectrum and its relation to the density of states in nickel. The temperature was held at 960 ± 7 °C to insure an oxide-free surface. Anumber of scans were summed to resolve detail that has not been resolved heretofore. Calculated transition probabilities appear to account for the observed L band always being narrower than the M.

A comparison of Al-$L_{2,3}$ and Ni-$M_{2,3}$ overlapping spectra from $NiAl_3$, NiAl, and 8 and 4% Al in nickel solid solutions together with the spectra of the pure metals, reveals certain major features of the soft X-ray spectra to be unrelated to crystal structure. The observed spectra suggest that the electronic structure of the aluminum undergoes a progressive change with increasing nickel content whereas the high energy X-ray L emission edge remains unshifted at least up to 50% Ni. In contrast to the Ni-Al system there is no overlap of the titanium-$M_{2,3}$ spectrum with the nickel-$M_{2,3}$ spectrum in the case of the Ti-Ni system. The nickel-$M_{2,3}$ from Ni in TiNi exhibits a peak at the same energy as that of the peak in the pure Ni spectrum but also exhibits a much larger peak about 3 eV lower in energy.

Key words: Aluminum; density of states; L-emission band; M-emission band; Ni-Al system; nickel; soft X-ray spectroscopy; TiNi intermetallic compound; transition probability energy.

Diffusion rates in solids, Dragoo, A. L., *Chapter IV in Atomic Energy Review,* O. Kubaschewski, *ed.,* **2,** *187–202 (International Atomic Energy Agency, Vienna, Austria, 1968).*

A discussion of the types of diffusion coefficients and of the experimental techniques for their determination is presented for inclusion in the International Atomic Energy Agency Monograph Series on the Physicochemical Properties of Nuclear Materials. The diffusion coefficients for tracer diffusion, self-diffusion, intrinsic diffusion, chemical inter-diffusion and grain-boundary diffusion are described. Experimental methods and limitations are discussed for (1) metallic and metalloid ion diffusion in borides, carbides, nitrides and oxides of Be, Ti, Zr, Hf, Nb, Ta, Mo, Th, and U; (2) diffusion of B, C, N, and O in metals; and (3) rare gas diffusion from compounds used as nuclear fuels.

Key words: Borides; carbides; diffusion rates; nitrides; oxides of nuclear materials.

Influence of irradiation rate on the production of *F* centers in LiF (TLD grade), Ehrlich, M., *Proc. Second Intern. Conf. Liminescence Dosimetry, Gatlinburg, Tenn., Sept. 23–26, 1968, J. A. Auzier, K. Becker, E. M. Robinson, ed., Paper No. CONF–680920 Health and Safety (TID–4500), pp. 322–326 (Oak Ridge National Laboratory, Oak Ridge, Tennessee, Sept. 1968).*

Optically polished samples of extruded plaques of LiF (TLD grade) were given ^{60}Co gamma-ray exposures ranging from about 30 000 *R*(9 C/kg) to 450 000 *R*(120 C/kg), at exposure rates between about $1.5 \times 10^3 R/h$ (0.39 C/kg *h*) and 5×10^6 *R*/*h* 1300 C/kg *h*). Over this range of exposures and exposure rates, the resulting absorption in the *F* band was found to be independent of exposure rate, and to increase with exposure, even for exposures for which the thermoluminesence exhibited saturation effects. After thermoluminescence readout at about 235 °C, practically all the absorption in the *F* band created by the ^{60}Co gamma-ray exposures had disappeared. These results are compatible with the dominant role given *F* centers in some of the current models for the thermoluminescence process in LiF (TLD grade).

Key words: ^{60}Co gamma radiation; *F*-center formation, LiF (TLD grade); ate dependence; thermoluminescence.

Thermoluminescence response of LiF to X- and gamma rays; a study of rate and energy dependence over a wide range of exposures, Ehrlich, M., *Proc. First Intern. Congress Radiation Protection, Rome, Italy, Sept. 5–10, 1966, pp. 429–434 (Pergamon Press Inc., New York, N.Y., 1968).*

The total thermoluminescence light emission ("response") of LiF (TLD grade) was studied as a function of exposure and exposure rate, and as a function of photon energy. Co^{60} gamma rays and a broad spectrum of low-energy bremsstrahlung were employed. No rate dependence of the response was detected over the entire range of exposures and exposure rates employed (from about 10^2 *R* to 2×10^7 *R*, and from about 10^2 *R*/*h* to 7×10^6 *R*/*h*, respectively). This represents further evidence that centers other than *F* centers are involved in the thermoluminescence of LiF (TLD grade).

A comparison of the curves of response versus exposure for the two photon spectra confirms Naylor's findings that the superlinearity region is steeper for Co^{60} gamma radiation than for low-energy x rays, and reveals that the effect is indeed dependent on photon energy rather than on exposure rate. These findings are compatible with an explanation of superlinearity as being due to the formation of additional traps by the radiation proper. For exposures above those causing superlinearity, the difference in curve shape again disappears. Also, there is no dependence on energy of the location and height of the response maximum, which suggests that the inhibiting mechanism is independent of photon energy.

Key words: Bremsstrahlung; Co^{60} photons; energy dependence; *F* centers; impurities; LiF (TLD); rate dependence; superlinearity; thermoluminescence; trap formation.

Nature of a colored by-product found in crude inosose phenylosazones, Fatiadi, A. J., *Carbohydrate Res.* **9,** *177–185 (1969).*

It has been shown that the crude inosose phenylosazones from D- and L-*myo*-inosose-1, *myo*-inosose-2, and DL-*epi*-inosose-2 contain a red, enolic impurity having a known structure, namely, *xylo*-2-oxo-1, 3-bis(phenylhydrazono)cyclohexane-4,5,6-triol. Similarly, the crude inosose phenylosazones from quebrachitol (1-*O*-methyl-*levo*-inositol) and pinitol (5-*O*-methyl-*dextro*-inositol) also contain a colored, enolic impurity having a structure analogous to that obtained from the above nonmethylated inosose phenylosazones.

Key words: Crude inosose; enols; formation; inositol; oxidation; phenylosazone.

Stress-induced dichroism at the absorption edge of $SrTiO_3$, Feldman, A., Horowitz, D., *Solid State Commun.* **6,** *607–612 (1968).*

The stress-induced dichroism at the absorption edge of $SrTiO_3$ has been measured at room temperature by the rotary transmission method. Stess- and strain-absorption coefficients were determined for the range of photon energies 3.15–3.22 eV. Our results, together with the selection rules derived by Casella, cast doubt upon the assignment of the absorption edge of $SrTiO_3$ to the transition $X_5' \rightarrow X_3$.

Key words: Absorption edge; dichroism; rotary transmission method; selection rules; $SrTiO_3$, uniaxial stress.

The laser absolute wavelength standard problem, Hall, J. L., *IEEE J. Quantum Elect.* **QE–4,** *No. 10, 638–641 (Oct. 1968).*

Stabilized lasers usually exhibit systematic frequency shifts larger than their resettability; this phenomenon is illustrated well by the 6328 Å Helium Neon laser. We describe a Lamb-dip stabilized laser which operates at 1.15259 microns in pure, low pressure (0.12 torr) neon. Optical heterodyne experiments indicate an accuracy exceeding 1 part in 10^9; short and medium term precisions of $1:10^{10}$ are easily achieved. We also report the successful operation of a wavelength reference based on the saturation of sharp molecular absorption. In the first experiments the P(7)-line of the ν_3 band of methane is saturated inside the cavity of a 3.39 micron Helium-neon laser. The saturation maximum at molecular line center produces an "emission" feature whose linewidth is less than 5 parts in 10^9. The pressure-induced offset is expected to be less than 1 part in 10^{10}. Size scaling is expected to improve these first results by at least 1 decade.

Key words: Laser wavelengths standards; wavelength stabilization; saturated molecular absorption.

Non-coherent scattering-IV. Doppler redistribution functions in moving atmospheres, Hummer, D. G., *Monthly Notices Roy. Astron. Soc.* **141,** *479–488 (Dec. 1968).*
Redistribution functions and their directional averages are derived for scattering by an assembly of atoms possessing a Maxwellian distribution in a frame moving with respect to the observer. Various assumptions concerning the form of the absorption coefficient and the coherence properties in the atom's rest frame are considered. The exact redistribution function for pure Doppler broadening is expanded in Legendre polynomials to facilitate evaluation of the source function. From the expansion it is clear that the use of direction-averaged redistribution functions will be significantly less accurate for moving than for static media.

Key words: Spectral line; redistribution function; non-coherent scattering; radiation transfer.

Mechanisms of microbial corrosion, Iverson, W. P. (*Proc. First Intern. Biodeterioration Symp., Southampton, England, Sept. 9–14, 1968*), *Chapter in Biodeterioration of Materials. Microbiological and Allied Aspects, pp. 28–43 (Elseyier Publ. Co., Ltd., Essex, England, 1968).*
A discussion of the general and specific mechanisms of microbial corrosion with special emphasis on anaerobic corrosion. General mechanisms include the production of corrosive metabolic products, the initiation of oxygen concentration cells and cathodic depolarization. Recent evidence to be presented indicates that the cathodic depolarization theory may at least in part explain the corrosion due to microorganisms in an anaerobic environment.

Key words: Microbial corrosion; corrosion mechamisms; cathodic depolarization; oxygen concentration cells; metabolic products; anaerobic corrosion.

Selection of the intermolecular potential. Part 2.—From data of state and transport properties taken in pairs, Klein, M., Hanley, H. J. M., *Trans. Faraday Soc.* **64,** *Part II, No. 551, 2927–2938 (Nov. 1968).*
A method previously developed to evaluate quantitatively the relationship between intermolecular potential functions and individual macroscopic properties is extended to the simultaneous fit of all possible pair combinations of these properties. As before the relationship between function families available at this time has been clarified. New results from this investigation give important information on the possible simultaneous fit of a simple function to more than one property. The function families studied were the m–6, Kihara, exp-6 and Morse functions. A reduced temperature range was found over which the simultaneous fit to pairs of properties is insensitive to the potential function. When a transport property is involved, this range is given by $2.0 < T_{12-6} < 5.0$ while if only equilibrium properties are involved, this range becomes $2.0 < T_{12-6} < 10.0$. Quantitative limits are given for the experimental error which can be tolerated without masking the sensitivity to the potential function outside these ranges.

Key words: Intermolecular potential function; experimental data; simultaneous correlation; transport properties; equilibrium properties.

Effects of excluded volume on light scattered from flexible macromolecules, McIntyre, D., Mazur, J., Wims, A. M., *J. Chem. Phys.* **49,** *No. 7, 2887–2895 (Oct. 1, 1968).*
The effect of the non-Gaussian behavior of the chain segment distribution in flexible polymer coils on the angular distribution of scattered light is discussed. The explicit form of a general spherical segment distribution function,

$$W(r, N)\,dr = \frac{t}{\Gamma(3/t)}\left[\frac{\Gamma(5/t)}{\Gamma(3/t)\langle R_N^2\rangle}\right]^{3/2} \exp-\left[\frac{\Gamma(5/t)r^2}{\Gamma(3/t)\langle R_N^2\rangle}\right]^{t/2} r^2 dr,$$

with different values of t, is used to evaluate the general scattering equation for the particle scattering factor $P(\theta)$.

$$P(\theta) = \frac{1}{N^2}\sum_i \sum_{i>j} \frac{\sin ksr_{ij}}{ksr_{ij}}.$$

In addition, the effects of excluded volume on the mean end-to-end chain separation is taken to be of the form

$$\langle R_N^2\rangle \approx N^{1+\epsilon},$$

where N is the number of chain steps and ϵ is a parameter, which measures the excluded volume effect on the $\langle R_N^2\rangle$. In this paper, an expansion of the $P(\theta)$ function to the first few terms is carried out and numerically evaluated for the dependence of $P(\theta)$ on the variable x, where $x = ks\langle R_{exp}\rangle$, k is the wave number of the incident light, s is related to the scattering angle and $\langle R_{exp}\rangle$ is the radius of gyration determined from experimental data of the scattering cross section. The computations were carried out for the polymer in good solvent, for which data for ϵ and t were adopted, based on the lattice model of non-self intersecting chain, and for polymer in theta solvent, for which Gaussian chain model was adopted. The computations were carried out for various degrees of polydispersity. A comparison was made between the theoretical and the experimental results on a polystyrene sample of molecular weight of 4.10^6 in cyclohexane at 35 °, 45 °, 55 °C and in benzene at 40 °C.

Key words: Chain-end distribution; excluded volume; light scattering; particle scattering factor; polydispersity.

A millimeter wave reflectometer, Little, W. E., Patty, O. L., Zanboorie, M. H., *IEEE Trans. Microwave Theory Tech.* **MTT-16,** *No. 2, 121 (Feb. 1968).*
This paper describes a millimeter wave reflectometer system that has been developed in WR–12 waveguide. A detailed description of the system circuitry, a discussion of sources of measurement error and some measurement results are presented.

Key words: Reflectometer; WR-waveguide; millimeter wave.

$SU(6)_W$ and high-energy photoproduction, Meshkov, S., Ponzini, R., *Phys. Rev.* **175,** *No. 5, 2030–2034 (Nov. 25, 1968).*
$SU(6)_W$ is used to make quantitative predictions for forward photoproduction cross sections at high energies. The predicted ratios for $\sigma(\gamma p|K^+\Sigma^0)/\sigma(\gamma p|K^+\Lambda)$ which vary from 0.5 to 1.0 for incident photons of energy 5–16 GeV are in good agreement with the SLAC experiments. This is in contrast to the quark model prediction of 1/27. Forward $\rho^0 p$ and ωp photoproduction cross sections also agree very well with experiment, but φp is too large by a factor of two.

Key words: Dominance; meson; photoproduction-meson; $SU(6)_W$; symmetry; vector.

Configuration interaction theory. Effects of overlapping resonances, Mies, F. H., *Phys. Rev.* **175,** *No. 1, 164–175 (Nov. 5, 1968).*
A generalized version of Fano's configuration interaction theory is presented which includes the interaction of many resonances with many continua and inelastic couplings between continuum states. In particular a new parameter is introduced; the overlap matrix between the continua to which neighboring resonances are coupled. Resonances which are coupled to the same channel states may be said to overlap. If their widths are comparable to their spacings the resultant effects on photoabsorption or on the scattering matrix can be quite profound. The apparent widths may bear little relation to the widths due to configuration interaction, and the resultant structure may not fit the usual Fano shapes for isolated resonances.
The effects of overlapping are examined for various models which are representative of atomic photoabsorption and electron-diatomic molecule scattering. It is demonstrated that without prior knowledge of the overlap matrix it is impossible to uniquely characterize a resonance from limited experimental observations. Scattering and photoabsorption experiments should be designed to examine all possible channels; both differential cross-sections and inelastic cross-sections. Even so, without the parallel support of theoretical estimates of partial widths, and the signs of the configuration interaction matrix elements, the interpretation of resonance phenomena and in particular the parameters which are extracted must be accepted with severe reservations.

Key words: Configuration interaction; resonances; overlapping resonances, autoionization, resonant scattering, photoionization, electron scattering.

Nuclear spin-lattice relaxation in very dilute solutions of orthohydrogen in parahydrogen, Miller, C. E., Lipsicas, M., *Phys. Rev.* **176,** *No. 1, 273–279 (Dec. 5, 1968).*
Measurements have been made of the proton spin lattice relaxation time in very dilute solutions of orthohydrogen in parahydrogen, as a function of temperature, density and fractional orthohydrogen concentration. Both the liquid phase, between 20K and 30K, and the gas phase, between 34K and 40K, have been studied. The salient features of the temperature and density dependences, qualitatively, fit an interpretation in terms of contributions from two particle and three particle correlations, as proposed by Deutch and Oppenheim.

Key words: Nuclear magnetic resonance; ortho hydrogen; relaxation time.

Matrix-isolation study of the vacuum-ultraviolet photolysis of difluorosilane. The infrared and ultraviolet spectra of the free radical SiF_2, Milligan, D. E., Jacox, M. E., *J. Chem. Phys.* **49,** *No. 10, 4269–4275 (Nov. 15, 1968).*
In studies of the vacuum-ultraviolet photolysis of $SiHF_3$ suspended in argon, nitrogen, and carbon monoxide matrices at 14 °K, evidence has been obtained indicating that H-atom detachment occurs and that the SiF_3 free radical is stabilized. All of the vibrational fundamental of SiF_3 have been observed in these experiments. The appearance of two stretching fundamentals requires that the molecule be nonplanar. A more detailed consideration of the pattern of vibrational absorptions indicates that the angle between each Si-F bond and the threefold symmetry axis of the molecule is approximately 71°, close to the value characteristic of sp^3 hybridization of the valence electrons about the central atom. Force constants have been estimated using a four-constant valence-force potential, and the thermodynamic properties of SiF_3 have been calculated.

Key words: Force constants; infrared spectrum; matrix isolation; SiF_3 free radical; thermodynamic properties; trifluorosilane; ultraviolet spectrum; vacuum; ultraviolet photolysis.

Matrix-isolation study of the vacuum-ultraviolet photolysis of trifluorosilane. The infrared spectrum of the free radical SiF_3, Milligan, D. E., Jacox, M. E., Guillory, W. A., *J. Chem. Phys.* **49,** *No. 12, 5330–5335 (Dec. 15, 1968).*
In studies of the vacuum-ultraviolet photolysis of $SiHF_3$ suspended in argon, nitrogen, and carbon monoxide matrices at 14 °K, evidence has been obtained indicating that H-atom detachment occurs and that the SiF_3 free radical is stabilized. All of the vibrational fundamentals of SiF_3 have been observed in these experiments. The appearance of two stretching fundamentals requires that the molecule be nonplanar. A more detailed consideration of the pattern of vibrational absorptions indicates that the angle between each Si-F bond and the threefold symmetry axis of the molecule is approximately 71°, close to the value characteristic of sp^3 hybridization of the valence electrons about the central atom. Force constants have been estimated using a four-constant valence-force potential, and the thermodynamic properties of SiF_3 have been calculated.

Key words: Force constants; infrared spectrum; matrix isolation; fluorosilane; ultraviolet spectrum; vacuum-ultraviolet photolysis.

Localized modes, resonant modes and impurity vibrational bands in vanadium alloys, Mozer, B., *Chapter in Neutron Inelastic Scattering,* **1,** *55–63 (Intern. Atomic Energy Agency, Vienna, Austria, 1968).*
Inelastic neutron scattering data have been obtained on Be-V, Ta-V, W-V, Ni-V, and Cr-V alloys in a search for defect modes of vibration, impurity vibrational bands, and effects on the vibrational spectrum arising from perturbed electron energy bands in some of these alloys. The results of these experiments show for the light mass beryllium atoms a single localized mode at 0.047 eV at low concentration and in agreement with theory for an isotopic defect; impurity bands with structure are observed at higher concentrations. A decay constant of 2.5 a_0^{-1} for the amplitude of a localized mode can be obtained from the observed splitting. Evidence is scant for resonant modes from heavy mass atoms in vanadium as observed in the very small difference between alloy vibrational spectra and the pure vanadium spectrum. Very small peaks are observed corresponding to a splitting of the resonant modes with no theoretical explanation available. Ni-V and Cr-V alloys of equal electron concentration show similar spectra but differing greatly from the pure vanadium spectrum. Arguments on how the electron density influences the magnitude of the high frequency vibrational spectra of the ions provide an indirect proof of the absence of bound electron states (localized states) associated with nickel ions in vanadium.

Key words: Alloys; bound states; inelastic neutron scattering; local modes; resonant modes.

Characteristic energy losses of 8-keV electrons in liquid Al, Bi, In, Ga, Hg, and Au, Powell, C. J., *Phys. Rev.* **175,** *No. 3, 972–982 (Nov. 15, 1968).*
Characteristic loss spectra have been obtained in a reflection scattering geometry for liquid Al, Bi, In, Ga, Hg, and Au and, in the case of Al, Bi and Au, for the same specimens in the solid phase. Peaks due to surface and volume plasmon excitation dominated the loss spectra for all elements except Au. The relative intensity of these peaks varied rapidly with scattering angle for the liquid and frozen specimens but there was little angular variation when Al, Bi, or Au was evaporated onto a frozen substrate of the same element. The Al plasmon losses varied with temperature and changed at the mp as would be expected from the known density variation. Changes in the Bi plasmon energy losses on melting and changes in other structure on melting have been interpreted in terms of band-structure changes. The peaks in the gold loss spectra appeared to become broader and less distinct on melting from which it was concluded that the Au excited states had shorter lifetimes with increased disorder. In general, however, the liquid and solid-state spectra of the same element were similar, thereby showing that for these materials there was not a large change in band structure on melting.

Key words: Aluminum; bismuth; electron energy loss; gallium; gold; indium; liquids; mercury; solids.

Interaction of electrons with solids, Powell, C. J., *Chapter 9.2 in Atomic and Electron Physics, Atomic Interactions, Vol.* **7,** *Methods of Experimental Physics, B. Bederson, ed., Part B, pp. 275–305 (Academic Press Inc., New York, N.Y., 1968).*
A review is given of methods and techniques useful in experiments where electrons of energy between 0 and 100 keV interact with solids. A general discussion is given firstly of common experimental components and procedures: electron guns, energy analyzers, and electron detectors; specimen preparation; and experimental strategy. The interaction of electrons with solids is considered firstly by assuming that the solid can be represented as an assemblage of atoms, thereby simplifying the analysis. Elastic and inelastic scattering measurements are discussed, followed by a survey of methods useful in situations where multiple scattering occurs and where secondary or higher order electrons and photons are generated. Finally, the relevance of angular anisotropics in elastic and inelastic electron scattering by crystalline solids is described.

Key words: Cross-sections; elastic scattering; electron detectors; electron energy analyzers; electron guns; electron scattering; electron-solid interactions; experimental techniques; inelastic scattering; multiple scattering; secondary processes; specimen preparation.

Franck-Condon factors for high rotational levels of nitrogen, Shumaker, J. B., Jr., *J. Quant. Spectry. Radiative Transfer* **9,** *153–156 (1969).*
Franck-Condon factors and band strengths of some strong bands of the first negative, first positive, and second positive systems of nitrogen are calculated in the Morse potential approximation and are shown to exhibit little dependence upon rotational level up to rotational quantum number 100.

Key words: Franck-Condon factor; band strength; rotation-vibration interactions; nitrogen.

Production of synthetic food materials: A statistical survey, Proc. Second Intern. Steel, N. M., *Conf. Women Engineers and Scientists, 30 pages (Women's Engr. Soc., London, England, 1968).*
This paper summarizes statistics on the production, sale, and value of synthetic vitamins, flavors, and amino acids in the United States

from 1945 to 1965 and discusses the observed trends. In absence of statistics on the production in other countries, U.S. import statistics and information from industrial journals are examined for indications regarding quantities manufactured in other countries. U.S. shipment statistics are given for yeasts and are evaluated as a measure of the quantities being made. Production statistics for feed grade synthetic urea are also presented. The foregoing data are discussed in relation to the potential roles of synthetic and biosynthetic materials in meeting the world food deficit.

Key words: Synthetic food materials; production of synthetic food; food problems; amino acids; urea; yeast; food additives.

Mössbauer spectroscopy with Ni^{61}, Travis, J. C., Spijkerman, J. J., *Chapter in Mössbauer Effect Methodology*, **4**, *237–259 (Plenum Press Inc., New York, N. Y., 1968).*

The practical application of Mössbauer spectroscopy to the study of nickel compounds has been retarded by two factors: 1) the late discovery of a suitable, single line source, and 2) the short half lives of both possible parent isotopes of ^{61}Ni. A suitable source of 15 percent Cr in Ni is activated by one hour of exposure to 100 MeV bremsstrahlung in the NBS linear electron accelerator. The source has a fractional effect of 0.1 ± 0.02, and yields an experimental linewidth of 0.097 ± 0.002 cm/s when extrapolated to zero thickness in source and absorber.

Adequate data have been obtained to determine a magnetic moment ratio, $\mu_e/\mu_g = -0.568 \pm 0.055$, and an estimate for the change in the nuclear charge radius, $\delta R/R = -2.5 \times 10^{-4}$. The ground state quadrupole moment is negligible for Mössbauer spectroscopy. Spectra which illustrate pure magnetic, pure quadrupolar, and mixed (Laves phase) interactions have been obtained.

This paper discusses the preparation of a single line source, the evaluation of nuclear parameters, theoretical studies of the nuclear hyperfine interactions, and theoretical prediction of the electric field gradient tensor.

Key words: Nickel Mössbauer spectroscopy; single line source; chemical shifts; quadrupole splitting; internal magnetic fields; magntic fields; magnetic moment ratio; nuclear hyperfine interactions; electronic configurations.

Tensile loading device for Kossel microdiffraction and metallography, Vieth, D. L., Yakowitz, H., *Rev. Sci. Instr.* **39,** *No. 12, 1929–1931 (Dec. 1968).*

A loading device used primarily in conjunction with Kossel (divergent beam) x-ray diffraction is described. The device is compatible with any standard upright metallograph as well. It is four inches (10.1 cm) in diameter and accommodates specimens one inch in reduced section by 1/4 inch wide. The device utilizes small load cells having ranges of 0 to 10 pounds (445N) and 0 to 100 pounds (445N) respectively. Load cell error is $\pm 0.5\%$ of the full load capacity. Load changes of 0.2% of load capacity can be observed. The load device is mechanically and electrically stable. Loads are read on a standard commercial universal indicator.

Key words: Strain measurement; Kossel x-ray method; metallography instrument design; tensile testing; x-ray microdiffraction.

Adiabatic calorimetry from 300 to 800 °K, West, E. D., Westrum, E. F., Jr., *Chapter 9 in Experimental Thermodynamics, Vol.* **I,** *Calorimetry of Nonreacting Systems, J. P., McCullough and D. W. Scott, ed., pp. 333–367 (Butterworth and Co., London, England, 1968).*

Adiabatic heat capacity calorimetry in the range 300 to 800 °K is reviewed with discussions of principles and two particular calorimeters. The general heat flow problem is discussed qualitatively as it pertains to the design of calorimeters of this type. Construction details are included in the examples and related to the principles. The advantages and disadvantages of different methods of operation are discussed.

Key words: Adiabatic calorimetry; calorimeter; calorimetry; cryoscopy; melting; phase transition; purity; and thermodynamics.

Adiabatic low-temperature calorimetry, Westrum, E. F., Jr., Furukawa, G. T., McCullough, J. P., *Chapter 5 in Experimental Thermodynamics, Vol.* **I** *Calorimetry of Nonreacting Systems, J. P. McCullough and D. W. Scott, ed., 133–214 (Butterworth and Co., London, England, 1968).*

Adiabatic heat-capacity calorimety in the range 4 to about 350 °K is reviewed with discussions in principles of calorimeter design, measurements, and analysis of data obtained. Measurements of temperature, power, and time are discussed with critical analysis of expected accuracy of circuitry and equipment used. Methods for transferring samples into the calorimeter vessel and various heat treatments in the calorimeter prior to measurements are suggested for substances that undergo phase transitions. Procedures are given for heat-leak, premelting, curvature, and vaporization corrections. Methods for smoothing the observed heat-capacity data and calculation of thermodynamic properties are discussed.

Key words: Calorimetry; calorimeters; cryostats; phase studies; phase transitions; thermometry; temperature; time; power; heat-leak correction; curvature correction; premelting correction; vaporization correction; purity; cryoscopy; thermodynamics; thermodynamic properties; low temperature calorimetry; adiabatic calorimetry; smoothing of observations.

Regularities in atomic oscillator strengths, Wiese, W. L., Weiss, A. W., *Phys. Rev.* **175,** *No. 1, 50–65 (Nov. 5, 1968).*

Many regularities and systematic trends among atomic oscillator strengths have been studied using the extensive material which has recently become available for the lighter elements. The quantum mechanical background for the existence of these regularities is discussed, and in particular the relationship between oscillator strength and nuclear charge as predicted from conventional perturbation theory is reviewed in detail. A number of characteristic numerical examples are then presented. The regularities are of great practical importance since they may be exploited to obtain additional oscillator strengths by simple interpolation techniques as well as to evaluate the reliability of existing data by the degree of fit into established systematic trends.

Key words: Atomic oscillator strengths; atomic spectroscopy; isoelectronic sequences; spectral series; spectroscopic regularities.

Other NBS Publications

J. Res. Nat. Bur. Stand. (U.S.), 73B (2) 59–189 (1969), $1.25.

An evaluation of linear least squares computer programs. R. H. Wampler.

The traffic assignment problem for a general network. S. C. Dafermos and F. T. Sparrow.

Sufficient conditions for the instability of numerical integration methods. A. I. A. Karim.

The second orthogonality conditions in the theory of proper and improper rotations. II. The intrinsic vector. H. Gelman.

The second orthogonality conditions in the theory of proper and improper rotations. III. The conjugacy theorem. H. Gelman.

Subgroups of $SL(t, z)$. M. Newman.

Cuttable and cut-reducible matrices. R. B. Marimont.

A theorem on automorphic integrals. J. Lehner.

A digital computer technique for calculating the step response of lumped or distributed networks. J. R. Andrews and N. S. Nahman.

Symmetry and the crossing number for complete graphs. T. L. Saaty.

Bryson, J. O., Gross, D., Techniques for the survey and evaluation of live floor loads and fire loads in modern office buildings, Bldg. Sci. Series 16 (Dec. 1968), 40 cents.

DeVoe, J. R., ed., Radiochemical Analysis Section: Summary of activities July 1967 to June 1968, Tech. Note 451 (Jan. 1969), $1.25.

Diamond, J. J., ed., Bibliography on the high temperature chemistry and physics of materials. October, November, December 1968, Spec. Publ. 315 (Jan. 1969), 70 cents.

Gross, D., Loftus, J. J., Lee, T. G., Gray, V. E., Smoke and gases produced by burning aircraft interior materials, Bldg. Sci. Series 18 (Feb. 1969), 35 cents.

Messina, C. G., Hilsenrath, J., Edpac: Utility programs for computer-assisted editing, copy-production, and data retrieval, Tech. Note 470 (Jan. 1969), 75 cents.

Barger, R. L., Hall, J. L., Pressure shift and broadening of methane line at 3.39μ studied by laser-saturated molecular absorption, Phys. Rev. Letters **22,** No. 1, 4–8 (Jan. 6, 1969).

Bay, Z., Luther, G. C., Locking a laser frequency to the time standard, Appl. Phys. Letters **13,** No. 9, 303–304 (Nov. 1, 1968).

Beatty, R. W., Fentress, G. H., An attenuation and phase shift divider circuit, Proc. IEEE **56,** No. 11, 2063–2064 (Nov. 1968).

Bennett, L. H., Swartzendruber, L. J., Some comments on the corrosion of materials in desalination plants, Desalination **4,** 389–390 (1968).

Botter, R., Rosenstock, H. M., Franck-Condon factors for NH_3 and H_2O, Chapter in Advances in Mass Spectrometry, **4,** 579–589 (Institute of Petroleum, London, England, 1968).

Brockman, J. F., Popular science writing, Proc. 1967 Inst. Technical Industrial Communications, Colorado State University, Fort Collins, Colo., June 12–16, 1967, pp. 96–100 (1967).

Casella, R. C., Time reversal and the K° meson decays, Phys. Rev. Letters **21,** No. 15, 1128–1131 (Oct. 7, 1968).

Ehrlich, M., Placious, R. C., Thermoluminescence response of CaF_2:Mn in polytetrafluoroethylene to electrons, Health Phys. **15,** 341–350 (1968).

Eisenhart, C., Zelen, M., Elements of probability, Chapter 12 in Handbook of Physics, Second Ed., E. U. Condon and H. Odishaw, ed., Part 1. Mathematics, pp. 1–163–1–197 (McGraw-Hill Book Co., New York, N.Y., 1967).

Evans, J. P., Sweger, D. M., Immersion cooler for freezing ice mantles on triple-point-of-water cells, Rev. Sci. Instr. **40,** No. 2, 376–377 (Feb. 1969).

Evenson, K. M., Broida, H. P., Wells, J. S., Mahler, R. J., Mizushima, M., Electron paramagnetic resonance absorption in oxygen with the HCN laser, Phys. Rev. Letters **21,** No. 15, 1038–1040 (Oct. 7, 1968).

Fatiadi, A. J., Esters of benzenepentol (pentahydroxybenzene), J. Chem. Eng. Data **14,** 118–119 (1969).

Feldman, A., Horowitz, D., Dispersion of the piezobirefringence of GaAs, J. Appl. Phys. **39,** No. 12, 5597–5599 (Nov. 1968).

Johnson, V. J., Development and operation of a specialized technical information and data center (The Cryogenic Data Center), J. Chem. Doc. **8,** No. 4, 219–224 (Nov. 1968).

Kahn, A. H., Polarons in anisotropic energy bands, Phys. Rev. **172,** No. 3, 813–815 (Aug. 15, 1968).

Lloyd, E. C., Erasable trance recording methods for chart recorders, Rev. Sci. Instr. **39,** No. 12, 1953–1954 (Dec. 1968).

Marzetta, L. A., Noise limitations in signal detectors, Instr. Technol. **16,** No. 2, 51–53 (Feb. 1969).

Moore, G. A., Wyman, L. L., Joseph, H. M., Comments on the possibilities of performing quantitative metallographic analyses with a digital computer, Chapter 13 in Quantitative Microscopy, pp. 380–403 (McGraw-Hill Inc., New York, N.Y., 1968).

Nemoto, T., Wait, D. F., Microwave circuit analysis using the equivalent generator concept, IEEE Trans. Microwave Theory Tech. **MTT-16,** No. 10, 866–873 (Oct. 1968).

Robbins, C. R., Growth of strontium titanate from a silica flux, J. Crystal Growth **2,** 402–404 (1968).

Rush, J. J., Melveger, A. J., Farrar, T. C., Tsang, T., Laser-Raman spectra and hindered rotation in the phosphonium halides, Chem. Phys. Letters **2,** No. 8, 621–624 (1968).

Schweitzer, W. G., Jr., Saturated absorption by neon inside a 6328 Å laser with a mixture of neon isotopes in its gain tube, Appl. Phys. Letters **13,** No. 11, 367–368 (Dec. 1, 1968).

Smith, E. W., Hooper, C. F., Jr., Comments on ion microfield distributions as used in plasma line broadening theories, J. Quant. Spectry. Radiative Transfer **8,** No. 9, 1617–1619 (Sept. 1968).

Stevens, M. E., Selected pattern recognition projects in Europe, Pattern Recognition **1,** 103–118 (Nov. 1968).

Weissler, P. G., International standard reference zero for audiometers, J. Acoust. Soc. Am. **44,** No. 1, 264–275 (July 1968).

Wilcox, R. M., Bounds for the isothermal, adiabatic, and isolated static susceptibility tensors, Phys. Rev. **174,** No. 2, 624–629 (Oct. 10, 1968).

Williams, E. S., A voltage converter for a new era, Meas. Data **2,** No. 6, 75–79 (Nov.-Dec. 1968).

Young, K. F., Forman, R. A., Use of polystyrene beads for manufacture of low loss coaxial lines for low temperature research, Rev. Sci. Instr. **39,** No. 12, 1964–1965 (Dec. 1968).

Young, R. D., Kuyatt, C. E., Resolution determination in field emission energy analyzers, Rev. Sci. Instr. **39,** No. 10, 1477–1480 (Oct. 1968).

**Publications for which a price is indicated are available by purchase from the Superintendent of Documents, U.S. Government Printing Office, Washington, D.C. 20402 (foreign postage, one-fourth additional). The NBS non-periodical series are also available from the Clearinghouse for Federal Scientific and Technical Information, Springfield, Va. 22151. Reprints from outside journals and the NBS Journal of Research may often be obtained directly from the authors.*

U.S. GOVERNMENT PRINTING OFFICE : 1969 OL—349-367

OCT 1969
UNIVERSITY MICROFILMS INC
ATTN SERIALS SECTION
300 NORTH ZEEB RD
ANN ARBOR MICH 48106

UNITED STATES
GOVERNMENT PRINTING OFFICE
DIVISION OF PUBLIC DOCUMENTS
WASHINGTON, D.C. 20402

OFFICIAL BUSINESS

POSTAGE AND FEES PAID
U.S. GOVERNMENT PRINTING OFFICE

JOURNAL OF RESEARCH of the National Bureau of Standards
A. Physics and Chemistry

Vol. 73A, No. 4 July–August 1969

Contents

Page

Classical path methods in line broadening. I. The classical path approximation. Earl W. Smith, C. R. Vidal, and J. Cooper. 389

Classical path methods in line broadening. II. Application to the Lyman series of hydrogen. Earl W. Smith, C. R. Vidal, and J. Cooper. 405

The second virial coefficient for the realistic pair potential. Harold W. Woolley. 421

Synthesis of barium ferrates in oxygen. Taki Negas and Robert S. Roth. 425

The system SrO-"chromium oxide" in air and oxygen. Taki Negas and Robert S. Roth. 431

Publications of the National Bureau of Standards. 443

Library of Congress Catalog Card Number: 62-37059

For sale by the Superintendent of Documents, U.S. Government Printing Office, Washington, D.C. 20402. Single copy price varies, This issue $1.25. Subscription price: $9.50 a year; $2.25 additional for foreign mailing.
UNITED STATES GOVERNMENT PRINTING OFFICE, WASHINGTON : 1969